Zhang, C-P, Liu, T, Yuan, J, Sanhueza, P, Traficante, A, Li, G-X, Li, D, Tatematsu, K, Wang, K, Lee, CW, Samal, MR, Eden, DJ, Marston, A, Liu, X-L, Zhou, J-J, Li, PS, Koch, PM, Xu, J-L, Wu, Y, Juvela, M, Zhang, T, Alina, D, Goldsmith, PF, Toth, L, Wang, J-J and Kim, K-T

The TOP-SCOPE Survey of PGCCs: PMO and SCUBA-2 Observations of 64 PGCCs in the Second Galactic Quadrant

The TOP-SCOPE survey of PGCCs: PMO and SCUBA-2 observations of 64 PGCCs in the 2nd Galactic Quadrant

Chuan-Peng Zhang[1,2,*], Tie Liu[3,4], Jinghua Yuan[1], Patricio Sanhueza[5], Alessio Traficante[6], Guang-Xing Li[7], Di Li[1], Ken'ichi Tatematsu[5], Ke Wang[8], Chang Won Lee[9,10], Manash R. Samal[11], David Eden[12], Anthony Marston[13], Xiao-Lan Liu[1], Jian-Jun Zhou[14], Pak Shing Li[15], Patrick M. Koch[16], Jin-Long Xu[1], Yuefang Wu[17], Mika Juvela[18], Tianwei Zhang[17], Dana Alina[19], Paul F. Goldsmith[20], L. V. Tóth[21], Jun-Jie Wang[1], Kee-Tae Kim[3]

ABSTRACT

In order to understand the initial conditions and early evolution of star formation in a wide range of Galactic environments, we carried out an investigation of 64 *Planck* Galactic Cold Clumps (PGCCs) in the second quadrant of the Milky Way. Using the ^{13}CO and C^{18}O $J = 1-0$ lines, and 850 μm continuum observations, we investigated cloud fragmentation and evolution associated with star formation. We extracted 468 clumps and 117 cores from the ^{13}CO line and 850 μm continuum maps, respectively. We make use of the Bayesian Distance Calculator and derived the distances of all 64 PGCCs. We found that in general, the mass-size plane follows a relation of $m \sim r^{1.67}$. At a given scale, the masses of our objects are around 1/10 of that of typical Galactic massive star-forming regions. Analysis of the clump and core masses, virial parameters, densities, and mass-size relation suggests that the PGCCs in our sample have a low core formation efficiency ($\sim$3.0%), and most PGCCs are likely low-mass star-forming candidates.

*Email: cpzhang@nao.cas.cn

[1]National Astronomical Observatories, Chinese Academy of Sciences, 100012 Beijing, PR China

[2]Max-Planck-Institut für Astronomie, Königstuhl 17, 69117 Heidelberg, Germany

[3]Korea Astronomy and Space Science Institute 776, Daedeokdae-ro, Yuseong-gu, Daejeon 34055, Korea

[4]East Asian Observatory, 660 N. A'ohōkū Place, Hilo, Hawaii 96720-2700, USA

[5]National Astronomical Observatory of Japan, National Institutes of Natural Sciences, 2-21-1 Osawa, Mitaka, Tokyo 181-8588, Japan

[6]IAPS - INAF, via Fosso del Cavaliere, 100, I-00133 Roma, Italy

[7]University Observatory Munich, Scheinerstrasse 1, D-81679 Munich, Germany

[8]European Southern Observatory, Karl-Schwarzschild-Str.2, D-85748 Garching bei München, Germany

[9]Korea Astronomy & Space Science Institute (KASI), 776 Daedeokdae-ro, Yuseong-gu, Daejeon 305-348, Republic of Korea

[10]University of Science & Technology, 176 Gajeong-dong, Yuseong-gu, Daejeon, Republic of Korea

[11]Graduate Institute of Astronomy, National Central University 300, Jhongli City, Taoyuan County 32001, Taiwan

[12]Astrophysics Research Institute, Liverpool John Moores University, IC2, Liverpool Science Park, 146 Brownlow Hill, Liverpool, L3 5RF, UK

[13]ESA/STScI, 3700 San Martin Dr, Baltimore, MD 21218, USA

[14]Xinjiang Astronomical Observatory, CAS, 150, Science 1-street, 830011 Urumqi, PR China

[15]Astronomy Department, University of California, Berkeley, CA 94720, USA

[16]Academia Sinica, Institute of Astronomy and Astrophysics, P.O. Box 23-141, Taipei 106, Taiwan

[17]Department of Astronomy, Peking University, 100871 Beijing, PR China

[18]Department of Physics, P.O.Box 64, FI-00014, University of Helsinki, Finland

[19]Physics Department, Nazarbayev University, Kabanbay batyr avenue 53, 010000 Astana, Kazakhstan

[20]Jet Propulsion Laboratory, California Institute of Technology, 4800 Oak Grove Drive, Pasadena, CA 91109, USA

[21]Loránd Eötvös University, Department of Astronomy, Pázmány P.s. 1/a, H-1117 Budapest, Hungary

Statistical study indicates that the 850 μm cores are more turbulent, more optically thick, and denser than the ^{13}CO clumps for star formation candidates, suggesting that the 850 μm cores are likely more appropriate future star-formation candidates than the ^{13}CO clumps.

Subject headings: ISM: clouds – ISM: dust – ISM: structure – stars: formation

1. Introduction

Stars form in the dense, cold regions within molecular clouds. However, the physical and chemical properties of the cold compact objects that breed stars are still poorly understood. Stars could form out of gravitationally bound substructures within a molecular cloud, but how the substructures themselves form is strongly debated (e.g., Johnstone et al. 2004). Investigating the cloud fragmentation from large scale to small scale may be one way to determine this. An important approach to improve our understanding is to perform a statistical study towards the cold dense clumps from unbiased large surveys in the Milky Way.

Fortunately, the *Planck* satellite has allowed for a systematically extracted inventory of Galactic cold clumps (Planck Collaboration et al. 2011a) using multiple bands from submillimeter to millimeter wavelengths. The Cold Core Catalogue of *Planck* Objects (C3PO) consisting of 10,783 cold cores (Planck Collaboration et al. 2011d), and the *Planck* Early Release Cold Cores Catalog (ECC), the sub-catalog, containing 915 of the most reliable detections were released in 2011 (Planck Collaboration et al. 2011b). The C3PO was the first unbiased, all-sky catalogue of cold objects, and gives an unprecedented statistical view to the properties of these potential pre-stellar clumps and offers a unique possibility for their classification in terms of their intrinsic properties and environment (Planck Collaboration et al. 2011d). The cores in C3PO have relatively high column densities ($0.1 \sim 1.6 \times 10^{22}$ cm^{-2}) and low dust temperatures ($\sim$10 – 15 K, Planck Collaboration et al. 2011c,d). This was followed by the *Planck* Catalogue of Galactic Cold Clumps (PGCCs; Planck Collaboration et al. 2016), an all-sky catalogue of Galactic cold clump candidates, containing 13,188 Galactic sources, detected by *Planck*. This catalogue is the full version of the ECC catalogue. The *Herschel* key programme "Galactic Cold Cores" was a follow-up to study the substructure and physics of selected C3PO sources (selection being performed on their intrinsic properties and their Galactic location). This study commenced during the *Herschel* Science Demonstration Phase Data (Juvela et al. 2010).

Further follow-up studies of PGCC objects have been carried out with ground-based telescopes to study the evolutionary conditions of PGCCs. These facilities include: the James Clerk Maxwell Telescope (JCMT), the Purple Mountain Observatory (PMO), the Nobeyama Radio Observatory, the Taeduk Radio Astronomy Observatory (TRAO), the Korean VLBI Network (KVN), the Caltech Submillimeter Observatory (CSO), the Submillimeter Array (SMA), and the Institut de radioastronomie millimétrique (IRAM) (Wu et al. 2012; Meng et al. 2013; Liu et al. 2012, 2013, 2015, 2016; Yuan et al. 2016; Zhang et al. 2016b; Kim et al. 2017; Tatematsu et al. 2017; Tang et al. 2018). These ground-based studies allow us to improve our understanding of dense cores and star formation in widely different environments at higher spatial resolution than the *Planck* observations, using different tracers from the continuum to spectral lines (e.g., CO, N_2H^+, HCO^+). For example, Wu et al. (2012) and Meng et al. (2013) carried out a survey towards 745 PGCCs in ^{12}CO, ^{13}CO, C^{18}O $J = 1 - 0$ using the PMO 13.7-m telescope. They found a variety of morphologies from extended diffuse to dense, isolated, cometary, and filamentary structures. They also found that the PGCCs are the most quiescent among the sample of weak-red IRAS, infrared dark clouds, UC H II candidates, extended green objects, and methanol maser sources. Liu et al. (2016) performed a series of observations with ground-based telescopes towards one PGCC in the λ Orionis complex to systematically investigate the effects of stellar feedback. Particularly they discovered an extremely young Class 0 protostellar object (G192N) and a proto-brown dwarf candidate (G192S), located in a gravitationally bound bright-rimmed clump. This provides a sample to study the earliest stage of star formation. Yuan et al. (2016) conducted the first large survey

of dense gas toward PGCCs in the $J = 1 - 0$ transitions of HCO^+ and HCN toward 621 molecular cores. On the basis of an inspection of the derived density information given in their PGCC catalog, Yuan et al. (2016) suggested that about 1000 out of 13,188 PGCCs show a sufficient reservoir of dense gas to form stars.

Based on the studies mentioned above, PGCCs are cold ($\sim$ 10-15 K), turbulence-dominated, and have relatively low column densities compared to other star-forming regions (Wu et al. 2012; Planck Collaboration et al. 2011c,d). Additionally, most clumps are quiescent and lack signs of star formation, indicating that the PGCCs are most likely in the very initial evolutionary stages of star formation (Wu et al. 2012; Yuan et al. 2016). Furthermore, previous studies indicate that gaseous CO abundance (or depletion) can be used as a tracer for the evolution of molecular clouds (Liu et al. 2013; Zhang et al. 2017a).

The work described here is part of the TOP-SCOPE[1] survey of PGCCs, which combines the TRAO 13.7-m telescope and the Submillimetre Common-User Bolometer Array 2 (SCUBA-2; Holland et al. 2013) instrument on board of the JCMT to observe around 1000 PGCCs (Eden et al., in prep.; Liu et al. 2018a). It is a follow-up study of Zhang et al. (2016b), who mainly used ^{12}CO and ^{13}CO $J = 1 - 0$ emission lines to investigate the gas content of 96 PGCCs from $98^\circ < l < 180^\circ$ and $-4^\circ < b < 10^\circ$ in the second quadrant of the Milky Way. The survey has covered most of the densest ECCs in the regions of the 2nd quadrant (see more details in Zhang et al. 2016b). Zhang et al. (2016b) discussed the properties and morphologies of these clumps combining the distributions of excitation temperature, velocity dispersion, and column density. The second quadrant is home to many well-known star formation regions, such as W3, W4, W5, NGC 7129, NGC 7538, and S235 (Dame et al. 1987, 2001; Heyer & Terebey 1998). A systematic cold core analysis of the second quadrant could thus be essential for understanding the properties of the initial star-forming conditions in the Outer Galaxy.

[1]TOP: TRAO observations of *Planck* cold clumps; SCOPE: SCUBA-2 Continuum Observations of Pre-protostellar Evolution

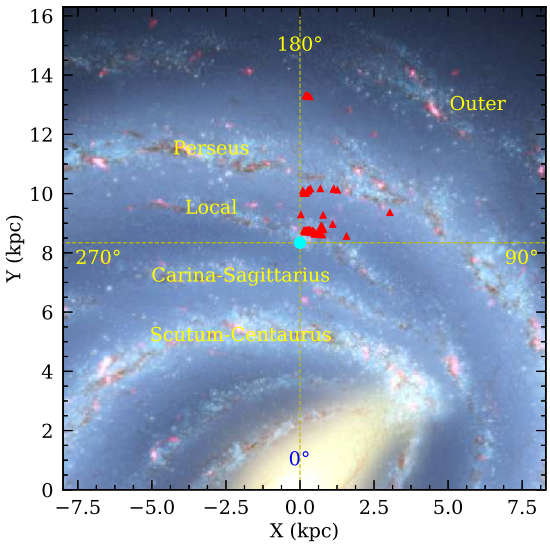

Fig. 1.— Distribution of the clumps (red-filled triangles) on the background of an artists conception of the Milky Way (R. Hurt: NASA/JPL-Caltech/SSC). All sources are located in the second quadrant of the Galaxy.

In the 96 Zhang et al. (2016b) PGCCs, there are 64 sources that have been covered by both the SCUBA-2 850 μm continuum and PMO ^{13}CO, C^{18}O $J = 1 - 0$ line observations. In this work, we study the 64 PGCCs mainly combining the continuum and line data mentioned above. The ^{13}CO are C^{18}O are more suitable tracers to study dense conditions of the PGCCs than the ^{12}CO and ^{13}CO investigation in Zhang et al. (2016b). These data are also compared with the WISE 12 and 22 μm emission. The full sample is presented in Table 1 and Fig. 1. Section 2 presents the observations and data reduction. Section 3 shows the results of observations and the data analysis. In Section 4, we discuss the fragmentation and evolution associated with star formation, and present a statistical analysis of the morphology, velocity dispersion, virial parameter, surface density, optical depth, and excitation temperature for the ^{13}CO clumps and 850 μm cores. Finally, a summary is presented in Section 5.

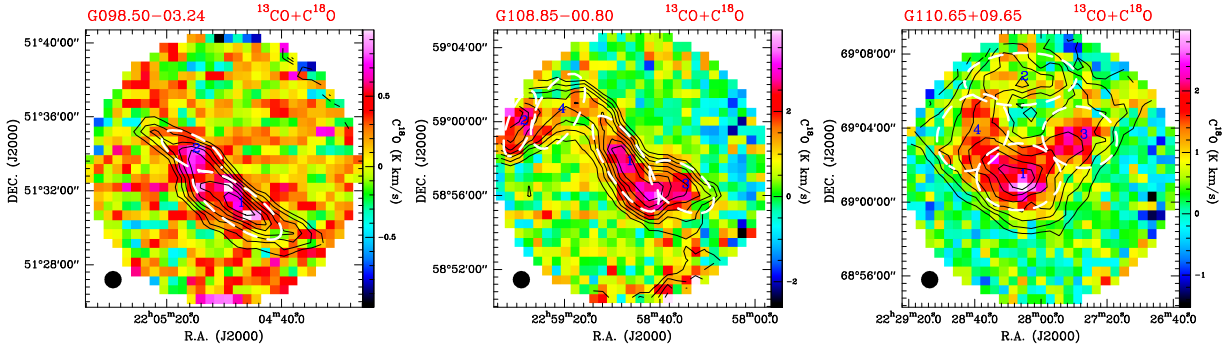

Fig. 2.— Integrated-intensity maps of $C^{18}O$ emission of each source with overlaid contours of the ^{13}CO line. The integrated velocity ranges used are indicated within the red window in the corresponding spectrum of Fig. 3. The contour levels of the ^{13}CO lines are drawn at 10% steps, starting with 30% of the peak value. The white ellipses indicate the extracted ^{13}CO clumps. The beam size of the ^{13}CO data is indicated in the bottom-left corner. `Supplementary figures can be downloaded in https://zcp521.github.io/pub/Figs.zip.`

2. Observations

2.1. The CO data of the PMO 13.7-m telescope

The CO observations were made during April – May 2011, and December 2011 – January 2012 using the 13.7-m millimeter telescope of Qinghai Station at the PMO[2]. The 9-beam SIS superconducting receiver with beams separated by around 180″, was used as the front end. The receiver was operated in the sideband separation of single sideband mode, allowing for simultaneous observations of three CO $J = 1 - 0$ isotopologues, with ^{12}CO in the upper sideband (USB) and ^{13}CO and $C^{18}O$ in the lower sideband (LSB). The half-power beam width (HPBW) is $52'' \pm 3''$, with a main beam efficiency of $\sim$50% for ^{13}CO and $C^{18}O$ observations. The ^{13}CO and $C^{18}O$ data are used here. The pointing and tracking accuracies are better than 5″. The typical system temperatures during the runs are $\sim$120 K at 110.2 GHz, and varied by $\sim$10% between beams. A fast Fourier transform (FFT) spectrometer was used as the back end with a total bandwidth of 1 GHz and 16,384 channels, giving a velocity resolution of $\sim 0.16\,\mathrm{km\,s^{-1}}$ for the ^{13}CO and $C^{18}O$ lines.

An on-the-fly (OTF) observing mode was used for the mapping observations at a scan speed of $50''\ \mathrm{s^{-1}}$. The off position for each "off" source was carefully chosen from an area within a 3° radius of each "on" source, where there is extremely weak or no CO emission (Dame et al. 1987, 2001). The antenna continuously scanned a region of $22' \times 22'$ centered on each clump, while only the central $14' \times 14'$ region is used due to the noisy edges of the OTF maps. The rms noise level was 0.1 K in the main beam antenna temperature T_A^* for ^{13}CO and $C^{18}O$ $J = 1 - 0$. The OTF data were resampled in a three-dimensional (3D) cube with a grid spacing of 30″. The IRAM software package GILDAS[3] was used for the data reduction. The reduced images are presented in Figs. 2 and 3. The integrated-intensity maps of ^{13}CO line are also overlaid on the WISE 12 and 22 μm emission maps in Figs. 4 and 5.

2.2. The 850 μm data of the JCMT 15-m telescope

The majority of the SCUBA-2 850 μm observations were conducted as part of the SCOPE project (Liu et al. 2018a). The rest of the data were collected from the JCMT data archive of the Canadian Astronomy Data Centre (CADC). SCUBA-2 is a bolometer detector at the JCMT 15-m telescope with ~10,000 pixels over eight science arrays which simultaneously observe 450 and 850 μm with a field-of-view of 8′, and the effective beam size is around 10″ at 450 μm and 14″

[2]http://www.dlh.pmo.cas.cn/

[3]http://iram.fr/IRAMFR/GILDAS/

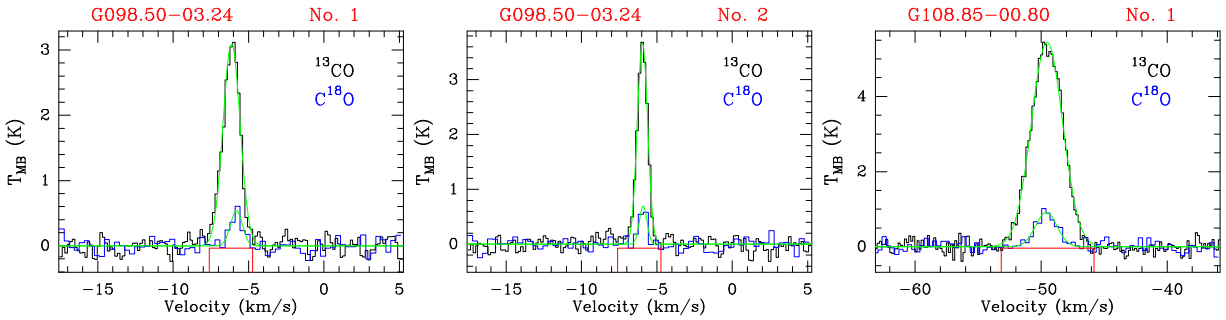

Fig. 3.— Averaged ^{13}CO (black line) and C^{18}O (blue lines) lines within the size of each extracted ^{13}CO clump (see Fig. 2). The green lines show the Gaussian fits in each spectrum. The red window indicates the velocity range corresponding to the ^{13}CO and C^{18}O integrated intensity maps (see Fig. 2). `Supplementary figures can be downloaded in https://zcp521.github.io/pub/Figs.zip.`

at 850 μm (Holland et al. 2013). The observations used the constant velocity (CV) Daisy mode (Bintley et al. 2014), which is more sensitive in the central 3′ radii, and designed for small and compact sources. The 225 GHz opacity during the observations was in the range of 0.09 to 0.11, therefore we only use the 850 μm data as the 450 μm data isn't photometric. The data were reduced using SMURF in the STARLINK package (Chapin et al. 2013; Dempsey et al. 2013). The mapped areas were about 12′ × 12′. The rms level in the central 3′ area of the maps was typically 6 – 10 mJy beam^{-1}. The images are presented in Fig. 6.

SCUBA-2 continuum observations at 850 μm are known to be affected by contamination from spectral lines (Johnstone et al. 2003; Parsons et al. 2018), especially the ^{12}CO $J = 3-2$ line at 345.796 GHz (Drabek et al. 2012). A typical level of the CO contamination is $<20\%$ (Nutter & Ward-Thompson 2007; Buckle et al. 2015; Rumble et al. 2015; Moore et al. 2015), which is not significant. In a study of 90 PGCCs, Juvela et al. (2017) found that the CO contamination levels in SCUBA-2 images are $\leqslant$5%. Therefore we don't correct for it here.

The observatory produced Flux Conversion Factor (FCF) was calculated using a 60″ aperture. If we have a clump that is bigger or smaller than this nominal FCF, we will need to adjust the flux values accordingly. The integrated flux density $S_{850\,\mu m}$ of each extracted core (see Section 3.2) has been corrected using aperture correction factor provided by Dempsey et al. (2013).

2.3. Archival WISE data

NASA's Wide-field Infrared Survey Explorer (WISE; Wright et al. 2010) mapped the sky at 3.4, 4.6, 12, and 22 μm (W1, W2, W3, and W4) with an angular resolution of 6.1″, 6.4″, 6.5″, and 12.0″ in the four bands, respectively. WISE achieved 5σ point source sensitivities better than 0.08, 0.11, 1, and 6 mJy in unconfused regions on the ecliptic in the four bands. The sensitivity was better toward the ecliptic poles due to denser coverage and lower zodiacal background. In this work, WISE 12 and 22 μm image data are used. Additionally, the AllWISE Data in VizieR Online Data Catalog (Cutri et al. 2013, 2014) are used for point source cross identification (within 10″ radii of the peak position of each 850 μm core) with our 850 μm catalog (using *Gaussclumps* procedure; see Section 3.2) listed in Table 5. The WISE images are presented in Figs. 4 and 5.

3. Results and Analysis

3.1. Distance Determination

The distances to the PGCCs are estimated using the Bayesian Distance Calculator[4] (Reid et al. 2016), which uses trigonometric parallaxes from the BeSSeL (Bar and Spiral Structure Legacy Survey[5]) and VERA (Japanese VLBI Exploration of Radio Astrometry[6]) projects, to significantly im-

[4]http://bessel.vlbi-astrometry.org/bayesian
[5]http://bessel.vlbi-astrometry.org/home
[6]http://veraserver.mtk.nao.ac.jp/

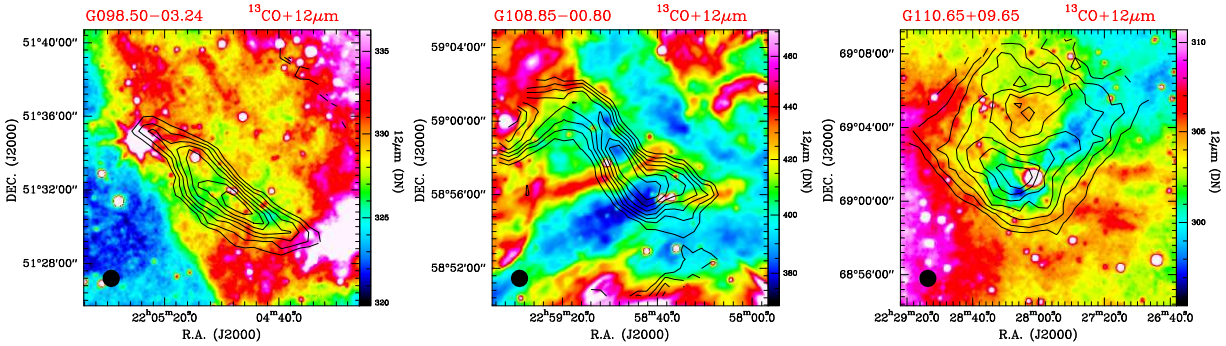

Fig. 4.— WISE 12 μm emission for each PGCC with overlaid ^{13}CO contours. The contour levels of the ^{13}CO lines are drawn at 10% steps, starting with 30% of the peak value. The beam size of ^{13}CO data is indicated in the bottom-left corner. `Supplementary figures can be downloaded in https://zcp521.github.io/pub/Figs.zip.`

prove the accuracy and reliability of kinematic distance estimates to other sources that are known to follow the Milky Way spiral structure. Based on the ^{13}CO centroid velocity of each 850 μm core No. 1 within each PGCC (see Table 4), the corresponding distance parameters (distributed between 0.42 and 5.0 kpc) are derived and listed in Table 1. The probabilities of the adopted distances are also listed in Table 1. In Fig. 1, we present the distribution of the PGCCs on an artist's conception of the Milky Way (Yuan et al. 2017). We find that most PGCCs are located in the Local and Perseus arms with a significant population in the corresponding interarm region, while only four PGCCs (G176.17-02.10, G177.09+02.85, G177.14-01.21, and G177.86+01.04) are located in the Outer arm. We note that some derived distances are different from those in Zhang et al. (2016b), who used only the Galactic rotation curve to acquire the kinematic distances (distribution between 0.1 and 28.7 kpc) following the method of Sofue (2011).

3.2. Fragment extraction and definition

The potential cloud fragments are extracted from the ^{13}CO integrated line intensity and 850 μm continuum maps with the *Gaussclumps* procedure (Kramer et al. 1998; Stutzki & Guesten 1990; Zhang et al. 2017b) in the GILDAS software package. *Gaussclumps* fits a 2-dimensional fragment to the local maximum of the input cube, subtracts this fragment from the cube, creating a residual map, and then continues with the maximum of this residual map (Gómez et al. 2014). This procedure is then repeated until a stop criterion is met. We only consider fragments with peak ^{13}CO and 850 μm intensities of above 5σ with the initial FWHM set at 1.1 times the beam size. The initial aperture FWHM and aperture cutoff are set as 2.0 and 8.0 times the beam size, respectively (see also detailed example of configurations in Belloche et al. 2011). Considering that some extracted sources are in filamentary structures, we have rejected sources with aspect ratios larger than 5 as the study of filaments in the SCOPE PGCCs will be the subject of a further study. The measured parameters are listed in Tables 2, 3, 4, and 5, and indicated with ellipses in Figs. 2 and 7.

In this work, we adopt "fragment" as the general name for both extracted clumps and cores. We consider a clump to have a typical size of 0.3 – 3 pc with a mass of 50 – 500 $M_\odot$ and cores are an order of magnitude lower with sizes of 0.03 – 0.2 pc with masses of 0.5 – 5 $M_\odot$ (e.g., Bergin & Tafalla 2007; Motte et al. 2017). Based on the effective radii in Tables 2 and 4, we thus refer to the ^{13}CO objects as clumps and the 850 μm objects as cores. Massive clouds tend to fragment into clusters of clumps and cores (Pokhrel et al. 2018), in which young stars form. Therefore, we can explore the habitats of clumps at larger scales and the cores at smaller scales, studying the fragmentation process[7].

[7] A caveat here is that the clumps and cores could just be dis-

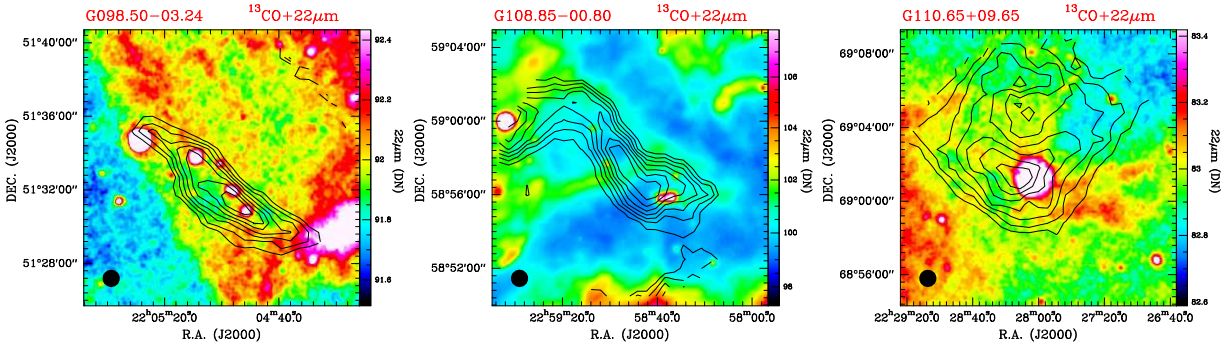

Fig. 5.— WISE 22 μm emission for each PGCC with overlaid ^{13}CO contours. The contour levels of the ^{13}CO lines are drawn at 10% steps, starting with 30% of the peak value. The beam size of ^{13}CO data is indicated in the bottom-left corner. `Supplementary figures can be downloaded in https://zcp521.github.io/pub/Figs.zip.`

3.3. ^{13}CO clumps

In total, we have extracted 468 ^{13}CO clumps having an effective radius range of 0.1 – 3.3 pc with a median value of 0.4 pc and a detected mass range of 1 – 6132 $M_\odot$ with a median value of 66 $M_\odot$ for the clumps. Figure 2 shows the C^{18}O emission with ^{13}CO contours overlaid. Some ^{13}CO clumps have weak or no corresponding C^{18}O emission. In Table 2, therefore, we only consider the sources that are detected in both the lines with main beam brightness temperatures $T_{^{13}\rm CO} > 3\sigma$ and $T_{\rm C^{18}O} > 3\sigma$. The white ellipses with numbers show the extracted ^{13}CO clumps. The average ^{13}CO and C^{18}O lines within each extracted ^{13}CO clump are presented in Fig. 3. We also display the Gaussian fitted lines with green curves. Most of the ^{13}CO and C^{18}O lines can be fitted with a single-velocity Gaussian component. For the multi-velocity components, we only consider the strongest peak or the velocity components with infrared emission.

In Fig. 2, morphologically we observed that some PGCCs show clearly filamentary structure (e.g. G108.85-00.80, G116.12+08.98) and spherical structure (e.g. G115.92+09.46, G133.48+09.02), and the others are morphologically complicated and don't belong to the both cases above. The filamentary structures are ubiquitous in the Milky Way (Rathborne et al. 2006; Csengeri et al. 2014; Motte et al. 2017; Zhang et al. 2017a). They are much elongated along the long axis of filament with aspect ratios $\gtrsim 5$ (Wang et al. 2011, 2014). For the spherical structure, the most massive fragments are often located at the center position of their parent clusters, with several low-mass fragments surrounding the most massive one. We find that the filamentary structures make up 23 (35.9%) sources in the 64 PGCCs, respectively. Dense clumps elongate along their parental filament axis. The clumps in filamentary structure seem to be more compact than the others in our sample. Könyves et al. (2015) suggested that the filamentary environment is more suitable for star formation than spherical structures. Lane et al. (2016) suggested that the dense core clusters tend to be elongated, perhaps indicating a formation mechanism linked to the filamentary structure within molecular clouds.

Figure 3 shows that only 56 (12.0%) of the ^{13}CO clumps show multi-velocity components in both ^{13}CO and C^{18}O emission, and the others have single velocity components. In the direction of the second quadrant of the Milky Way, there are at most three spiral arms in line of sight, and they are located at relatively near distances without kinematic distance ambiguity. The relatively optically thick ^{13}CO line has similar profiles to the optically thin C^{18}O line for most clumps, but shows a slightly broader width. Comparing the ^{12}CO line as a dynamical tracer with the ^{13}CO line, Zhang et al. (2016b) also found that clumps are mostly dynamically quiescent and lack star forming activity, further indicating that the PGCCs are

crete self-gravitating structures in a large-scale cloud (see also Section 3.6).

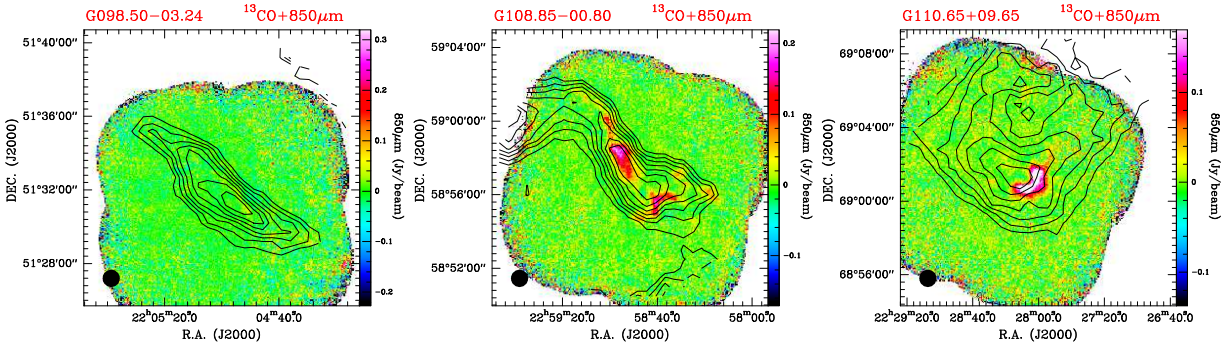

Fig. 6.— SCUBA-2 850 μm emission for each PGCC with overlaid ^{13}CO contours. The contour levels of the ^{13}CO lines are drawn at 10% steps, starting with 30% of the peak value. The beam size of ^{13}CO data is indicated in the bottom-left corner. `Supplementary figures can be downloaded in https://zcp521.github.io/pub/Figs.zip.`

most likely in a very early evolutionary stage of star formation (Wu et al. 2012; Yuan et al. 2016).

In Figs. 4 and 5, ^{13}CO emission is plotted on maps of WISE 12 and 22 μm emission. This is helpful for understanding the related infrared emission distribution in the background, and to predict the interaction relationship between the ionized gas and molecular clouds (see details in Section 4.2).

3.4. 850 μm cores

All 64 PGCCs have been observed at 850 μm with SCUBA-2, but only 28 (43.8%) are detected above 5σ (σ is the rms noise of the image). The PGCCs G142.49+07.48 and G150.44+03.95 are not adequately covered by the 850 μm observations, which may reduce the detection number of 850 μm cores, but have no significantly affect on the detection statistics. The low detection rate suggests that the PGCCs have a relatively low core formation efficiency (CFE; see Section 4.7). In total, we extracted 117 850μm cores having an effective radius range of 0.03 – 0.48 pc with a median value of 0.07 pc and a detected mass range of 0.4 – 311 $M_\odot$ with a median value of 8 $M_\odot$ for the cores. Figure 6 shows the 850 μm emission map (*color scale*) with ^{13}CO contours overlaid. About 26 (22.2%) of the 117 cores have weak ($< 3\sigma$) or no corresponding C^{18}O emission (see Fig. 8 and Table 4). The 850 μm cores are strongly associated with the peak positions of C^{18}O emission.

In Table 5, we list the positional associations between our extracted 850 μm cores and the AllWISE Data (Cutri et al. 2013, 2014). We only search for WISE point sources within 10″ radii of the peak position of each 850 μm core. In Fig. 7, we show the distribution of the extracted 850 μm cores. We find that 74 (63.2%) of the 117 850μm cores have corresponding WISE infrared point sources, some of which may happen to be the sources in line of sight.

In Fig. 8, we present the ^{13}CO and C^{18}O lines extracted from the 117 850 μm cores. We find that only 26 (22.2%) of the 850 μm cores show multi-velocity components in ^{13}CO and C^{18}O lines, suggesting that most detections correspond to a single object along the line of sight. Compared with ^{13}CO clumps, the 850 μm cores have few multi-peak spectra, indicating that majority ^{13}CO clumps at large scale are relatively more dynamically complex than the 850 μm cores at small scale (see the error analysis in Section 4.1).

3.5. Opacity, excitation temperature, column density, and mass

We use the approach of Wong et al. (2008) to derive the opacity, excitation temperature, and column density of each clump combining ^{13}CO and C^{18}O $J = 1 - 0$. The integrated velocity ranges for each clump are shown in Figs. 3 and 8. The relationship between opacities (τ) and main-beam brightness temperatures ($T_{\rm MB}$) for ^{13}CO and C^{18}O (Myers et al. 1983; Zhang & Wang 2012)

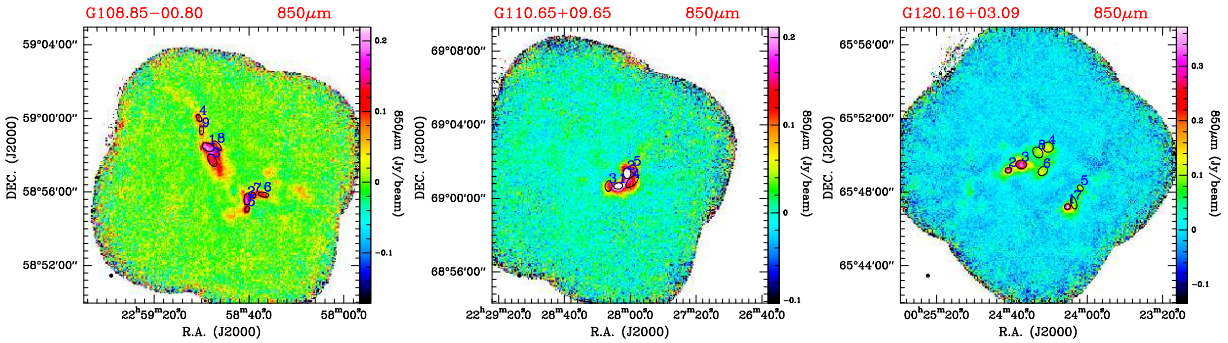

Fig. 7.— The extracted 850 μm cores (*black ellipse*) superimposed on 850 μm emission. The beam size of 850 μm data is indicated in the bottom-left corner. `Supplementary figures can be downloaded in https://zcp521.github.io/pub/Figs.zip.`

is

$$\frac{T_{\rm MB}(^{13}{\rm CO})}{T_{\rm MB}({\rm C}^{18}{\rm O})} = \frac{1-\exp(-\tau_{13})}{1-\exp(-\tau_{18})} = \frac{1-\exp(-\lambda\tau_{18})}{1-\exp(-\tau_{18})}. \quad (1)$$

Equation (1) assumes a single excitation temperature for both molecules and throughout the line of sight, and assumes $\tau_{13} = \lambda\tau_{18}$, where λ is the abundance ratio between $^{13}{\rm C}^{16}{\rm O}$ and $^{12}{\rm C}^{18}{\rm O}$. λ can be derived from relation in Wilson & Rood (1994) and Pineda et al. (2013) to be as

$$\lambda = \frac{[^{13}{\rm C}^{16}{\rm O}]}{[^{12}{\rm C}^{18}{\rm O}]} = \frac{58.8R_{\rm GC}+37.1}{4.7R_{\rm GC}+25.05}, \quad (2)$$

where $R_{\rm GC}$ is the Galactocentric distance. We only consider the sources detected with main beam brightness temperatures $T_{^{13}{\rm CO}} > 3\sigma$ and $T_{{\rm C}^{18}{\rm O}} > 3\sigma$ (see Table 3). Furthermore, the excitation temperature $T_{\rm ex}$ is derived from the radiative transfer equation:

$$J(T) = {\rm T}_0/[\exp({\rm T}_0/T)-1] \quad (3)$$

$$T_{\rm MB} = f[J(T_{\rm ex})-J(T_{\rm bg})][1-\exp(-\tau)] \quad (4)$$

where f is the beam filling factor which we assume as $f = 1$, $T_{bg} = 2.73\,{\rm K}$ is the cosmic microwave background temperature and $T_0 = h\nu/k = 5.29\,{\rm K}$ for the $J = 1-0$ transition of ^{13}CO (Wong et al. 2008). We then obtain the molecular ^{13}CO column density $N(^{13}{\rm CO})$ from the relation (Bourke et al. 1997):

$$N(^{13}{\rm CO})_{\rm thin} = \frac{T_{\rm ex}+0.88}{1-\exp(-5.29/T_{\rm ex})} \times \frac{2.42\times10^{14}}{J(T_{\rm ex})-J(T_{\rm bg})}\int T_{\rm MB}(^{13}{\rm CO})dv, \quad (5)$$

where $N(^{13}{\rm CO})_{\rm thin}$ and v are in units of ${\rm cm}^{-2}$ and ${\rm km\,s}^{-1}$, respectively. We then apply a correction factor $\tau/(1-\exp(-\tau))$ to the ^{13}CO column density (Pineda et al. 2010; Liu et al. 2013):

$$N'(^{13}{\rm CO})_{\rm corrected} = N(^{13}{\rm CO})_{\rm thin} \times \frac{\tau_{13}}{1-\exp(-\tau_{13})} \quad (6)$$

Finally, the molecular hydrogen column $N_{\rm H_2}$ was calculated, assuming that the $[{\rm H_2}/^{13}{\rm CO}]$ abundance ratio is 7×10^5 (Frerking et al. 1982).

The ^{13}CO clump mass is given by the integral of the column density across the source via formula (Kauffmann et al. 2008):

$$M_{\rm H_2}^{^{13}{\rm CO}} = \mu_{\rm H_2} m_{\rm H} D^2 \int N_{\rm H_2} d\Omega, \quad (7)$$

where $\mu_{\rm H_2} = 2.8$, $m_{\rm H} = 1.008\,{\rm u}$, D, and Ω are the mean molecular weight, the mass of a hydrogen atom, the distance, and the solid angle of the source, respectively. The masses of all extracted ^{13}CO clumps are listed in Table 3.

3.6. Virial analysis

The virial theorem can be used to test whether fragments are in a stable state. Under the assumption of a simple spherical fragment with a density distribution of $\rho = r^{-2}$, ignoring magnetic fields and bulk motions of the gas, the virial mass of a fragment can be estimated from the formula (MacLaren et al. 1988; Evans 1999):

$$M_{\rm vir} \simeq 126\, R_{\rm eff}\, \Delta V^2_{{\rm C}^{18}{\rm O}}\, (M_\odot), \quad (8)$$

where $R_{\rm eff} = {\rm FWHM}/(2\sqrt{\ln 2})$ is the effective radius of the fragment in pc, and $\Delta V_{{\rm C}^{18}{\rm O}}$ (listed in

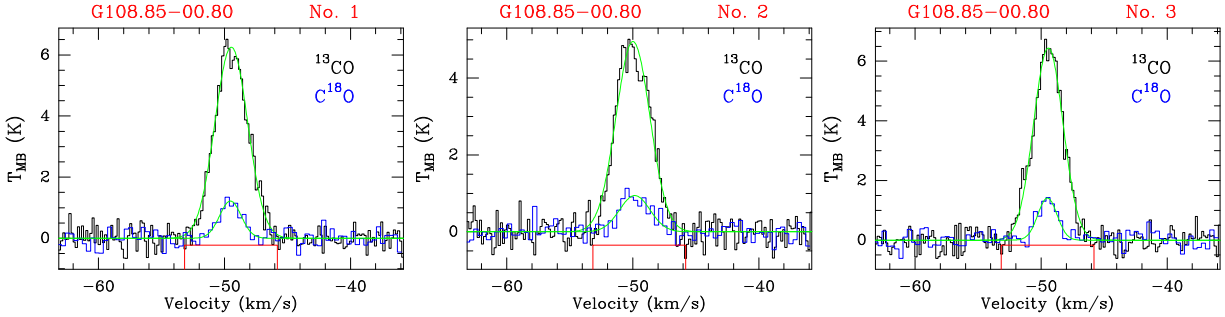

Fig. 8.— ^{13}CO (black line) and C^{18}O (blue line) lines within each extracted 850 μm core (see Fig. 7). The green lines show the Gaussian fits in each spectrum. The red window indicates the velocity range of corresponding ^{13}CO and C^{18}O integrated intensity maps (see Fig. 2). `Supplementary figures can be downloaded in https://zcp521.github.io/pub/Figs.zip.`

Tables 2 and 4) is the FWHM of the line profile in km s^{-1}. $\Delta V_{\rm C^{18}O}$ is the measured C^{18}O linewidth using Gaussian line fitting. For a typical cold cloud ($<$ 20 K), the thermal width is only a few tenths narrower than the observed linewidth, thus the observed linewidth is presumed to be representative of the turbulent velocity structure. The spatial resolution of the C^{18}O data is somewhat larger than the sizes of individual cores, hence we just consider the C^{18}O spectrum within one pixel corresponding to the peak position of each core (see error analysis in Section 4.1). The virial parameter $\alpha_{\rm vir}$ is defined by $\alpha_{\rm vir} = M_{\rm vir}/M$. The virial masses and virial parameters are listed in Tables 3 and 5.

3.7. Dust mass and surface density

We assume that the dust emission is optically thin and the gas-to-dust ratio is 100. The fragment masses are calculated using dust opacity κ_ν = 0.0182 cm^2 g^{-1} at 850 μm (Kauffmann et al. 2008) assuming a gas to dust mass ratio of 100 for a model of dust grains with thin ice mantles at a gas density of 10^6 cm^{-3}(Ossenkopf & Henning 1994). The total mass, $M_{\rm H_2}^{850\mu{\rm m}}$, of the 850 μm sources can therefore be calculated via the formula (Kauffmann et al. 2008):

$$\left(\frac{M_{\rm H_2}^{850\mu{\rm m}}}{M_\odot}\right) = 0.12\left(e^{14.39\left(\frac{\lambda}{\rm mm}\right)^{-1}\left(\frac{T_{\rm dust}}{\rm K}\right)^{-1}} - 1\right) \times \left(\frac{\kappa_\nu}{\rm cm^2 g^{-1}}\right)^{-1}\left(\frac{S_\nu}{\rm Jy}\right)\left(\frac{D}{\rm kpc}\right)^2\left(\frac{\lambda}{\rm mm}\right)^3, \quad (9)$$

where λ is the observed wavelength in mm, $T_{\rm dust}$ is the dust temperature in K, S_ν is the integrated flux in Jy, and D is the distance to the source in kpc. For all fragments, we adopt the associated excitation temperature of ^{13}CO $J = 1 - 0$ as an approximated dust temperature (Liu et al. 2013). The surface density (Σ) can be derived from $\Sigma = M/(\pi R_{\rm eff}^2)$ in units of g cm^{-2}, and here $R_{\rm eff}$ is the effective radius of the fragment, and FWHM is the source size. These corresponding parameters are also listed in Tables 4 and 5.

4. Discussion

We have surveyed 64 PGCCs with CO and in the 850 μm continuum in the second quadrant of the Milky Way. The CO observations have low spatial resolution, and therefore trace relatively extended molecular clouds and clumps at larger scales, whilst the 850 μm-continuum observations have relatively high spatial resolution and are used to trace the dense cores at smaller scales, embedded within the molecular clouds. Investigating the fragments at different scales, and comparing their differences will help us to improve our understanding of the early stages of the star-formation process. By combining CO isotopologues (^{13}CO and C^{18}O), important physical parameters can be quantitatively estimated to characterize and increase our knowledge of the clump properties. 5 of the PGCCs, G108.85-00.80, G112.52+08.38, G120.67+02.66, G120.98+02.66, and G121.92-01.71, are distributed over larger regions than the scan map size (14′×14′) and further

observations over a larger region are needed for a complete analysis.

4.1. Error analysis of different beam sizes

The CO and 850 μm observations have beam sizes of around 52″ and 14″, respectively. To derive some parameters of 850 μm cores, such as velocity dispersion and temperature, we have to use the CO line data observations for estimation. However, there is no simple way of assigning CO emission to each 850 μm core when they form a tight cluster, for example, in G172.85+02.27. That is, the CO emission toward each one of these six 850 μm cores is contaminated by emission from nearby cores. If the 850 μm cores are not located in a tight cluster, it seems that we can use a reasonable filling factor, $f = (14/52)^2$, to estimate the excitation temperature assuming all integrated-intensity of ^{13}CO clump emits from the dense and isolated 850 μm core. However, the large 52″ beam means that the velocity gradients from, e.g., accretion along filaments, rotation, and even molecular outflows, will overestimate the velocity dispersion of each 850 μm core. Therefore, this will lead to high uncertainties for our estimation. The velocity dispersion, virial mass and virial parameter of the 850 μm cores will be overestimated, and the excitation temperature at the position of each 850 μm core will be underestimated.

4.2. Infrared emission

The extended 12 μm emission originates mainly from polycyclic aromatic hydrocarbons (Watson et al. 2008), which are excited by UV radiation at the interface between the expanding H II region and the ambient interstellar medium (Zhang et al. 2016a). The extended 22 μm emission is mostly produced by relatively hot dust (Anderson et al. 2012; Faimali et al. 2012), and is a good tracer of early star formation activity.

Figures 4 and 5 compare infrared emission of WISE 12 and 22 μm with the ^{13}CO emission contours. The morphological distribution of the ^{13}CO emission is correlated or uncorrelated with the 12 and 22 μm emission, which correspond to infrared-bright and infrared-dark PGCCs, respectively. We find that $\sim$30% of PGCCs are infrared bright after visually inspecting the image, whilst $\sim$70% sources are infrared dark. We also note that $\sim$15% of the infrared dark PGCCs have more than one infrared bright core, which are also correlated with a peak in the ^{13}CO emission. Positionally matching the AllWISE Catalog (Cutri et al. 2013, 2014) with the extracted 850 μm sources (see Table 5), we find that 74 of the 117 850μm cores have corresponding WISE infrared point sources. Those with or without infrared point sources may be protostellar or infrared quiet/starless cores, respectively (Yuan et al. 2017). This suggests that the infrared dark PGCCs with infrared bright cores are more evolved, but are younger than the infrared bright PGCCs.

We find no infrared dust bubbles (Churchwell et al. 2006, 2007), which would show strong 22 μm emission surrounded by a ringlike 12 μm emission shell. The 12 and 22 μm emission have no significant morphological differences. Compact H II regions or bright infrared cores may have an effect on the evolution of early star formation (Zhang et al. 2017b). The integrated-intensity maps of some PGCCs show steep gradients, e.g. G098.50-03.24, G127.88+02.66, G151.08+04.46 (see Fig. 2). This suggests that the molecular clouds have been compressed by nearby warm clouds, such as G035.39-00.33 (Liu et al. 2018b), possibly indicating cloud-cloud collisions, such as in the case of G178.28-00.61 (Zhang et al., in prep.).

4.3. Fragmentation

In Fig. 3, we present the ^{13}CO and C^{18}O line spectra extracted from the identified 468 ^{13}CO clumps in our sample of 64 PGCCs. They typically have sizes of $\sim$0.2 – 2 pc. This shows that each of the PGCCs fragments into an average of $\sim$7.3 ^{13}CO clumps. The G144.84+00.76 PGCC fragments into 14 clumps. We suggest that the fragmentation is ubiquitous and a necessary process of the early stage of star formation. Analysis shows that most of the clumps are associated with CO structures. Only 68 sources of the ^{13}CO clumps were not detected with C^{18}O lines, suggesting that most of the clumps are relatively dense.

Figure 7 shows examples of 850 μm emission maps with extracted cores overlaid. In total, 117 cores are extracted at 850 μm. Less than half (28) of the 64 PGCCs have been detected with 850 μm continuum, indicating that each PGCC fragments into 4.2 cores on average with an effective radius

of 0.03 – 0.48 pc. We suggest that the number of the fragments is strongly associated with the fragment size, and the results might also be dependent on the sensitivity (Pokhrel et al. 2018).

4.4. Mass-size relation

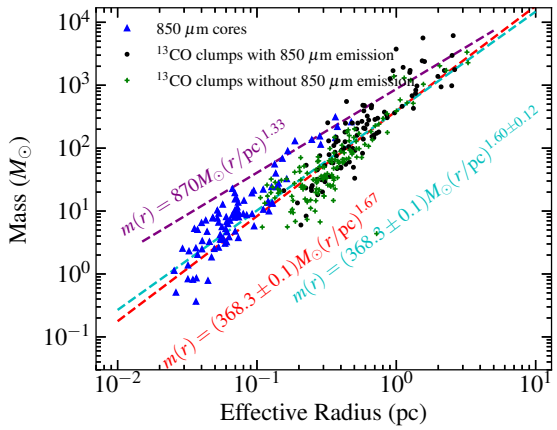

Fig. 9.— *Mass-Radius* distributions of Gaussian 850 μm cores (*blue triangles*), ^{13}CO clumps with (*black dots*) and without (*green crosses*) 850 μm emission. Their masses and effective radii are listed in Tables 3 and 5, respectively. The purple line delineates the threshold introduced by Kauffmann & Pillai (2010), separating the regimes into high-mass and low-mass star forming candidates. The red line shows a power-law fit using least-squares fitting in log-space with a fixed exponent 1.67 to the mass-size relation for clumps that undergo quasi-isolated gravitational collapse in a turbulent medium (Li 2017; Zhang & Li 2017). The cyan line presents a power-law fit of all the data point using least-squares fitting. The corresponding formulas are also shown nearby the lines.

Li (2017) derived a scaling relation of $m \sim r^{5/3}$ to describe the properties of the gravitationally bound structures, where the multiplication factor of the relationship is determined by the level of ambient turbulence. A higher level of turbulence leads to a higher mass at a given scale. It has been found that the scaling provides a good description to the fragments observed from sub-pc scales to those of a few pc (Zhang et al. 2017a). In Fig. 9, the red dashed line shows the mass-size relation derived assuming $m \sim r^{5/3}$ from Li (2017) and Zhang et al. (2017a). Figure 9 also displays the mass-size relation derived from a linear fit to the data. In general, the results obtained from these fits are very similar. This clearly demonstrates that these clumps do not obey "Larson's third law", where the power-law exponent is ~ 1.9 (Larson 1981; Solomon et al. 1987), but is consistent with the prediction made in Li (2017).

Having established the relation, it is possible to use the properties of the observed clumps to estimate the turbulence in the ambient medium. In our sample, we found that our structures satisfy the relationship, $m(r) = (368.3\pm0.1)M_{\odot}(r/\mathrm{pc})^{1.67}$ (see Figure 9). The multiplication factor is small compared to that found in high-mass star-forming regions by Urquhart et al. (2014), who had a relationship of $m(r) = 2630M_{\odot}(r/\mathrm{pc})^{1.67}$, and Zhang et al. (2017a), $m(r) = 7079M_{\odot}(r/\mathrm{pc})^{1.67}$. The sample in Zhang et al. (2017a) are more massive and denser than those in Urquhart et al. (2014). At a given scale, the masses of gas condensation in our PGCC sample are around 1/10 of that of typical Galactic high-mass star-forming regions (Urquhart et al. 2014). Using the scaling relation presented in Li (2017), this implies that the energy dissipation rate of the ambient turbulence should be 1/30 of that of the Galactic massive star-forming regions, where we expect the observed velocity dispersion of the molecular gas in our PGCC sample to be 1/3 times of the averaged Galactic value on a given scale[8]. In general, the level of turbulence in PGCC sample is significantly lower than the Galactic average. This is consistent with our previous findings in Zhang et al. (2016b).

4.5. Low-mass star formation

In Fig. 9, we present the mass-size plane for the extracted ^{13}CO clumps and 850 μm cores. Comparison with the high-mass star formation threshold of $m(r) > 870M_{\odot}(r/\mathrm{pc})^{1.33}$ empirically proposed by Kauffmann & Pillai (2010) allows us to determine whether these fragments are capable of giving birth to massive stars. The data points are

[8] These numbers are obtained using the scaling relations presented in Li (2017), where the mass-size relation is determined by $m \approx \epsilon_{\mathrm{cascade}}^{2/3}\eta^{-2/3}G^{-1}r^{5/3}$ (where m is the critical mass, r is the source size, and $\epsilon_{\mathrm{cascade}} \approx \eta\sigma_{\mathrm{v}}^3/l$ is the turbulence energy dissipation rate of the ambient medium).

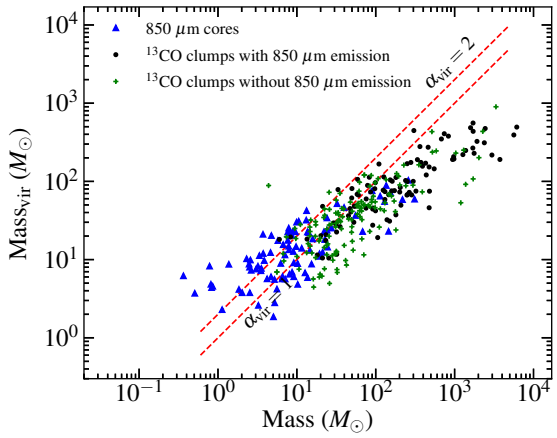

Fig. 10.— *Mass*$_{\rm vir}$-*Mass* distributions of Gaussian 850 μm cores (*blue triangles*), ^{13}CO clumps with (*black dots*) and without (*green crosses*) 850 μm emission. The parameters are listed in Tables 3 and 5. Two dashed lines delineate the thresholds of $\alpha_{\rm vir} = 1$ and $\alpha_{\rm vir} = 2$.

mostly distributed below the threshold, given by the purple dashed line. Therefore, it appears that the majority of ^{13}CO clumps and 850 μm cores are low-mass star-forming region candidates.

In Fig. 10, we present virial mass vs. fragment mass distributions for the ^{13}CO clumps and 850 μm cores. Two dashed lines show the thresholds with virial parameters $\alpha_{\rm vir} = 1$ and $\alpha_{\rm vir} = 2$. We find that $\sim$26% of ^{13}CO clumps have $\alpha_{\rm vir} > 1$, and $\sim$5% have $\alpha_{\rm vir} > 2$, whilst $\sim$71% of the 850 μm cores have $\alpha_{\rm vir} > 1$, with $\sim$37% having $\alpha_{\rm vir} > 2$. This indicates that most of the 850 μm cores are gravitationally unbound and are either stable or expanding (Hindson et al. 2013), relatively to the ^{13}CO clumps. It is also likely that kinetic energy is larger than the gravitational energy, suggesting that such cores have to be confined by some external pressure (Bertoldi & McKee 1992; Pattle et al. 2015). Therefore, a long timescale for star formation is required for most of our local PGCCs, or they will never form stars.

Mass surface density, Σ, is a commonly used parameter to assess the high-mass star formation potential. Urquhart et al. (2014) suggested that the surface density of 0.05 g cm^{-2} might represent a minimum threshold of efficient massive star formation, as is suitable for pc-scale clumps. According to this threshold, parts of the ^{13}CO clumps are potential candidates of massive star formation. However, we note that most of the candidates have a typical size less than 1.0 pc. Traficante et al. (2018) argued that $\Sigma = 0.12$ g cm^{-2} may represent the minimum surface density at clump scales for high-mass star formation to occur, based on the analysis of dynamic activity associated with their parent clump. Krumholz & McKee (2008) suggest that a minimum mass surface density of 1 g cm^{-2} is required to prevent fragmentation into low-mass cores through radiative feedback, thus allowing high-mass star formation. For the ^{13}CO clumps and 850 μm cores in this work, we find that the mean values of surface densities are 0.13 and 0.39 g cm^{-2}, respectively (see Figure 12). Therefore, the surface densities further prove that some of ^{13}CO clumps and 850 μm cores have potential to form high-mass stars but the majority would form low-mass stars.

4.6. Core mass function

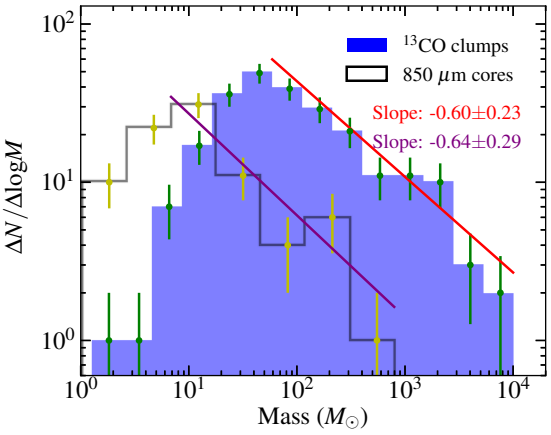

Fig. 11.— Mass distribution for ^{13}CO clumps (*blue*) and 850 μm cores (*black*). The parameters are listed in Tables 3 and 5. The slopes of the fitted power law index are shown in the histogram. The error bars represent the standard deviation of a Poisson distribution $\sqrt{\Delta N/\Delta \log M}$.

The core mass function (CMF) generally has a comparable slope with the stellar initial mass function and, consequently, the Salpeter power-law with a logarithmic slope of -1.35 (Zinnecker & Yorke

2007; Salpeter 1955). Previous observations show that massive stars usually form in dense clusters, so competitive accretion of protostars from their common gas reservoir was used to explain the observed Salpeter stellar mass distribution for massive stars (Bonnell et al. 2001; Klessen & Burkert 2001). To investigate the intermediate- and high-mass star formation, in Fig. 11, we simply fit the mass spectra in the mass ranges between 400 and 8000 $M_\odot$ for ^{13}CO clumps and between 7 and 800 $M_\odot$ for 850 μm cores with a linear least square method using the obtained clump and core masses in our observations, respectively. The lower mass limit used to define the power law tail is derived from the peak positions (at $\sim$400 $M_\odot$ for the clumps, and $\sim$7 $M_\odot$ for the cores) from low-mass to high-mass end of the mass spectra distributions in Figure 11. The derived two slopes of the mass spectrum are similar to each other with clump scope $k_{\rm clump} = -0.60 \pm 0.23$ and core slope $k_{\rm core} = -0.64 \pm 0.29$, which are much flatter than the Salpeter stellar initial mass function and the CMFs of massive star-forming candidates (e.g., Beuther & Schilke 2004; Bontemps et al. 2010; Ohashi et al. 2016; Csengeri et al. 2017b). For low-mass star-forming objects, Marsh et al. (2016) obtained a slope of -0.55 ± 0.07 in the Taurus L1495 cloud, Elia et al. (2013) derived a slope of -0.7 ± 0.3 for the gas clump distribution in the third Galaxy quadrant, and Kim et al. (2004) also derived a shallower mass function slope of -0.59 ± 0.32 for their clump sample named CMa OB1 and G220.8-1.7. The three cases above are consistent with our results. The similar slopes may be resulted from their similar initial conditions. We also have to note that the sample distribution at different distances and the contamination from large scale structure may lead to uncertain slopes (Moore et al. 2007; Reid et al. 2010).

4.7. Core formation efficiency

The core formation efficiency (CFE) describes the fraction of clump mass that has converted into denser cores (Elia et al. 2013; Veneziani et al. 2017). Hence the CFE is defined as:

$$\mathrm{CFE} = \frac{M_{\rm core}}{M_{\rm core} + M_{\rm clump}}, \qquad (10)$$

where $M_{\rm core}$ is the mass of 850 μm cores, and $M_{\rm clump}$ is mass of the ^{13}CO clump that hosts those associated 850 μm cores. Considering that $M_{\rm clump}$ is estimated from the extracted Gaussian clumps, the diffuse gas component of the cloud will be missing. Additionally, the clump masses are estimated by ^{13}CO which will be depleted in low temperatures ($<$ 18 K) (Pillai et al. 2007, 2011), hence, $M_{\rm clump}$ will be underestimated. The cores in our sample are considered to be gravitationally bound objects. Using the core and clump masses of the entire sample to estimate the CFE, we get a CFE of 3.0%[9]. Of all 64 PGCCs, only 28 (43.8%) are detected at 850 μm with emission above 5σ, indicating a low CFE. Our estimated CFE is much lower than those estimated from the conversion of molecular clouds to clumps across the first quadrant (5 – 8%; Eden et al. 2012, 2013); the first and second quadrants (5 – 23%; Battisti & Heyer 2014); the fourth quadrant (8 – 39%; Veneziani et al. 2017), and the Galactic Centre (10 – 13%; Csengeri et al. 2016).

4.8. Statistics

4.8.1. ^{13}CO clumps and 850 μm cores

Figure 12 presents histograms of the velocity dispersions, optical depths, excitation temperatures, surface densities, and virial parameters for the ^{13}CO clumps and the 850 μm cores.

The velocity dispersion ($\sigma_{\rm v}$) histogram in Fig. 12 shows that the median value is $0.40 \pm 0.15\,{\rm km\,s^{-1}}$ for ^{13}CO clumps, smaller than that ($0.57 \pm 0.19\,{\rm km\,s^{-1}}$) of 850 μm cores, indicating that the 850 μm cores are more dynamically active at a small scale, and being consistent with the fact that 850 μm cores are mainly located at the peak positions of ^{13}CO clumps (see Fig. 6), or that some cores with IR emission are forming stars. It seems that the 850 μm cores are generally more turbulent than ^{13}CO clumps. Another possibility is that there is active star formation injecting turbulence in the 850 μm cores.

From the optical depth ($\tau_{^{13}\rm CO}$) distribution in Fig. 12, we find that the median values are 0.89 ± 0.65 for the ^{13}CO clumps and 1.75 ± 0.46 for the 850 μm cores. Most of the ^{13}CO clumps have optical depths < 1.0. This indicates that most of

[9] Here we consider all the extracted clumps and cores.

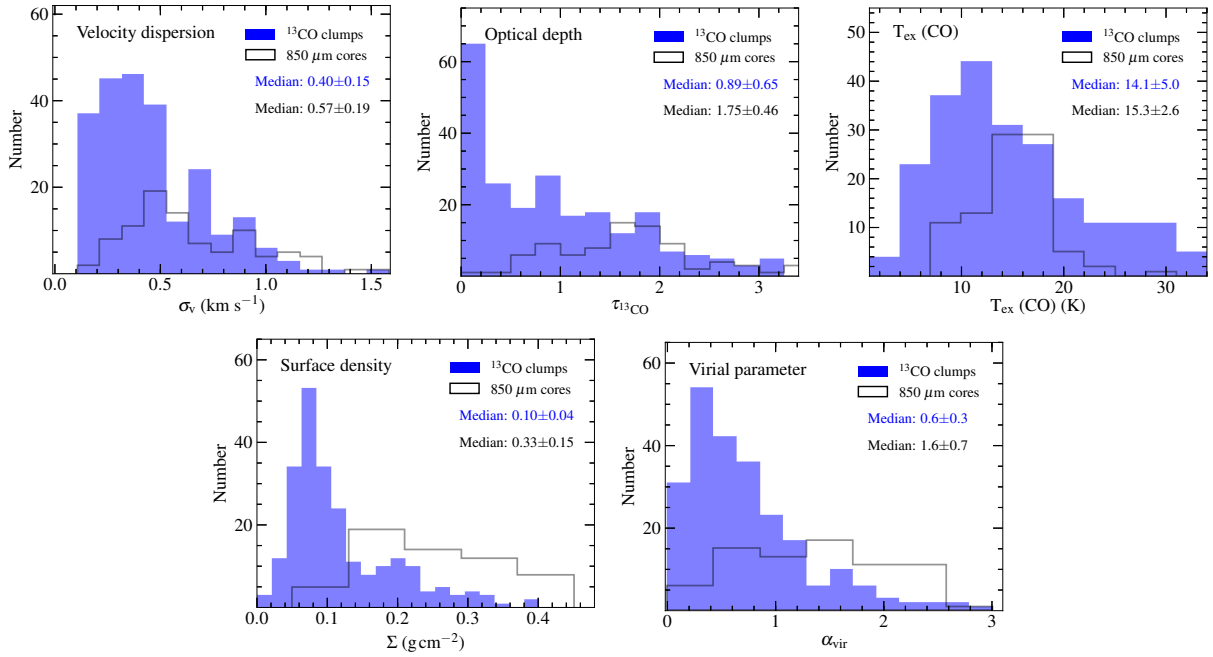

Fig. 12.— Histograms of velocity dispersion, optical depth, excitation temperature, surface density, and virial parameter for ^{13}CO clumps (*blue*) and 850 μm cores (*black*). The parameters are listed in Tables 2, 3, 4, and 5. The corresponding median value is presented in each frame. The uncertainty on each median calculated represents median absolute deviation.

the ^{13}CO clumps are more optically thin than the 850 μm cores.

The excitation temperature (T_{ex}) histogram in Fig. 12 shows that the median value is 14.1 ± 5.0 K for ^{13}CO clumps, and it is 15.3 ± 2.6 K for 850 μm cores. Considering the 850 μm cores are smaller than the ^{13}CO beam, the filling factors should be $f < 1$. However, we adopt $f = 1$ to estimate excitation temperature, which will lead to underestimate the excitation temperature for 850 μm cores (see also error analysis in Section 4.1). It suggests that the internal parts of the clumps have higher temperatures than the outer parts, probably indicating an internal heating mechanism.

The surface density (Σ) histogram in Fig. 12 shows that the median value is 0.10 ± 0.04 g cm^{-2} for the ^{13}CO clumps, while it is 0.33 ± 0.15 g cm^{-2} for the 850 μm cores. The median value of surface densities of 850 μm cores is much larger than that of ^{13}CO clumps, indicating that some 850 μm cores that are gravitationally bound are denser and represent the precise locations where the stars would form inside the clumps.

The virial parameter (α_{vir}) histogram in Fig. 12 shows that the median value is 0.6 ± 0.3 for the ^{13}CO clumps, while it is 1.6 ± 0.7 for the 850 μm cores. The virial parameters above 2.0 may indicate that the fragments have difficulty in forming stars (Kauffmann et al. 2008), without the help of external pressure. Based on the virial parameters in this work, most of the ^{13}CO clumps are candidates to form dense cores. Further checking their embedded cores at 850 μm, the median value of their virial parameters is around 1.6. Therefore, our cores are mostly gravitationally unbound, and may be dispersing at the core scale, or estimates based on ^{13}CO overestimate the in-core turbulence. We also note that 76 out of 117 cores at 850 μm have WISE counterparts (see Section 4.2). It is likely that many cores have already formed stars and may be in the process of expansion.

4.8.2. PGCCs with and without 850 μm emission

Figure 13 presents histograms of the velocity dispersions, optical depths, excitation tempera-

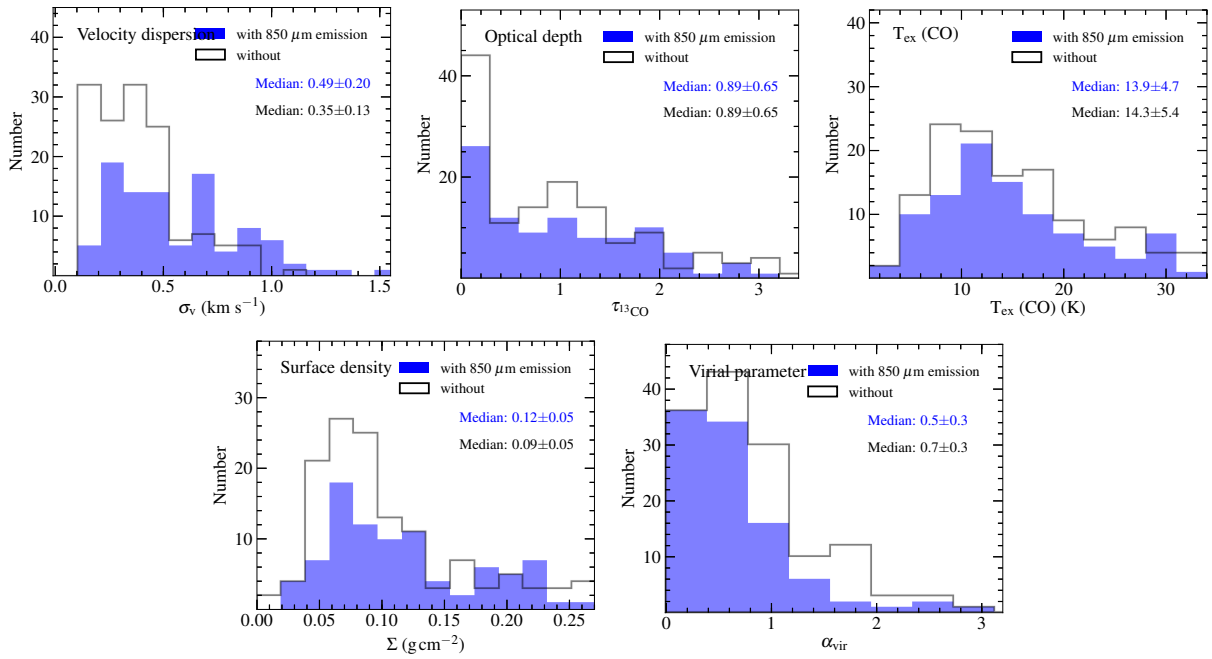

Fig. 13.— Histograms of velocity dispersion, optical depth, excitation temperature, surface density, and virial parameter for the ^{13}CO clumps in the 64 PGCCs with (*blue*) and without (*black*) 850 μm extracted emission. The parameters are listed in Tables 2, 3, 4, and 5. The corresponding median value is presented in each sub-histogram. The uncertainty on each median calculated represents median absolute deviation.

tures, surface densities, and virial parameters for the detected ^{13}CO clumps associated with and without 850 μm emission.

The velocity dispersion ($\sigma_{\rm v}$) histogram in Fig. 13 shows that for PGCCs with and without 850 μm emission the median values are 0.49 ± 0.20 and $0.35 \pm 0.13\,{\rm km\,s^{-1}}$, respectively. This indicates that the PGCCs with 850 μm emission are more dynamically active and turbulent than those without 850 μm emission.

The optical depth ($\tau_{^{13}{\rm CO}}$) histogram (using ^{13}CO as the tracer) in Fig. 13 shows that the median values are the same (0.89 ± 0.65), for PGCCs with and without 850 μm emission.

The excitation temperature ($T_{\rm ex}$) histogram in Fig. 13 shows that for PGCCs with and without 850 μm emission, the median values are 13.9 ± 4.7 and 14.3 ± 5.4 K, respectively. Therefore, the two groups are practically are at the same temperature.

The surface density (Σ) histogram in Fig. 13 shows that for PGCCs with and without 850 μm emission, the median values are 0.12 ± 0.05 and $0.09 \pm 0.05\,{\rm g\,cm^{-2}}$. This indicates that the densities are similar for the both.

The virial parameter ($\alpha_{\rm vir}$) histogram in Fig. 13 shows that for PGCCs with and without 850 μm emission the median values are 0.5 ± 0.3 and 0.7 ± 0.3, respectively. Based on the virial parameters in this work, the PGCCs with 850 μm emission probably have a slightly greater potential to form stars than those without 850 μm emission.

4.8.3. Comparison with other studies

Other studies such as those of IRDCs (e.g. Zhang et al. 2017a) found that the linewidth of the C^{18}O $J = 1 - 0$ line ranges from around 2.0 to 6.0 km s^{-1} and the volume density from 870 μm continuum measurements is greater than $5.0 \times 10^4\,{\rm cm^{-3}}$, and most cores have virial parameters $\alpha_{\rm vir} < 1.0$. Most ATLASGAL clumps and cores (e.g., Csengeri et al. 2014, 2017a; Wienen et al. 2015, 2018; König et al. 2017; Urquhart et al. 2018) are also dynamically active, dense, and

gravitationally bound, and are high-mass star formation candidates. In this work, however, we find that the 64 PGCCs are dynamically quiescent, optically thin, non-dense, and gravitationally unbound, the typical values of which are $\sigma_{\rm v} < 1.5\,{\rm km\,s^{-1}}$, $\tau_{^{13}{\rm CO}} < 1.0$, $\Sigma < 0.3\,{\rm cm^{-2}}$, and $\alpha_{\rm vir} \gtrsim 1.0$. Wu et al. (2012), Liu et al. (2013), and Meng et al. (2013) detected relatively low column densities, velocity dispersions, and high virial parameters ($\alpha_{\rm vir} > 1.0$) towards other PGCCs with star formation activities. The consistent results further confirm that the PGCCs are mostly quiescent and lack star forming activities, or are most likely at the very initial evolutionary stages of star formation.

5. Summary

To make progress in understanding the early evolution of molecular clouds and dense cores in a wide range of Galactic environments, we carry out an investigation of 64 PGCCs in the second quadrant of the Milky Way, using ^{13}CO, C^{18}O, and 850 μm observations. Through the survey, we study their fragmentation and evolution associated with star formation, and show statistical analysis of the extracted ^{13}CO clumps and 850 μm cores.

We present the maps of all ^{13}CO, C^{18}O, and 850 μm observations. Using the *Gaussclumps* procedure in GILDAS, we extracted 468 clumps from the ^{13}CO integrated line intensity maps and 117 cores from the 850 μm continuum images. We present all the observational spectra and the derived integrated-intensity maps of ^{13}CO and C^{18}O, compute and list the physical parameters of the lines and the extracted fragments.

Using the Bayesian Distance Calculator (Reid et al. 2016), we derived the distances of all 64 PGCCs in our samples, which are distributed between 0.42 and 5.0 kpc in the second quadrant of the Milky Way. We find that 60 PGCCs are located in the Local and Perseus arms or the associated interarm region, with 4 PGCCs in the Outer arm.

Fragmentation analysis show that each PGCC fragments into 7.3 clumps on average in ^{13}CO emission with sizes of around 0.1 – 3.2 pc, and each PGCC detected at 850 μm fragments into 4.2 cores at 850 μm with effective radii of 0.03 – 0.48 pc. We suggest that the fragmentation number may be associated with the fragment size, and the relationship between fragmentation number and the fragment size may reflect the nature of clump and core formation efficiency.

We further studied the the properties of the fragments in mass-size plane. We found that in general, the structure follows a relation that is close to $m \sim r^{1.67}$, which is much shallower than what is predicted by Larson (1981), but is consistent if these objects undergo quasi-isolated gravitational collapse in a turbulent medium (Li 2017; Zhang et al. 2017a). At a given scale, the masses of our PGCCs are around 1/10 of that of the typical Galactic massive star-forming regions. This reflects the uniqueness of the PGCC sample: according to (Li 2017), the normalization of mass-size relation is determined by the energy dissipation rate of the ambient turbulence. In our sample the mass-size relation can be explained if the turbulence observed in these clumps is 1/3 times (measured in velocity dispersion) the averaged Galactic value.

Statistics indicate that the 850 μm cores are more turbulent, more optically thick, and denser than the ^{13}CO clumps, suggesting that most 850 μm cores are better star-forming candidates than the ^{13}CO clumps. The excitation temperature histogram may suggest that the inner parts of the clumps have higher temperatures than the outer parts, probably indicating an internal heating mechanism. The PGCCs with 850 μm emission are more dynamically active, and have more potential to form stars than those without 850 μm emission.

Analysis of the clump and core masses, virial parameter, surface density, and mass-size relation suggests that the PGCCs in the second quadrant of the Milky Way have a low core formation efficiency of ∼3.0%, and most are candidates of low-mass star formation. Comparison with previous studies suggests that the PGCCs are mostly quiescent and lack star forming activities, or are most likely at the very initial evolutionary stages of star formation. As evident from the physical parameters, it seems clear that the clumps/cores in this PGCC sample are not able to form high-mass stars.

We firstly thank the anonymous referee for prompting many clarifications of this paper. This

work is supported by the National Key Basic Research Program of China (973 Program) 2015CB857100, and the National Natural Science Foundation of China through grants 11703040, 11503035 and 11573036. C.-P. Zhang acknowledges support by the China Scholarship Council in Germany as a postdoctoral researcher (No. 201704910137). Tie Liu is supported by EACOA fellowship. C.W. L. was supported by Basic Science Research Program though the National Research Foundation of Korea (NRF) funded by the Ministry of Education, Science, and Technology (NRF-2016R1A2B4012593). M.J. acknowledges the support of the Academy of Finland Grant No. 285769. G.-X. Li is supported by the DFG Cluster of Excellence "Origin and Structure of the Universe". K.W. is supported by grant WA3628-1/1 of the German Research Foundation (DFG) through the priority program 1573 ("Physics of the Interstellar Medium"). L.V. Toth acknowledges the support of the OTKA grant NN-111016. We are grateful to the staff at the Qinghai Station of PMO for their assistance during the observations. This publication makes use of data products from the Wide-field Infrared Survey Explorer, which is a joint project of the University of California, Los Angeles, and the Jet Propulsion Laboratory/California Institute of Technology, funded by the National Aeronautics and Space Administration. The JCMT is operated by the East Asian Observatory on behalf of The National Astronomical Observatory of Japan, Academia Sinica Institute of Astronomy and Astrophysics, the Korea Astronomy and Space Science Institute, the National Astronomical Observatories of China and the Chinese Academy of Sciences (Grant No. XDB09000000), with additional funding support from the Science and Technology Facilities Council of the United Kingdom and participating universities in the United Kingdom and Canada. The SCUBA-2 data mainly taken in this paper were observed under project code M16AL002.

Facilities: PMO, JCMT, WISE.

REFERENCES

Anderson, L. D., Zavagno, A., Deharveng, L., et al. 2012, A&A, 542, A10

Battisti, A. J. & Heyer, M. H. 2014, ApJ, 780, 173

Belloche, A., Schuller, F., Parise, B., et al. 2011, A&A, 527, A145

Bergin, E. A. & Tafalla, M. 2007, ARA&A, 45, 339

Bertoldi, F. & McKee, C. F. 1992, ApJ, 395, 140

Beuther, H. & Schilke, P. 2004, Science, 303, 1167

Bintley, D., Holland, W. S., MacIntosh, M. J., et al. 2014, in Proc. SPIE, Vol. 9153, Millimeter, Submillimeter, and Far-Infrared Detectors and Instrumentation for Astronomy VII, 915303

Bonnell, I. A., Bate, M. R., Clarke, C. J., & Pringle, J. E. 2001, MNRAS, 323, 785

Bontemps, S., Motte, F., Csengeri, T., & Schneider, N. 2010, A&A, 524, A18

Bourke, T. L., Garay, G., Lehtinen, K. K., et al. 1997, ApJ, 476, 781

Buckle, J. V., Drabek-Maunder, E., Greaves, J., et al. 2015, MNRAS, 449, 2472

Chapin, E. L., Berry, D. S., Gibb, A. G., et al. 2013, MNRAS, 430, 2545

Churchwell, E., Povich, M. S., Allen, D., et al. 2006, ApJ, 649, 759

Churchwell, E., Watson, D. F., Povich, M. S., et al. 2007, ApJ, 670, 428

Csengeri, T., Bontemps, S., Wyrowski, F., et al. 2017a, A&A, 601, A60

Csengeri, T., Bontemps, S., Wyrowski, F., et al. 2017b, A&A, 600, L10

Csengeri, T., Urquhart, J. S., Schuller, F., et al. 2014, A&A, 565, A75

Csengeri, T., Weiss, A., Wyrowski, F., et al. 2016, A&A, 585, A104

Cutri, R. M., Wright, E. L., Conrow, T., et al. 2013, VizieR Online Data Catalog, 2328

Cutri, R. M., Wright, E. L., Conrow, T., et al. 2014, VizieR Online Data Catalog, 2328

Dame, T. M., Hartmann, D., & Thaddeus, P. 2001, ApJ, 547, 792

Dame, T. M., Ungerechts, H., Cohen, R. S., et al. 1987, ApJ, 322, 706

Dempsey, J. T., Friberg, P., Jenness, T., et al. 2013, MNRAS, 430, 2534

Drabek, E., Hatchell, J., Friberg, P., et al. 2012, MNRAS, 426, 23

Eden, D. J., Moore, T. J. T., Morgan, L. K., Thompson, M. A., & Urquhart, J. S. 2013, MNRAS, 431, 1587

Eden, D. J., Moore, T. J. T., Plume, R., & Morgan, L. K. 2012, MNRAS, 422, 3178

Elia, D., Molinari, S., Fukui, Y., et al. 2013, ApJ, 772, 45

Evans, II, N. J. 1999, ARA&A, 37, 311

Faimali, A., Thompson, M. A., Hindson, L., et al. 2012, MNRAS, 426, 402

Frerking, M. A., Langer, W. D., & Wilson, R. W. 1982, ApJ, 262, 590

Gómez, L., Wyrowski, F., Schuller, F., Menten, K. M., & Ballesteros-Paredes, J. 2014, A&A, 561, A148

Heyer, M. H. & Terebey, S. 1998, ApJ, 502, 265

Hindson, L., Thompson, M. A., Urquhart, J. S., et al. 2013, MNRAS, 435, 2003

Holland, W. S., Bintley, D., Chapin, E. L., et al. 2013, MNRAS, 430, 2513

Johnstone, D., Boonman, A. M. S., & van Dishoeck, E. F. 2003, A&A, 412, 157

Johnstone, D., Di Francesco, J., & Kirk, H. 2004, ApJ, 611, L45

Juvela, M., He, J., Pattle, K., et al. 2017, ArXiv e-prints: 1711.09425

Juvela, M., Ristorcelli, I., Montier, L. A., et al. 2010, A&A, 518, L93

Kauffmann, J., Bertoldi, F., Bourke, T. L., Evans, II, N. J., & Lee, C. W. 2008, A&A, 487, 993

Kauffmann, J. & Pillai, T. 2010, ApJ, 723, L7

Kim, B. G., Kawamura, A., Yonekura, Y., & Fukui, Y. 2004, PASJ, 56, 313

Kim, J., Lee, J.-E., Liu, T., et al. 2017, ApJS, 231, 9

Klessen, R. S. & Burkert, A. 2001, ApJ, 549, 386

König, C., Urquhart, J. S., Csengeri, T., et al. 2017, A&A, 599, A139

Könyves, V., André, P., Men'shchikov, A., et al. 2015, A&A, 584, A91

Kramer, C., Stutzki, J., Rohrig, R., & Corneliussen, U. 1998, A&A, 329, 249

Krumholz, M. R. & McKee, C. F. 2008, Nature, 451, 1082

Lane, J., Kirk, H., Johnstone, D., et al. 2016, ApJ, 833, 44

Larson, R. B. 1981, MNRAS, 194, 809

Li, G.-X. 2017, MNRAS, 465, 667

Liu, T., Kim, K.-T., Juvela, M., et al. 2018a, ApJS, 234, 28

Liu, T., Li, P. S., Juvela, M., et al. 2018b, ArXiv e-prints: 1803.09457

Liu, T., Wu, Y., Mardones, D., et al. 2015, Publication of Korean Astronomical Society, 30, 79

Liu, T., Wu, Y., & Zhang, H. 2012, ApJS, 202, 4

Liu, T., Wu, Y., & Zhang, H. 2013, ApJ, 775, L2

Liu, T., Zhang, Q., Kim, K.-T., et al. 2016, ApJS, 222, 7

MacLaren, I., Richardson, K. M., & Wolfendale, A. W. 1988, ApJ, 333, 821

Marsh, K. A., Kirk, J. M., André, P., et al. 2016, MNRAS, 459, 342

Meng, F., Wu, Y., & Liu, T. 2013, ApJS, 209, 37

Moore, T. J. T., Bretherton, D. E., Fujiyoshi, T., et al. 2007, MNRAS, 379, 663

Moore, T. J. T., Plume, R., Thompson, M. A., et al. 2015, MNRAS, 453, 4264

Motte, F., Bontemps, S., & Louvet, F. 2017, ArXiv e-prints: 1706.00118

Myers, P. C., Linke, R. A., & Benson, P. J. 1983, ApJ, 264, 517

Nutter, D. & Ward-Thompson, D. 2007, MNRAS, 374, 1413

Ohashi, S., Sanhueza, P., Chen, H.-R. V., et al. 2016, ApJ, 833, 209

Ossenkopf, V. & Henning, T. 1994, A&A, 291, 943

Parsons, H., Dempsey, J. T., Thomas, H. S., et al. 2018, ApJS, 234, 22

Pattle, K., Ward-Thompson, D., Kirk, J. M., et al. 2015, MNRAS, 450, 1094

Pillai, T., Kauffmann, J., Wyrowski, F., et al. 2011, A&A, 530, A118

Pillai, T., Wyrowski, F., Hatchell, J., Gibb, A. G., & Thompson, M. A. 2007, A&A, 467, 207

Pineda, J. L., Goldsmith, P. F., Chapman, N., et al. 2010, ApJ, 721, 686

Pineda, J. L., Langer, W. D., Velusamy, T., & Goldsmith, P. F. 2013, A&A, 554, A103

Planck Collaboration, Ade, P. A. R., Aghanim, N., et al. 2011a, A&A, 536, A1

Planck Collaboration, Ade, P. A. R., Aghanim, N., et al. 2011b, A&A, 536, A7

Planck Collaboration, Ade, P. A. R., Aghanim, N., et al. 2011c, A&A, 536, A22

Planck Collaboration, Ade, P. A. R., Aghanim, N., et al. 2011d, A&A, 536, A23

Planck Collaboration, Ade, P. A. R., Aghanim, N., et al. 2016, A&A, 594, A28

Pokhrel, R., Myers, P. C., Dunham, M. M., et al. 2018, ApJ, 853, 5

Rathborne, J. M., Jackson, J. M., & Simon, R. 2006, ApJ, 641, 389

Reid, M. A., Wadsley, J., Petitclerc, N., & Sills, A. 2010, ApJ, 719, 561

Reid, M. J., Dame, T. M., Menten, K. M., & Brunthaler, A. 2016, ApJ, 823, 77

Rumble, D., Hatchell, J., Gutermuth, R. A., et al. 2015, MNRAS, 448, 1551

Salpeter, E. E. 1955, ApJ, 121, 161

Sofue, Y. 2011, PASJ, 63, 813

Solomon, P. M., Rivolo, A. R., Barrett, J., & Yahil, A. 1987, ApJ, 319, 730

Stutzki, J. & Guesten, R. 1990, ApJ, 356, 513

Tang, M., Liu, T., Qin, S.-L., et al. 2018, ApJ, 856, 141

Tatematsu, K., Liu, T., Ohashi, S., et al. 2017, ApJS, 228, 12

Traficante, A., Fuller, G. A., Smith, R. J., et al. 2018, MNRAS, 473, 4975

Urquhart, J. S., König, C., Giannetti, A., et al. 2018, MNRAS, 473, 1059

Urquhart, J. S., Moore, T. J. T., Csengeri, T., et al. 2014, MNRAS, 443, 1555

Veneziani, M., Schisano, E., Elia, D., et al. 2017, A&A, 599, A7

Wang, K., Zhang, Q., Testi, L., et al. 2014, MNRAS, 439, 3275

Wang, K., Zhang, Q., Wu, Y., & Zhang, H. 2011, ApJ, 735, 64

Watson, C., Povich, M. S., Churchwell, E. B., et al. 2008, ApJ, 681, 1341

Wienen, M., Wyrowski, F., Menten, K. M., et al. 2015, A&A, 579, A91

Wienen, M., Wyrowski, F., Menten, K. M., et al. 2018, A&A, 609, A125

Wilson, T. L. & Rood, R. 1994, ARA&A, 32, 191

Wong, T., Ladd, E. F., Brisbin, D., et al. 2008, MNRAS, 386, 1069

Wright, E. L., Eisenhardt, P. R. M., Mainzer, A. K., et al. 2010, AJ, 140, 1868

Wu, Y., Liu, T., Meng, F., et al. 2012, ApJ, 756, 76

Yuan, J., Wu, Y., Ellingsen, S. P., et al. 2017, ApJS, 231, 11

Yuan, J., Wu, Y., Liu, T., et al. 2016, ApJ, 820, 37

Zhang, C.-P. & Li, G.-X. 2017, MNRAS, 469, 2286

Zhang, C.-P., Li, G.-X., Wyrowski, F., et al. 2016a, A&A, 585, A117

Zhang, C. P. & Wang, J. J. 2012, A&A, 544, A11

Zhang, C.-P., Yuan, J.-H., Li, G.-X., Zhou, J.-J., & Wang, J.-J. 2017a, A&A, 598, A76

Zhang, C.-P., Yuan, J.-H., Xu, J.-L., et al. 2017b, Research in Astronomy and Astrophysics, 17, 057

Zhang, T., Wu, Y., Liu, T., & Meng, F. 2016b, ApJS, 224, 43

Zinnecker, H. & Yorke, H. W. 2007, ARA&A, 45, 481

This 2-column preprint was prepared with the AAS LaTeX macros v5.2.

TABLE 1
64 *Planck* COLD CLUMPS IN THE SECOND QUADRANT

Name	R.A.(J2000) hh:mm:ss	DEC.(J2000) dd:mm:ss	Distance kpc	Prob.[a]
G098.50-03.24	22:05:00.08	+51:33:11.69	1.59(0.25)	0.76
G108.85-00.80	22:58:51.53	+58:57:27.09	3.21(0.38)	0.56
G110.65+09.65	22:28:00.22	+69:01:48.10	0.82(0.11)	1.00
G112.52+08.38	22:52:47.62	+68:49:28.31	0.78(0.10)	1.00
G112.60+08.53	22:52:54.76	+68:59:53.90	0.78(0.10)	1.00
G115.92+09.46	23:24:04.62	+71:08:08.69	0.73(0.08)	1.00
G116.08-02.38	23:56:41.79	+59:45:13.19	0.72(0.09)	1.00
G116.12+08.98	23:28:14.03	+70:45:12.38	0.73(0.08)	1.00
G120.16+03.09	00:24:26.01	+65:49:27.59	1.28(0.65)	0.88
G120.67+02.66	00:29:41.95	+65:26:39.99	0.90(0.29)	0.97
G120.98+02.66	00:32:38.94	+65:28:07.08	0.92(0.04)	1.00
G121.35+03.39	00:35:48.66	+66:13:13.29	0.70(0.08)	1.00
G121.90-01.54	00:42:52.64	+61:18:23.20	0.59(0.20)	0.91
G121.92-01.71	00:43:06.34	+61:08:21.59	0.58(0.20)	0.91
G125.66-00.55	01:14:52.20	+62:11:16.60	0.61(0.16)	0.53
G126.49-01.30	01:21:14.55	+61:21:34.60	0.93(0.15)	0.57
G126.95-01.06	01:25:19.48	+61:32:36.19	0.60(0.17)	0.52
G127.22-02.25	01:26:10.18	+60:19:29.30	0.88(0.19)	1.00
G127.88+02.66	01:38:39.10	+65:05:06.49	0.89(0.11)	1.00
G128.95-00.18	01:43:15.17	+62:04:39.09	0.92(0.18)	0.59
G131.72+09.70	02:39:57.51	+70:42:11.60	0.57(0.16)	1.00
G132.07+08.80	02:39:18.17	+69:44:01.11	0.59(0.15)	1.00
G132.03+08.95	02:39:33.56	+69:53:21.08	0.59(0.15)	1.00
G133.28+08.81	02:51:42.22	+69:14:13.39	0.58(0.15)	1.00
G133.48+09.02	02:54:44.50	+69:19:57.59	0.61(0.14)	0.62
G136.31-01.77	02:36:07.02	+58:21:09.09	0.51(0.17)	1.00
G140.49+06.07	03:37:46.12	+63:07:27.29	1.23(0.49)	0.63
G140.77+05.00	03:34:18.18	+62:05:35.89	0.56(0.14)	0.74
G142.49+07.48	03:59:13.56	+62:58:52.40	0.55(0.14)	0.79
G142.62+07.29	03:59:00.66	+62:45:12.60	0.54(0.14)	1.00
G144.84+00.76	03:40:20.80	+56:16:28.09	2.20(0.28)	1.00
G146.11+07.80	04:23:14.52	+60:44:31.20	0.52(0.14)	1.00
G146.71+02.05	03:56:37.16	+56:07:23.10	0.47(0.15)	1.00
G147.01+03.39	04:04:41.36	+56:56:16.79	0.50(0.14)	1.00
G148.00+00.09	03:54:48.04	+53:47:19.89	2.15(0.28)	0.83
G148.24+00.41	03:57:26.18	+53:52:36.30	2.17(0.29)	0.77
G149.23+03.07	04:14:48.52	+55:12:03.29	0.47(0.15)	1.00
G149.41+03.37	04:17:09.06	+55:17:39.39	0.47(0.15)	1.00
G149.52-01.23	03:56:52.61	+51:48:01.70	0.51(0.14)	0.87
G149.58+03.45	04:18:23.93	+55:13:30.59	0.47(0.15)	1.00
G149.65+03.54	04:19:11.24	+55:14:44.39	0.47(0.15)	1.00
G150.22+03.91	04:23:51.69	+55:06:22.50	0.46(0.14)	1.00
G150.44+03.95	04:25:07.08	+54:58:32.39	0.46(0.14)	1.00
G151.08+04.46	04:30:42.87	+54:51:53.89	0.46(0.14)	1.00
G151.45+03.95	04:29:56.25	+54:14:51.70	0.46(0.14)	1.00
G154.90+04.61	04:48:27.03	+52:06:30.39	0.45(0.14)	1.00
G156.04+06.03	05:00:19.24	+52:06:45.60	0.42(0.13)	1.00
G156.20+05.26	04:57:00.65	+51:31:08.89	0.44(0.14)	1.00
G157.25-01.00	04:32:09.45	+46:37:25.00	0.46(0.14)	1.00
G159.52+03.26	04:59:55.05	+47:40:52.20	1.97(0.35)	0.82

TABLE 1—*Continued*

Name	R.A.(J2000) hh:mm:ss	DEC.(J2000) dd:mm:ss	Distance kpc	Prob.[a]
G162.79+01.34	05:02:42.87	+43:55:05.70	0.45(0.14)	0.83
G169.14-01.13	05:12:20.07	+37:20:57.09	1.87(0.23)	0.92
G171.03+02.66	05:33:35.43	+37:56:42.69	1.82(0.22)	0.81
G171.34+02.59	05:34:06.95	+37:38:47.30	1.78(0.20)	0.80
G172.85+02.27	05:36:51.80	+36:11:58.29	1.71(0.13)	0.77
G175.20+01.28	05:38:55.10	+33:41:05.89	1.69(0.12)	0.78
G175.53+01.34	05:39:59.24	+33:26:08.80	1.69(0.12)	0.75
G176.17-02.10	05:27:55.18	+31:01:34.99	4.96(0.44)	0.39
G176.35+01.92	05:44:23.17	+33:02:58.99	1.70(0.13)	0.63
G176.94+04.63	05:57:00.77	+33:55:16.30	1.78(0.22)	0.53
G177.09+02.85	05:50:02.12	+32:53:35.90	4.97(0.57)	0.49
G177.14-01.21	05:33:52.82	+30:42:36.29	5.00(0.48)	0.46
G177.86+01.04	05:44:35.76	+31:17:57.40	4.99(0.64)	0.53
G178.28-00.61	05:39:03.83	+30:04:05.90	0.96(0.02)	0.36

[a]The distance probabilities derived by the Bayesian Distance Calculator.

Table 2

Observed parameters of extracted CO clumps

Name	Offset(R.A. DEC.)[a] ($''$ $''$)	$V_{^{13}CO}$ km s^{-1}	$\Delta V_{^{13}CO}$ km s^{-1}	$T_{^{13}CO}$ K	$V_{C^{18}O}$ km s^{-1}	$\Delta V_{C^{18}O}$[b] km s^{-1}	$T_{C^{18}O}$ K	$\tau_{^{13}CO}$[c]	$T_{ex}(^{13}CO)$[d] K
G098.50-03.24_1	-42.41, -118.79	-6.12 ± 0.01	1.33 ± 0.03	3.09 ± 0.11	-5.80 ± 0.07	0.93 ± 0.18	0.54 ± 0.10	0.93 ± 0.50	10.11 ± 1.80
G098.50-03.24_2	103.25, 56.95	-5.95 ± 0.01	0.81 ± 0.02	3.67 ± 0.12	-5.91 ± 0.04	0.59 ± 0.12	0.70 ± 0.09	1.19 ± 0.40	11.10 ± 1.07
G108.85-00.80_1	21.64, 16.41	-49.53 ± 0.01	2.94 ± 0.03	5.44 ± 0.15	-49.59 ± 0.08	2.00 ± 0.19	0.91 ± 0.12	0.93 ± 0.38	16.93 ± 2.35
G108.85-00.80_2	364.31, 146.82	-49.78 ± 0.02	2.68 ± 0.04	6.02 ± 0.24	-49.75 ± 0.07	1.52 ± 0.15	1.42 ± 0.20	1.97 ± 0.50	15.46 ± 0.85
G108.85-00.80_3	-160.17, -58.88	-50.51 ± 0.02	2.92 ± 0.05	4.16 ± 0.19	-50.49 ± 0.14	2.45 ± 0.31	0.66 ± 0.15	0.79 ± 0.60	14.10 ± 3.94
G108.85-00.80_4	241.50, 186.31	-49.55 ± 0.02	2.31 ± 0.04	4.68 ± 0.16	-49.74 ± 0.11	1.55 ± 0.20	0.64 ± 0.14	0.41 ± 0.14	21.10 ± 7.03
G110.65+09.65_1	70.87, -26.19	-4.28 ± 0.01	1.55 ± 0.01	5.69 ± 0.09	-4.33 ± 0.02	1.03 ± 0.04	1.50 ± 0.07	2.25 ± 0.17	14.52 ± 0.25
G110.65+09.65_2	65.76, 290.64	-4.62 ± 0.01	1.68 ± 0.02	4.16 ± 0.10	-4.57 ± 0.06	1.15 ± 0.15	0.59 ± 0.08	0.41 ± 0.35	18.83 ± 6.28
G110.65+09.65_3	-126.92, 102.11	-4.33 ± 0.01	1.42 ± 0.02	4.56 ± 0.11	-4.44 ± 0.03	1.12 ± 0.08	1.00 ± 0.08	1.61 ± 0.26	12.66 ± 0.53
G110.65+09.65_4	219.56, 117.51	-4.20 ± 0.01	1.36 ± 0.01	5.19 ± 0.08	-4.22 ± 0.03	1.01 ± 0.07	1.10 ± 0.08	1.51 ± 0.22	14.34 ± 0.51
G112.52+08.38_1	225.49, 286.31	-5.37 ± 0.01	1.90 ± 0.03	3.56 ± 0.12	-5.63 ± 0.10	1.17 ± 0.35	0.55 ± 0.12	0.61 ± 0.57	13.55 ± 5.48
G112.52+08.38_2	62.60, 120.64	-5.26 ± 0.01	1.19 ± 0.01	4.31 ± 0.08	–	–	–	–	–
G112.52+08.38_3	-11.56, 379.79	-4.89 ± 0.02	1.69 ± 0.04	3.37 ± 0.17	–	–	–	–	–
G112.52+08.38_4	-154.70, 296.51	-5.13 ± 0.02	1.45 ± 0.04	2.52 ± 0.15	-5.53 ± 0.07	0.33 ± 0.07	0.31 ± 0.10	0.20 ± 0.05	50.00 ± 5.00
G112.52+08.38_5	297.07, 27.03	-5.16 ± 0.01	1.07 ± 0.02	3.06 ± 0.09	–	–	–	–	–
G112.60+08.53_1	88.57, -83.18	-5.03 ± 0.01	1.87 ± 0.01	3.60 ± 0.07	-5.08 ± 0.07	1.81 ± 0.15	0.34 ± 0.04	0.20 ± 0.05	25.84 ± 8.61
G112.60+08.53_2	168.07, -346.67	-5.46 ± 0.02	1.82 ± 0.04	3.70 ± 0.17	-5.60 ± 0.19	2.19 ± 0.52	0.43 ± 0.13	0.25 ± 0.06	22.60 ± 7.53
G112.60+08.53_3	-150.67, 222.54	-4.77 ± 0.01	1.85 ± 0.03	2.72 ± 0.09	-4.97 ± 0.15	1.85 ± 0.29	0.24 ± 0.07	0.20 ± 0.05	20.72 ± 6.91
G112.60+08.53_4	-29.65, -305.67	-5.08 ± 0.01	1.64 ± 0.03	3.30 ± 0.12	-5.26 ± 0.18	1.98 ± 0.36	0.23 ± 0.07	0.20 ± 0.05	29.34 ± 9.78
G112.60+08.53_5	224.69, 126.61	-5.02 ± 0.01	1.50 ± 0.02	3.64 ± 0.07	-5.09 ± 0.08	1.48 ± 0.17	0.36 ± 0.06	0.21 ± 0.05	25.23 ± 8.41
G112.60+08.53_6	368.93, 169.82	-5.01 ± 0.03	1.82 ± 0.06	2.77 ± 0.19	-4.84 ± 0.04	0.33 ± 0.07	0.66 ± 0.18	1.88 ± 0.95	7.74 ± 0.87
G112.60+08.53_7	-340.99, 84.70	-4.49 ± 0.03	1.86 ± 0.07	2.14 ± 0.17	–	–	–	–	–
G112.60+08.53_8	40.39, 332.32	-4.70 ± 0.01	1.50 ± 0.03	2.57 ± 0.09	–	–	–	–	–
G115.92+09.46_1	-40.18, 29.56	-3.35 ± 0.01	1.58 ± 0.03	3.59 ± 0.10	-3.50 ± 0.09	1.04 ± 0.22	0.34 ± 0.07	0.20 ± 0.05	25.27 ± 8.42
G115.92+09.46_2	42.52, 209.09	-3.92 ± 0.01	0.63 ± 0.03	4.04 ± 0.20	-3.91 ± 0.07	0.37 ± 0.10	0.71 ± 0.10	0.96 ± 0.40	12.89 ± 1.93
G115.92+09.46_3	-38.44, -185.70	-3.10 ± 0.02	1.15 ± 0.04	2.28 ± 0.13	-3.56 ± 0.10	0.33 ± 0.07	0.23 ± 0.07	0.22 ± 0.05	15.65 ± 5.22
G115.92+09.46_4	237.75, -208.00	-3.38 ± 0.03	1.01 ± 0.09	2.01 ± 0.20	–	–	–	–	–
G115.92+09.46_5	-197.65, 243.71	-2.29 ± 0.05	1.69 ± 0.12	1.43 ± 0.19	–	–	–	–	–
G115.92+09.46_6	84.44, -58.39	-2.95 ± 0.02	1.71 ± 0.04	2.40 ± 0.12	–	–	–	–	–
G115.92+09.46_7	177.70, 179.51	-4.06 ± 0.01	0.58 ± 0.03	2.80 ± 0.17	-2.62 ± 0.15	0.33 ± 0.07	0.31 ± 0.09	0.24 ± 0.06	17.93 ± 5.98
G116.08-02.38_1	13.48, 29.31	-1.03 ± 0.01	1.66 ± 0.03	3.35 ± 0.11	-0.97 ± 0.07	1.51 ± 0.15	0.59 ± 0.09	0.99 ± 0.42	10.73 ± 1.46
G116.08-02.38_2	273.23, -229.61	-0.64 ± 0.02	1.33 ± 0.04	3.19 ± 0.18	-0.72 ± 0.08	0.73 ± 0.18	0.63 ± 0.14	1.31 ± 0.69	9.50 ± 1.36
G116.08-02.38_3	-343.22, 89.77	-1.69 ± 0.02	1.24 ± 0.05	2.84 ± 0.21	–	–	–	–	–
G116.08-02.38_4	-24.68, -218.51	-0.78 ± 0.02	1.56 ± 0.03	2.94 ± 0.13	-0.81 ± 0.08	0.87 ± 0.34	0.53 ± 0.11	1.05 ± 0.58	9.31 ± 1.59
G116.08-02.38_5	-179.22, 0.06	-1.46 ± 0.02	1.58 ± 0.04	2.87 ± 0.13	-1.49 ± 0.11	1.08 ± 0.27	0.43 ± 0.11	0.53 ± 0.18	11.72 ± 6.80
G116.08-02.38_6	-160.83, 177.51	-1.38 ± 0.02	1.68 ± 0.05	2.85 ± 0.16	-1.50 ± 0.11	0.98 ± 0.26	0.47 ± 0.14	0.79 ± 0.78	9.89 ± 3.65
G116.08-02.38_7	245.32, 27.51	-0.59 ± 0.02	1.57 ± 0.05	2.24 ± 0.15	–	–	–	–	–
G116.12+08.98_1	33.51, 15.77	-1.68 ± 0.02	1.47 ± 0.04	2.23 ± 0.10	-1.36 ± 0.09	0.58 ± 0.19	0.27 ± 0.08	0.20 ± 0.05	50.00 ± 5.00
G116.12+08.98_2	-135.37, 89.61	-1.59 ± 0.02	1.65 ± 0.06	1.98 ± 0.12	–	–	–	–	–
G116.12+08.98_3	133.67, -156.31	-2.00 ± 0.01	1.11 ± 0.03	2.76 ± 0.12	–	–	–	–	–
G116.12+08.98_4	44.63, -386.87	-2.45 ± 0.02	1.06 ± 0.06	2.48 ± 0.20	–	–	–	–	–
G116.12+08.98_5	218.49, -318.66	-1.96 ± 0.02	0.86 ± 0.05	2.71 ± 0.18	–	–	–	–	–
G120.16+03.09_1	-22.48, 33.58	-19.53 ± 0.01	2.79 ± 0.01	5.65 ± 0.08	-19.58 ± 0.03	2.24 ± 0.07	1.12 ± 0.06	1.34 ± 0.17	15.79 ± 0.53
G120.16+03.09_2	378.42, -81.46	-18.94 ± 0.02	2.52 ± 0.04	5.56 ± 0.20	-18.85 ± 0.05	1.67 ± 0.15	1.23 ± 0.13	1.66 ± 0.35	14.91 ± 0.83

TABLE 2—*Continued*

Name	Offset(R.A. DEC.)[a] ($''$ $''$)	$V_{^{13}CO}$ km s^{-1}	$\Delta V_{^{13}CO}$ km s^{-1}	$T_{^{13}CO}$ K	$V_{C^{18}O}$ km s^{-1}	$\Delta V_{C^{18}O}$[b] km s^{-1}	$T_{C^{18}O}$ K	$\tau_{^{13}CO}$[c]	$T_{ex}(^{13}CO)$[d] K
G120.16+03.09_3	227.97, -125.30	-19.10 ± 0.01	2.65 ± 0.02	4.96 ± 0.10	-19.12 ± 0.05	2.12 ± 0.12	0.85 ± 0.07	0.90 ± 0.23	15.79 ± 1.40
G120.16+03.09_4	-339.30, -79.48	-19.18 ± 0.02	2.69 ± 0.03	4.54 ± 0.15	-19.47 ± 0.13	2.52 ± 0.28	0.49 ± 0.10	0.23 ± 0.06	28.76 ± 9.59
G120.16+03.09_5	-95.33, -182.45	-19.65 ± 0.01	2.38 ± 0.02	5.09 ± 0.10	-19.71 ± 0.03	1.94 ± 0.07	1.06 ± 0.06	1.49 ± 0.19	14.14 ± 0.50
G120.16+03.09_6	-82.44, -385.11	-19.74 ± 0.02	1.61 ± 0.04	4.92 ± 0.23	-19.79 ± 0.07	1.23 ± 0.21	0.90 ± 0.14	1.11 ± 0.47	14.73 ± 1.97
G120.67+02.66_1	-268.36, 38.59	-17.42 ± 0.01	1.83 ± 0.03	5.32 ± 0.14	-17.40 ± 0.06	1.45 ± 0.16	0.68 ± 0.09	0.20 ± 0.05	43.44 ± 14.48
G120.67+02.66_2	39.59, -23.71	-17.66 ± 0.01	2.23 ± 0.02	4.39 ± 0.07	-17.78 ± 0.08	2.19 ± 0.18	0.49 ± 0.06	0.24 ± 0.06	27.44 ± 9.15
G120.67+02.66_3	308.68, -202.02	-17.31 ± 0.01	1.64 ± 0.03	4.48 ± 0.13	-17.53 ± 0.11	2.11 ± 0.28	0.47 ± 0.09	0.23 ± 0.06	29.16 ± 9.72
G120.67+02.66_4	214.22, 240.74	-16.72 ± 0.01	1.77 ± 0.04	2.91 ± 0.11	–	–	–	–	–
G120.67+02.66_5	-301.58, 264.36	-17.31 ± 0.03	1.63 ± 0.08	3.85 ± 0.34	–	–	–	–	–
G120.67+02.66_6	223.27, -94.80	-17.77 ± 0.01	1.86 ± 0.02	4.29 ± 0.10	-18.03 ± 0.07	1.54 ± 0.16	0.62 ± 0.08	0.45 ± 0.34	18.48 ± 7.19
G120.67+02.66_7	-43.70, 201.96	-16.92 ± 0.01	1.64 ± 0.02	3.80 ± 0.09	-17.08 ± 0.12	1.57 ± 0.46	0.36 ± 0.08	0.20 ± 0.05	27.15 ± 9.05
G120.67+02.66_8	97.40, -222.10	-17.70 ± 0.01	1.29 ± 0.02	4.51 ± 0.11	–	–	–	–	–
G120.98+02.66_1	-81.42, -14.81	-17.15 ± 0.01	1.62 ± 0.02	4.88 ± 0.09	-17.18 ± 0.04	1.32 ± 0.10	0.74 ± 0.07	0.57 ± 0.24	18.62 ± 3.56
G120.98+02.66_2	36.17, 366.70	-16.32 ± 0.05	2.65 ± 0.15	2.40 ± 0.23	-15.97 ± 0.06	0.69 ± 0.12	0.74 ± 0.13	2.92 ± 0.89	6.41 ± 0.69
G120.98+02.66_3	128.44, 79.31	-16.53 ± 0.02	2.13 ± 0.04	2.46 ± 0.10	–	–	–	–	–
G120.98+02.66_4	-177.09, 350.49	-16.87 ± 0.04	1.32 ± 0.09	2.36 ± 0.29	–	–	–	–	–
G120.98+02.66_5	241.17, 259.50	-15.62 ± 0.02	1.53 ± 0.05	2.83 ± 0.17	–	–	–	–	–
G120.98+02.66_6	111.75, -136.49	-16.27 ± 0.01	1.61 ± 0.03	2.66 ± 0.11	–	–	–	–	–
G120.98+02.66_7	-286.73, -286.12	-16.76 ± 0.02	0.94 ± 0.05	3.34 ± 0.25	–	–	–	–	–
G120.98+02.66_8	-135.92, -379.72	-16.43 ± 0.03	1.08 ± 0.07	2.83 ± 0.27	–	–	–	–	–
G120.98+02.66_9	332.14, -111.82	-15.27 ± 0.02	1.14 ± 0.06	2.12 ± 0.16	–	–	–	–	–
G120.98+02.66_10	-26.32, -326.39	-16.09 ± 0.02	1.14 ± 0.04	2.29 ± 0.14	–	–	–	–	–
G121.35+03.39_1	-50.68, 70.57	-5.43 ± 0.01	1.51 ± 0.02	3.44 ± 0.10	-5.34 ± 0.03	0.96 ± 0.06	1.06 ± 0.07	2.88 ± 0.31	9.13 ± 0.28
G121.35+03.39_2	290.02, -15.02	-5.77 ± 0.02	1.84 ± 0.04	2.44 ± 0.13	-5.69 ± 0.13	1.57 ± 0.24	0.42 ± 0.11	0.91 ± 0.72	8.10 ± 2.18
G121.35+03.39_3	-214.68, 330.09	-5.20 ± 0.03	1.85 ± 0.06	2.98 ± 0.20	-5.21 ± 0.11	1.69 ± 0.27	0.78 ± 0.15	2.24 ± 0.76	8.13 ± 0.71
G121.35+03.39_4	208.90, 327.68	-6.13 ± 0.03	1.69 ± 0.08	2.44 ± 0.20	-6.18 ± 0.10	1.06 ± 0.24	0.69 ± 0.15	2.50 ± 0.91	6.60 ± 0.66
G121.35+03.39_5	136.58, 205.61	-5.37 ± 0.01	1.24 ± 0.03	3.84 ± 0.12	-5.34 ± 0.04	0.89 ± 0.10	0.89 ± 0.10	1.81 ± 0.39	10.65 ± 0.54
G121.35+03.39_6	259.22, -291.72	-5.70 ± 0.03	1.55 ± 0.07	2.70 ± 0.23	–	–	–	–	–
G121.35+03.39_7	-138.51, -197.58	-5.34 ± 0.03	1.90 ± 0.07	1.87 ± 0.12	-5.13 ± 0.14	1.24 ± 0.44	0.25 ± 0.08	0.30 ± 0.10	10.46 ± 3.49
G121.35+03.39_8	-314.28, 75.58	-5.30 ± 0.03	1.40 ± 0.08	2.42 ± 0.23	–	–	–	–	–
G121.90-01.54_1	102.50, -22.74	-14.08 ± 0.01	1.60 ± 0.03	3.45 ± 0.10	-13.95 ± 0.09	0.99 ± 0.17	0.39 ± 0.09	0.24 ± 0.06	21.66 ± 7.22
G121.90-01.54_2	62.89, 367.78	-13.34 ± 0.01	1.43 ± 0.03	3.81 ± 0.16	-13.25 ± 0.08	0.81 ± 0.17	0.58 ± 0.13	0.62 ± 0.57	14.35 ± 5.70
G121.90-01.54_3	69.11, -375.24	-13.94 ± 0.01	0.99 ± 0.03	3.91 ± 0.17	-14.33 ± 0.10	0.55 ± 0.27	0.56 ± 0.15	0.40 ± 0.13	18.03 ± 6.01
G121.90-01.54_4	168.66, 227.79	-14.08 ± 0.01	1.33 ± 0.03	3.18 ± 0.13	–	–	–	–	–
G121.90-01.54_5	-115.22, -92.25	-13.91 ± 0.01	0.92 ± 0.02	4.31 ± 0.10	-14.01 ± 0.05	0.69 ± 0.09	0.67 ± 0.09	0.63 ± 0.36	15.97 ± 3.94
G121.90-01.54_6	315.70, 80.41	-14.43 ± 0.02	1.34 ± 0.04	3.05 ± 0.16	-14.51 ± 0.04	0.33 ± 0.07	0.70 ± 0.13	1.77 ± 0.65	8.59 ± 0.74
G121.90-01.54_7	235.59, -314.20	-14.03 ± 0.02	1.17 ± 0.05	3.52 ± 0.25	–	–	–	–	–
G121.90-01.54_8	58.28, -211.62	-14.06 ± 0.01	1.08 ± 0.02	3.82 ± 0.13	-14.19 ± 0.07	0.69 ± 0.16	0.59 ± 0.11	0.62 ± 0.47	14.31 ± 4.60
G121.92-01.71_1	29.74, 29.56	-14.03 ± 0.01	1.43 ± 0.02	3.69 ± 0.08	-14.02 ± 0.06	1.41 ± 0.17	0.48 ± 0.06	0.20 ± 0.05	26.52 ± 8.84
G121.92-01.71_2	-54.04, 399.89	-13.93 ± 0.02	1.03 ± 0.05	4.70 ± 0.31	-13.93 ± 0.08	0.43 ± 0.12	1.14 ± 0.24	1.95 ± 0.77	12.61 ± 1.14
G121.92-01.71_3	198.58, -335.67	-13.28 ± 0.02	1.14 ± 0.03	3.90 ± 0.20	-13.48 ± 0.08	1.14 ± 0.16	0.70 ± 0.12	1.05 ± 0.51	12.14 ± 1.91
G121.92-01.71_4	51.66, -193.85	-13.96 ± 0.01	1.47 ± 0.02	3.82 ± 0.12	-14.06 ± 0.05	1.17 ± 0.14	0.79 ± 0.09	1.43 ± 0.36	11.05 ± 0.74
G121.92-01.71_5	171.84, 361.30	-14.17 ± 0.04	1.43 ± 0.09	2.53 ± 0.26	–	–	–	–	–
G121.92-01.71_6	141.39, 268.56	-13.81 ± 0.01	1.18 ± 0.03	3.29 ± 0.15	-13.54 ± 0.12	1.05 ± 0.31	0.34 ± 0.10	0.22 ± 0.06	21.75 ± 7.25

TABLE 2—*Continued*

Name	Offset(R.A. DEC.)[a] ($''$ $''$)	$V_{^{13}CO}$ km s^{-1}	$\Delta V_{^{13}CO}$ km s^{-1}	$T_{^{13}CO}$ K	$V_{C^{18}O}$ km s^{-1}	$\Delta V_{C^{18}O}$[b] km s^{-1}	$T_{C^{18}O}$ K	$\tau_{^{13}CO}$[c]	$T_{ex}(^{13}CO)$[d] K
G121.92-01.71_7	-342.04, 230.79	-13.60 ± 0.04	0.82 ± 0.09	2.91 ± 0.46	–	–	–	–	–
G121.92-01.71_8	-34.69, 276.71	-13.86 ± 0.01	1.09 ± 0.03	3.62 ± 0.16	-13.81 ± 0.12	1.09 ± 0.26	0.44 ± 0.13	0.20 ± 0.05	50.00 ± 5.00
G121.92-01.71_9	-239.73, -2.71	-14.23 ± 0.02	1.08 ± 0.05	2.50 ± 0.17	–	–	–	–	–
G121.92-01.71_10	304.44, -98.21	-13.18 ± 0.03	1.38 ± 0.08	1.49 ± 0.15	-15.31 ± 0.09	0.45 ± 0.14	0.41 ± 0.11	2.46 ± 1.12	4.14 ± 0.45
G125.66-00.55_1	-1.87, -3.71	-12.59 ± 0.04	0.55 ± 0.12	1.95 ± 0.10	–	–	–	–	–
G125.66-00.55_2	-201.48, -328.04	-11.69 ± 0.07	5.30 ± 0.12	2.09 ± 0.22	–	–	–	–	–
G125.66-00.55_3	184.22, 71.68	-13.73 ± 0.04	5.88 ± 0.08	2.15 ± 0.12	-15.61 ± 0.11	1.63 ± 0.26	0.50 ± 0.10	1.85 ± 0.73	6.04 ± 0.55
G125.66-00.55_4	-169.21, -194.67	-10.65 ± 0.04	4.25 ± 0.09	2.06 ± 0.12	-9.68 ± 0.14	1.53 ± 0.35	0.49 ± 0.10	1.88 ± 0.72	5.78 ± 0.53
G125.66-00.55_5	373.43, 70.57	-13.71 ± 0.10	3.86 ± 0.22	1.23 ± 0.18	–	–	–	–	–
G125.66-00.55_6	-282.12, 24.55	-12.75 ± 0.06	4.98 ± 0.12	1.51 ± 0.15	-11.34 ± 0.13	0.97 ± 0.23	0.35 ± 0.11	1.78 ± 1.10	4.37 ± 0.67
G125.66-00.55_7	-150.35, 334.33	-12.38 ± 0.14	0.54 ± 0.11	0.79 ± 0.15	–	–	–	–	–
G125.66-00.55_8	12.71, 239.14	-14.71 ± 0.05	1.99 ± 0.12	1.89 ± 0.21	–	–	–	–	–
G125.66-00.55_9	-90.17, -408.37	-11.47 ± 0.18	4.41 ± 0.47	1.80 ± 0.40	–	–	–	–	–
G125.66-00.55_10	-344.86, 207.32	-13.09 ± 0.14	3.44 ± 0.47	1.12 ± 0.27	–	–	–	–	–
G126.49-01.30_1	-105.00, 368.78	-12.80 ± 0.03	2.49 ± 0.06	3.65 ± 0.25	-12.50 ± 0.12	1.51 ± 0.32	0.72 ± 0.16	1.31 ± 0.70	10.81 ± 1.65
G126.49-01.30_2	-307.13, 200.24	-12.31 ± 0.03	2.47 ± 0.06	3.28 ± 0.20	-12.20 ± 0.09	1.45 ± 0.31	0.71 ± 0.14	1.56 ± 0.64	9.41 ± 1.03
G126.49-01.30_3	-37.05, -61.98	-11.85 ± 0.01	2.04 ± 0.02	3.68 ± 0.09	-11.79 ± 0.04	1.43 ± 0.09	0.73 ± 0.06	1.29 ± 0.24	10.92 ± 0.58
G126.49-01.30_4	129.49, 379.21	-12.54 ± 0.04	1.85 ± 0.09	3.39 ± 0.32	-12.57 ± 0.06	0.62 ± 0.13	1.11 ± 0.22	3.15 ± 1.00	8.95 ± 0.89
G126.49-01.30_5	315.68, 224.10	-11.94 ± 0.05	1.95 ± 0.12	2.34 ± 0.29	-12.47 ± 0.06	0.33 ± 0.07	0.76 ± 0.22	3.13 ± 1.45	6.22 ± 0.86
G126.49-01.30_6	104.09, 231.96	-12.06 ± 0.02	1.97 ± 0.04	2.70 ± 0.13	-12.26 ± 0.22	1.59 ± 0.60	0.30 ± 0.08	0.24 ± 0.06	17.18 ± 5.73
G126.49-01.30_7	-170.02, -368.87	-11.38 ± 0.03	1.43 ± 0.06	3.37 ± 0.28	-11.19 ± 0.04	0.47 ± 0.20	1.31 ± 0.20	4.03 ± 1.00	8.81 ± 0.72
G126.49-01.30_8	-153.57, 227.44	-12.18 ± 0.02	2.38 ± 0.05	2.95 ± 0.15	-11.92 ± 0.11	1.74 ± 0.24	0.51 ± 0.10	0.91 ± 0.57	9.73 ± 2.12
G126.49-01.30_9	-270.00, 24.81	-11.71 ± 0.02	1.95 ± 0.04	2.70 ± 0.12	-11.68 ± 0.13	2.03 ± 0.27	0.33 ± 0.07	0.20 ± 0.05	50.00 ± 5.00
G126.49-01.30_10	218.65, 1.24	-11.36 ± 0.01	1.37 ± 0.03	2.86 ± 0.12	-11.44 ± 0.04	0.71 ± 0.10	0.53 ± 0.07	1.10 ± 0.38	8.93 ± 1.00
G126.95-01.06_1	-13.45, 59.83	-11.61 ± 0.01	2.28 ± 0.03	2.59 ± 0.08	-11.91 ± 0.06	1.24 ± 0.21	0.40 ± 0.06	0.64 ± 0.37	9.72 ± 2.37
G126.95-01.06_2	275.72, -223.07	-11.92 ± 0.03	2.42 ± 0.06	2.46 ± 0.15	–	–	–	–	–
G126.95-01.06_3	-310.76, 123.36	-11.78 ± 0.05	3.09 ± 0.11	1.78 ± 0.17	–	–	–	–	–
G126.95-01.06_4	-76.87, -348.44	-12.72 ± 0.02	1.81 ± 0.06	2.45 ± 0.15	-12.76 ± 0.09	0.68 ± 0.20	0.41 ± 0.11	0.86 ± 0.74	8.27 ± 2.54
G126.95-01.06_5	-224.27, -128.38	-10.65 ± 0.04	3.08 ± 0.08	1.94 ± 0.15	–	–	–	–	–
G126.95-01.06_6	48.67, 294.37	-11.28 ± 0.03	2.09 ± 0.08	2.27 ± 0.17	–	–	–	–	–
G127.22-02.25_1	48.35, 116.47	-10.86 ± 0.03	2.54 ± 0.06	1.64 ± 0.10	–	–	–	–	–
G127.22-02.25_2	-90.12, -70.73	-10.61 ± 0.03	2.38 ± 0.06	1.60 ± 0.10	–	–	–	–	–
G127.22-02.25_3	142.83, -236.72	-11.21 ± 0.04	1.60 ± 0.09	1.45 ± 0.15	–	–	–	–	–
G127.22-02.25_4	-64.77, -224.45	-11.05 ± 0.03	2.27 ± 0.08	1.68 ± 0.13	–	–	–	–	–
G127.22-02.25_5	-241.16, 232.55	-9.56 ± 0.06	1.90 ± 0.14	1.27 ± 0.17	–	–	–	–	–
G127.22-02.25_6	-33.61, -328.85	-10.88 ± 0.04	1.42 ± 0.09	1.85 ± 0.19	–	–	–	–	–
G127.22-02.25_7	-238.38, -155.87	-10.40 ± 0.06	1.93 ± 0.15	1.29 ± 0.18	–	–	–	–	–
G127.22-02.25_8	176.83, -97.86	-11.21 ± 0.05	1.76 ± 0.12	1.48 ± 0.18	–	–	–	–	–
G127.22-02.25_9	-236.84, 93.95	-9.87 ± 0.16	3.47 ± 0.31	0.73 ± 0.22	–	–	–	–	–
G127.22-02.25_10	-95.72, 182.15	-10.98 ± 0.10	2.35 ± 0.30	1.32 ± 0.26	–	–	–	–	–
G127.22-02.25_11	-330.43, -80.73	-10.80 ± 0.07	1.92 ± 0.19	0.87 ± 0.16	–	–	–	–	–
G127.88+02.66_1	-8.77, -131.31	-11.31 ± 0.01	1.47 ± 0.01	4.88 ± 0.08	-11.28 ± 0.05	1.08 ± 0.12	0.53 ± 0.06	0.24 ± 0.06	30.73 ± 10.24
G127.88+02.66_2	15.45, 142.74	-11.77 ± 0.01	1.45 ± 0.02	4.86 ± 0.11	-11.81 ± 0.04	1.11 ± 0.10	0.77 ± 0.07	0.71 ± 0.25	16.95 ± 2.50
G127.88+02.66_3	190.01, -6.47	-11.73 ± 0.01	1.27 ± 0.02	5.47 ± 0.11	-11.89 ± 0.04	0.79 ± 0.09	0.83 ± 0.08	0.60 ± 0.26	20.16 ± 3.96

TABLE 2—*Continued*

Name	Offset(R.A. DEC.)[a] ($''$ $''$)	$V_{^{13}CO}$ km s^{-1}	$\Delta V_{^{13}CO}$ km s^{-1}	$T_{^{13}CO}$ K	$V_{C^{18}O}$ km s^{-1}	$\Delta V_{C^{18}O}$[b] km s^{-1}	$T_{C^{18}O}$ K	$\tau_{^{13}CO}$[c]	$T_{ex}(^{13}CO)$[d] K
G127.88+02.66_4	-202.75, 220.07	-11.41 ± 0.02	1.43 ± 0.04	3.30 ± 0.16	–	–	–	–	–
G128.95-00.18_1	-231.47, 0.76	-14.75 ± 0.01	1.28 ± 0.03	3.55 ± 0.11	-14.75 ± 0.05	0.84 ± 0.19	0.62 ± 0.09	0.95 ± 0.41	11.48 ± 1.63
G128.95-00.18_2	171.86, -167.56	-14.14 ± 0.03	1.40 ± 0.06	3.16 ± 0.25	-14.02 ± 0.07	0.78 ± 0.15	0.54 ± 0.10	0.91 ± 0.56	10.42 ± 2.47
G128.95-00.18_3	65.91, 146.24	-14.57 ± 0.01	1.07 ± 0.02	3.95 ± 0.12	-14.59 ± 0.04	0.68 ± 0.11	0.81 ± 0.09	1.41 ± 0.35	11.43 ± 0.74
G128.95-00.18_4	403.40, -23.36	-14.16 ± 0.01	0.86 ± 0.03	4.89 ± 0.25	–	–	–	–	–
G128.95-00.18_5	329.22, 87.12	-14.18 ± 0.01	0.80 ± 0.03	4.34 ± 0.18	-14.16 ± 0.05	0.59 ± 0.12	0.83 ± 0.14	1.22 ± 0.50	12.86 ± 1.50
G128.95-00.18_6	237.94, 172.73	-14.03 ± 0.01	1.08 ± 0.04	3.75 ± 0.17	-13.95 ± 0.06	0.78 ± 0.14	0.76 ± 0.13	1.41 ± 0.54	10.90 ± 1.11
G128.95-00.18_7	-113.55, -342.17	-14.68 ± 0.03	1.27 ± 0.07	2.10 ± 0.19	–	–	–	–	–
G128.95-00.18_8	0.18, -117.19	-14.55 ± 0.00	1.25 ± 0.03	3.67 ± 0.14	-14.43 ± 0.05	0.81 ± 0.13	0.58 ± 0.08	0.72 ± 0.37	13.04 ± 2.73
G128.95-00.18_9	-272.52, -233.46	-14.99 ± 0.02	1.07 ± 0.05	2.57 ± 0.18	–	–	–	–	–
G131.72+09.70_1	64.10, 5.50	-8.38 ± 0.01	1.54 ± 0.02	3.42 ± 0.10	-8.51 ± 0.07	0.89 ± 0.14	0.48 ± 0.09	0.37 ± 0.12	16.61 ± 5.54
G131.72+09.70_2	77.45, -330.62	-8.46 ± 0.01	1.11 ± 0.03	3.36 ± 0.15	-8.53 ± 0.05	0.33 ± 0.07	0.80 ± 0.14	1.90 ± 0.61	9.33 ± 0.65
G131.72+09.70_3	-31.44, -199.94	-8.30 ± 0.01	1.03 ± 0.02	4.41 ± 0.12	-8.40 ± 0.06	0.67 ± 0.11	0.57 ± 0.11	0.20 ± 0.05	34.37 ± 11.46
G131.72+09.70_4	-5.37, 376.52	-7.91 ± 0.10	4.31 ± 0.22	1.15 ± 0.19	–	–	–	–	–
G131.72+09.70_5	-131.35, -51.09	-8.44 ± 0.01	1.17 ± 0.02	4.13 ± 0.11	-8.57 ± 0.04	0.62 ± 0.11	0.79 ± 0.11	1.19 ± 0.41	12.38 ± 1.17
G131.72+09.70_6	385.19, -7.17	-9.45 ± 0.04	1.42 ± 0.09	1.97 ± 0.23	–	–	–	–	–
G131.72+09.70_7	216.00, 350.27	-8.95 ± 0.13	1.62 ± 0.28	1.32 ± 0.43	–	–	–	–	–
G131.72+09.70_8	-171.55, 211.65	-8.49 ± 0.06	2.25 ± 0.13	1.15 ± 0.15	–	–	–	–	–
G131.72+09.70_9	213.94, 117.56	-8.92 ± 0.04	1.95 ± 0.10	1.83 ± 0.18	–	–	–	–	–
G131.72+09.70_10	210.85, -197.48	-8.49 ± 0.02	0.95 ± 0.04	2.91 ± 0.18	–	–	–	–	–
G131.72+09.70_11	118.46, 293.90	-8.85 ± 0.04	1.71 ± 0.11	1.58 ± 0.18	–	–	–	–	–
G131.72+09.70_12	-219.30, 41.73	-8.61 ± 0.02	1.23 ± 0.04	2.76 ± 0.16	–	–	–	–	–
G132.07+08.80_1	32.70, -30.88	-12.15 ± 0.01	1.70 ± 0.03	3.30 ± 0.10	-12.12 ± 0.07	0.82 ± 0.15	0.36 ± 0.07	0.24 ± 0.06	21.16 ± 7.05
G132.07+08.80_2	48.73, 366.57	-11.51 ± 0.02	1.65 ± 0.06	3.07 ± 0.20	-11.44 ± 0.12	0.83 ± 0.31	0.52 ± 0.15	0.85 ± 0.80	10.35 ± 3.48
G132.07+08.80_3	-43.98, -300.43	-12.73 ± 0.02	1.65 ± 0.04	2.94 ± 0.14	–	–	–	–	–
G132.07+08.80_4	-76.89, 176.42	-11.98 ± 0.02	1.75 ± 0.04	2.67 ± 0.13	–	–	–	–	–
G132.07+08.80_5	313.65, 205.27	-12.35 ± 0.04	1.81 ± 0.09	2.06 ± 0.21	–	–	–	–	–
G132.07+08.80_6	-115.93, -399.93	-13.09 ± 0.02	1.09 ± 0.06	3.88 ± 0.31	–	–	–	–	–
G132.03+08.95_1	42.67, 18.01	-12.30 ± 0.02	2.32 ± 0.05	2.41 ± 0.12	–	–	–	–	–
G132.03+08.95_2	375.03, -95.57	-12.88 ± 0.03	1.16 ± 0.06	3.80 ± 0.32	-13.04 ± 0.10	0.88 ± 0.20	0.85 ± 0.21	1.71 ± 0.86	10.64 ± 1.39
G132.03+08.95_3	-8.86, -406.84	-11.98 ± 0.04	1.76 ± 0.10	3.13 ± 0.35	–	–	–	–	–
G132.03+08.95_4	236.83, 233.85	-11.60 ± 0.04	2.26 ± 0.08	2.09 ± 0.18	–	–	–	–	–
G132.03+08.95_5	-96.88, -275.79	-11.72 ± 0.02	1.75 ± 0.05	2.57 ± 0.16	–	–	–	–	–
G132.03+08.95_6	139.31, -374.38	-12.14 ± 0.07	1.94 ± 0.15	2.26 ± 0.43	–	–	–	–	–
G132.03+08.95_7	269.04, -165.02	-12.79 ± 0.02	0.92 ± 0.06	3.67 ± 0.30	-12.93 ± 0.13	1.04 ± 0.28	0.68 ± 0.20	1.13 ± 0.89	11.27 ± 2.71
G133.28+08.81_1	63.92, -24.09	-11.06 ± 0.05	2.02 ± 0.12	1.95 ± 0.23	-10.81 ± 0.16	1.55 ± 0.32	0.59 ± 0.18	2.80 ± 1.40	5.24 ± 0.69
G133.28+08.81_2	-161.66, -115.49	-10.63 ± 0.07	1.88 ± 0.18	1.44 ± 0.26	-10.39 ± 0.12	0.99 ± 0.32	0.35 ± 0.11	1.94 ± 1.22	4.15 ± 0.88
G133.28+08.81_3	195.98, 292.97	-11.39 ± 0.23	0.45 ± 0.13	0.53 ± 0.14	–	–	–	–	–
G133.28+08.81_4	-28.19, 104.83	-10.98 ± 0.06	2.07 ± 0.16	1.89 ± 0.28	-10.73 ± 0.09	0.53 ± 0.22	0.92 ± 0.28	5.54 ± 2.77	4.96 ± 0.72
G133.28+08.81_5	-179.85, 164.58	-11.15 ± 0.15	2.40 ± 0.66	0.92 ± 0.30	–	–	–	–	–
G133.28+08.81_6	-42.69, 393.91	-10.40 ± 0.18	2.77 ± 0.56	0.98 ± 0.30	–	–	–	–	–
G133.28+08.81_7	199.91, -201.01	-11.31 ± 0.07	2.00 ± 0.17	1.28 ± 0.21	-11.26 ± 0.22	0.34 ± 0.07	0.50 ± 0.13	4.11 ± 1.78	3.54 ± 0.47
G133.28+08.81_8	-39.82, 194.61	-11.22 ± 0.08	1.81 ± 0.26	1.12 ± 0.24	–	–	–	–	–
G133.28+08.81_9	-353.68, -38.86	-11.02 ± 0.06	1.39 ± 0.15	1.16 ± 0.20	–	–	–	–	–

TABLE 2—*Continued*

Name	Offset(R.A. DEC.)[a] ($'' \; ''$)	$V_{^{13}CO}$ km s^{-1}	$\Delta V_{^{13}CO}$ km s^{-1}	$T_{^{13}CO}$ K	$V_{C^{18}O}$ km s^{-1}	$\Delta V_{C^{18}O}$[b] km s^{-1}	$T_{C^{18}O}$ K	$\tau_{^{13}CO}$[c]	$T_{ex}(^{13}CO)$[d] K
G133.48+09.02_1	-68.03, 41.28	-16.22 ± 0.03	2.99 ± 0.06	6.22 ± 0.36	-16.19 ± 0.05	2.62 ± 0.12	1.32 ± 0.11	1.52 ± 0.31	16.61 ± 1.31
G133.48+09.02_2	94.14, 270.16	-16.35 ± 0.07	3.12 ± 0.15	3.62 ± 0.48	-16.31 ± 0.16	3.72 ± 0.39	0.61 ± 0.13	0.88 ± 0.66	11.99 ± 4.01
G133.48+09.02_3	125.04, -228.34	-14.72 ± 0.06	2.29 ± 0.15	3.57 ± 0.51	-14.63 ± 0.09	1.66 ± 0.29	0.84 ± 0.13	1.87 ± 0.71	9.90 ± 1.75
G133.48+09.02_4	-265.02, 248.58	-14.99 ± 0.15	3.77 ± 0.55	2.27 ± 0.41	–	–	–	–	–
G133.48+09.02_5	-264.64, -21.07	-15.38 ± 0.04	2.32 ± 0.10	3.51 ± 0.32	-15.92 ± 0.16	2.47 ± 0.38	0.53 ± 0.13	0.57 ± 0.19	13.78 ± 7.69
G136.31-01.77_1	-6.76, -40.87	-8.73 ± 0.02	1.58 ± 0.04	2.95 ± 0.13	-8.60 ± 0.08	1.21 ± 0.16	0.51 ± 0.09	0.93 ± 0.50	9.67 ± 1.78
G136.31-01.77_2	156.05, 377.85	-9.41 ± 0.04	1.43 ± 0.12	2.28 ± 0.29	–	–	–	–	–
G136.31-01.77_3	333.11, 188.10	-9.90 ± 0.06	2.34 ± 0.16	1.46 ± 0.21	–	–	–	–	–
G136.31-01.77_4	63.17, -367.20	-8.75 ± 0.04	1.39 ± 0.09	2.20 ± 0.21	–	–	–	–	–
G136.31-01.77_5	105.15, 168.31	-9.37 ± 0.02	1.64 ± 0.06	1.77 ± 0.10	–	–	–	–	–
G136.31-01.77_6	396.39, -68.64	-10.21 ± 0.05	1.37 ± 0.13	1.85 ± 0.28	–	–	–	–	–
G136.31-01.77_7	-71.74, -310.33	-9.19 ± 0.04	1.50 ± 0.12	1.33 ± 0.17	–	–	–	–	–
G140.49+06.07_1	-63.35, 3.28	-17.20 ± 0.01	2.18 ± 0.03	3.07 ± 0.10	-17.37 ± 0.13	1.97 ± 0.29	0.28 ± 0.06	0.20 ± 0.05	22.53 ± 7.51
G140.49+06.07_2	-183.43, 343.69	-18.25 ± 0.03	1.53 ± 0.07	3.78 ± 0.30	-18.15 ± 0.09	0.54 ± 0.11	0.64 ± 0.21	0.93 ± 0.91	12.23 ± 4.05
G140.49+06.07_3	-159.30, -311.64	-16.28 ± 0.03	1.67 ± 0.06	3.23 ± 0.23	-15.68 ± 0.10	0.70 ± 0.23	0.50 ± 0.15	0.65 ± 0.22	12.00 ± 6.13
G140.49+06.07_4	207.65, 63.38	-17.58 ± 0.01	1.21 ± 0.02	3.99 ± 0.12	-17.59 ± 0.12	1.15 ± 0.29	0.38 ± 0.09	0.20 ± 0.05	28.26 ± 9.42
G140.49+06.07_5	-28.86, -222.00	-16.57 ± 0.02	1.63 ± 0.05	3.04 ± 0.19	-16.64 ± 0.15	1.15 ± 0.37	0.34 ± 0.11	0.24 ± 0.06	19.24 ± 6.41
G140.49+06.07_6	-87.96, 215.14	-17.39 ± 0.02	1.99 ± 0.05	2.68 ± 0.13	–	–	–	–	–
G140.77+05.00_1	74.56, -45.41	-13.61 ± 0.01	1.36 ± 0.01	4.22 ± 0.07	-13.54 ± 0.04	1.17 ± 0.08	0.59 ± 0.05	0.38 ± 0.23	19.87 ± 6.50
G140.77+05.00_2	54.93, -384.27	-13.88 ± 0.01	1.34 ± 0.02	5.39 ± 0.14	-13.89 ± 0.11	1.22 ± 0.33	0.56 ± 0.14	0.22 ± 0.06	35.05 ± 11.68
G140.77+05.00_3	-271.93, 145.07	-13.88 ± 0.02	1.50 ± 0.04	2.72 ± 0.15	-13.93 ± 0.11	0.78 ± 0.22	0.36 ± 0.11	0.26 ± 0.06	16.57 ± 5.52
G140.77+05.00_4	49.69, -259.11	-13.78 ± 0.01	1.49 ± 0.02	3.45 ± 0.09	-13.86 ± 0.08	1.09 ± 0.18	0.36 ± 0.07	0.23 ± 0.06	22.63 ± 7.54
G140.77+05.00_5	-371.83, 4.89	-13.80 ± 0.04	1.43 ± 0.11	2.12 ± 0.23	–	–	–	–	–
G140.77+05.00_6	-108.78, 48.41	-14.02 ± 0.01	1.06 ± 0.03	2.92 ± 0.10	-14.20 ± 0.12	0.92 ± 0.31	0.24 ± 0.08	0.20 ± 0.05	23.06 ± 7.69
G140.77+05.00_7	176.04, -273.09	-14.06 ± 0.02	1.50 ± 0.04	2.59 ± 0.12	-14.22 ± 0.16	0.40 ± 0.08	0.29 ± 0.09	0.24 ± 0.06	16.57 ± 5.52
G142.49+07.48_1	-46.91, -80.24	-13.51 ± 0.02	1.72 ± 0.05	1.92 ± 0.11	-13.36 ± 0.12	0.97 ± 0.33	0.33 ± 0.09	0.91 ± 0.76	6.42 ± 1.85
G142.49+07.48_2	228.36, 131.68	-13.73 ± 0.02	1.14 ± 0.04	2.32 ± 0.13	–	–	–	–	–
G142.49+07.48_3	127.48, 386.95	-13.65 ± 0.02	0.60 ± 0.05	3.84 ± 0.29	–	–	–	–	–
G142.49+07.48_4	-366.16, -63.49	-13.22 ± 0.02	0.93 ± 0.04	2.67 ± 0.18	-13.31 ± 0.07	0.44 ± 0.18	0.74 ± 0.14	2.48 ± 0.79	7.22 ± 0.61
G142.49+07.48_5	392.32, 11.18	-13.66 ± 0.03	1.26 ± 0.07	2.12 ± 0.21	-11.85 ± 0.05	0.33 ± 0.07	0.67 ± 0.18	3.02 ± 1.28	5.65 ± 0.62
G142.49+07.48_6	-99.68, 386.49	-13.52 ± 0.03	0.87 ± 0.07	2.52 ± 0.27	–	–	–	–	–
G142.49+07.48_7	-227.92, -157.23	-13.25 ± 0.02	1.26 ± 0.05	2.31 ± 0.16	–	–	–	–	–
G142.49+07.48_8	73.99, 330.61	-13.67 ± 0.02	0.79 ± 0.05	2.98 ± 0.25	–	–	–	–	–
G142.49+07.48_9	102.41, 14.94	-13.38 ± 0.02	1.60 ± 0.05	2.23 ± 0.14	–	–	–	–	–
G142.49+07.48_10	224.03, -131.91	-13.34 ± 0.07	2.09 ± 0.17	0.96 ± 0.17	–	–	–	–	–
G142.49+07.48_11	-21.14, -427.92	–	–	–	–	–	–	–	–
G142.49+07.48_12	74.85, -229.61	-14.01 ± 0.03	1.14 ± 0.07	1.85 ± 0.17	-13.59 ± 0.06	0.33 ± 0.07	0.45 ± 0.14	2.00 ± 1.11	5.16 ± 0.70
G142.62+07.29_1	-3.79, -74.43	-11.43 ± 0.01	1.00 ± 0.02	2.94 ± 0.10	-11.37 ± 0.05	0.50 ± 0.10	0.46 ± 0.08	0.67 ± 0.44	10.83 ± 2.95
G142.62+07.29_2	-408.10, -75.40	-11.39 ± 0.04	1.21 ± 0.10	2.44 ± 0.33	–	–	–	–	–
G142.62+07.29_3	-29.94, 98.29	-12.24 ± 0.01	1.05 ± 0.03	2.44 ± 0.11	-12.27 ± 0.11	0.68 ± 0.20	0.26 ± 0.08	0.23 ± 0.06	16.12 ± 5.37
G142.62+07.29_4	-321.77, -51.78	-11.32 ± 0.03	1.31 ± 0.07	1.89 ± 0.17	–	–	–	–	–
G142.62+07.29_5	-132.01, -207.83	-12.67 ± 0.04	1.82 ± 0.08	1.35 ± 0.14	–	–	–	–	–
G142.62+07.29_6	-0.84, 244.23	-12.57 ± 0.02	0.98 ± 0.04	2.08 ± 0.13	–	–	–	–	–
G142.62+07.29_7	-162.20, 122.77	-12.61 ± 0.05	1.21 ± 0.20	1.37 ± 0.19	–	–	–	–	–

TABLE 2—*Continued*

Name	Offset(R.A. DEC.)[a] ($'' \; ''$)	$V_{^{13}CO}$ km s^{-1}	$\Delta V_{^{13}CO}$ km s^{-1}	$T_{^{13}CO}$ K	$V_{C^{18}O}$ km s^{-1}	$\Delta V_{C^{18}O}$[b] km s^{-1}	$T_{C^{18}O}$ K	$\tau_{^{13}CO}$[c]	$T_{ex}(^{13}CO)$[d] K
G142.62+07.29_8	-353.36, -208.13	–	–	–	–	–	–	–	–
G144.84+00.76_1	-92.04, 17.23	-30.34 ± 0.08	3.45 ± 0.18	2.13 ± 0.30	–	–	–	–	–
G144.84+00.76_2	216.26, -27.80	-30.12 ± 0.05	2.22 ± 0.12	2.62 ± 0.31	–	–	–	–	–
G144.84+00.76_3	33.66, -188.76	-29.48 ± 0.06	2.66 ± 0.14	2.11 ± 0.26	–	–	–	–	–
G144.84+00.76_4	337.97, -203.89	-30.25 ± 0.05	1.49 ± 0.10	2.51 ± 0.35	–	–	–	–	–
G144.84+00.76_5	407.64, -37.77	-30.81 ± 0.05	1.36 ± 0.12	3.17 ± 0.45	–	–	–	–	–
G144.84+00.76_6	-358.29, -183.75	-29.93 ± 0.10	2.27 ± 0.24	1.39 ± 0.33	–	–	–	–	–
G144.84+00.76_7	14.46, -410.93	–	–	–	–	–	–	–	–
G144.84+00.76_8	-240.48, 330.61	-32.16 ± 0.04	0.35 ± 0.16	3.20 ± 0.71	–	–	–	–	–
G144.84+00.76_9	-363.35, 42.35	–	–	–	–	–	–	–	–
G144.84+00.76_10	-58.47, 213.76	-30.73 ± 0.08	2.03 ± 0.23	1.87 ± 0.37	–	–	–	–	–
G144.84+00.76_11	106.33, -344.41	-28.91 ± 0.12	2.20 ± 0.26	1.65 ± 0.48	–	–	–	–	–
G144.84+00.76_12	-250.11, -284.31	–	–	–	–	–	–	–	–
G144.84+00.76_13	282.01, 105.46	-31.22 ± 0.17	2.94 ± 0.51	1.24 ± 0.40	–	–	–	–	–
G144.84+00.76_14	-164.50, -191.40	-29.26 ± 0.09	2.73 ± 0.24	1.48 ± 0.28	–	–	–	–	–
G146.11+07.80_1	15.88, -21.69	-11.83 ± 0.01	1.31 ± 0.02	3.18 ± 0.08	-11.77 ± 0.04	0.95 ± 0.09	0.60 ± 0.06	1.17 ± 0.29	9.74 ± 0.72
G146.11+07.80_2	160.33, 157.17	-12.17 ± 0.02	1.39 ± 0.04	2.26 ± 0.11	–	–	–	–	–
G146.11+07.80_3	39.73, -215.09	-11.84 ± 0.01	1.28 ± 0.03	2.92 ± 0.13	-11.90 ± 0.05	0.74 ± 0.12	0.62 ± 0.08	1.54 ± 0.44	8.44 ± 0.67
G146.11+07.80_4	-17.55, 324.27	-11.52 ± 0.03	1.36 ± 0.07	1.49 ± 0.13	–	–	–	–	–
G146.11+07.80_5	230.86, -56.99	-12.15 ± 0.01	0.75 ± 0.02	3.08 ± 0.13	-12.08 ± 0.08	0.70 ± 0.15	0.33 ± 0.08	0.23 ± 0.06	20.00 ± 6.67
G146.11+07.80_6	-37.70, -357.81	-11.88 ± 0.04	1.10 ± 0.09	1.52 ± 0.20	–	–	–	–	–
G146.71+02.05_1	34.98, 15.55	2.36 ± 0.01	0.97 ± 0.04	3.88 ± 0.21	2.35 ± 0.07	0.78 ± 0.15	0.52 ± 0.09	0.28 ± 0.07	22.15 ± 7.38
G146.71+02.05_2	-225.82, -58.60	2.25 ± 0.01	0.84 ± 0.03	3.52 ± 0.19	2.33 ± 0.11	0.80 ± 0.32	0.41 ± 0.11	0.25 ± 0.06	21.73 ± 7.24
G146.71+02.05_3	171.63, -193.06	1.45 ± 0.04	2.04 ± 0.08	1.76 ± 0.15	–	–	–	–	–
G146.71+02.05_4	363.97, -102.25	1.43 ± 0.07	2.70 ± 0.14	1.27 ± 0.19	–	–	–	–	–
G146.71+02.05_5	-352.29, -208.03	2.40 ± 0.02	0.78 ± 0.04	3.65 ± 0.30	–	–	–	–	–
G146.71+02.05_6	235.44, -11.45	2.39 ± 0.02	0.75 ± 0.05	3.15 ± 0.22	–	–	–	–	–
G146.71+02.05_7	-133.28, -251.97	2.44 ± 0.02	0.83 ± 0.05	2.23 ± 0.17	–	–	–	–	–
G146.71+02.05_8	-224.57, 167.84	1.94 ± 0.02	0.75 ± 0.06	1.93 ± 0.17	1.07 ± 0.06	0.33 ± 0.07	0.54 ± 0.13	2.49 ± 0.99	5.24 ± 0.55
G147.01+03.39_1	-9.23, 9.90	-4.70 ± 0.01	0.74 ± 0.02	3.33 ± 0.13	-4.67 ± 0.08	0.68 ± 0.17	0.41 ± 0.10	0.20 ± 0.05	50.00 ± 5.00
G148.00+00.09_1	387.97, -71.98	-32.49 ± 0.02	2.53 ± 0.05	3.93 ± 0.19	-32.66 ± 0.14	1.82 ± 0.52	0.65 ± 0.16	0.90 ± 0.70	12.85 ± 3.39
G148.00+00.09_2	188.20, -15.39	-33.34 ± 0.01	2.52 ± 0.03	3.01 ± 0.10	-33.31 ± 0.12	2.13 ± 0.21	0.39 ± 0.08	0.28 ± 0.07	17.38 ± 5.79
G148.00+00.09_3	389.81, 118.97	-33.42 ± 0.03	1.27 ± 0.09	4.83 ± 0.45	–	–	–	–	–
G148.00+00.09_4	19.59, -150.16	-33.95 ± 0.01	1.85 ± 0.03	3.49 ± 0.10	-33.86 ± 0.05	1.17 ± 0.13	0.61 ± 0.07	1.07 ± 0.31	10.90 ± 0.99
G148.00+00.09_5	297.62, -237.61	-33.20 ± 0.01	1.42 ± 0.04	3.93 ± 0.17	-33.14 ± 0.07	0.76 ± 0.20	0.75 ± 0.15	1.32 ± 0.60	11.55 ± 1.38
G148.00+00.09_6	170.56, 232.03	-34.31 ± 0.01	1.52 ± 0.03	2.93 ± 0.12	-34.33 ± 0.13	1.02 ± 0.23	0.30 ± 0.09	0.22 ± 0.06	19.54 ± 6.51
G148.00+00.09_7	-27.64, -356.72	-33.48 ± 0.03	2.12 ± 0.07	2.08 ± 0.17	–	–	–	–	–
G148.00+00.09_8	-73.40, 124.98	-34.06 ± 0.02	1.44 ± 0.04	2.88 ± 0.14	–	–	–	–	–
G148.00+00.09_9	-55.45, 359.08	-33.93 ± 0.02	1.19 ± 0.05	3.42 ± 0.23	–	–	–	–	–
G148.00+00.09_10	334.72, 20.50	-33.17 ± 0.02	2.23 ± 0.04	3.81 ± 0.16	-32.68 ± 0.05	0.62 ± 0.12	0.93 ± 0.15	2.12 ± 0.59	10.34 ± 0.61
G148.00+00.09_11	-293.87, -150.48	-33.92 ± 0.04	1.31 ± 0.10	2.08 ± 0.26	–	–	–	–	–
G148.00+00.09_12	416.96, -96.60	-32.53 ± 0.03	2.43 ± 0.06	4.26 ± 0.28	-32.81 ± 0.12	1.43 ± 0.25	0.95 ± 0.24	1.81 ± 0.86	11.69 ± 1.23
G148.00+00.09_13	-143.90, -238.07	-33.79 ± 0.02	1.65 ± 0.05	2.63 ± 0.17	–	–	–	–	–
G148.24+00.41_1	-348.83, 124.41	-33.50 ± 0.02	2.13 ± 0.04	4.34 ± 0.19	-34.07 ± 0.05	0.76 ± 0.15	1.02 ± 0.16	1.99 ± 0.55	11.72 ± 0.71

TABLE 2—*Continued*

Name	Offset(R.A. DEC.)[a] ($'' \; ''$)	$V_{^{13}CO}$ km s^{-1}	$\Delta V_{^{13}CO}$ km s^{-1}	$T_{^{13}CO}$ K	$V_{C^{18}O}$ km s^{-1}	$\Delta V_{C^{18}O}$[b] km s^{-1}	$T_{C^{18}O}$ K	$\tau_{^{13}CO}$[c]	$T_{ex}(^{13}CO)$[d] K
G148.24+00.41_2	-214.68, 79.88	-33.73 ± 0.01	2.05 ± 0.03	4.09 ± 0.13	-33.79 ± 0.06	1.75 ± 0.13	0.80 ± 0.09	1.40 ± 0.34	11.83 ± 0.78
G148.24+00.41_3	-321.90, -176.71	-33.52 ± 0.03	2.49 ± 0.08	2.56 ± 0.18	-33.25 ± 0.19	1.82 ± 0.40	0.40 ± 0.13	0.75 ± 0.25	9.08 ± 4.19
G148.24+00.41_4	29.19, 46.36	-34.80 ± 0.01	1.59 ± 0.02	3.14 ± 0.09	-34.78 ± 0.05	1.17 ± 0.12	0.61 ± 0.07	1.39 ± 0.33	9.25 ± 0.59
G148.24+00.41_5	-24.59, -376.60	-33.95 ± 0.04	3.05 ± 0.09	1.53 ± 0.12	–	–	–	–	–
G148.24+00.41_6	-148.60, -47.74	-33.80 ± 0.02	2.20 ± 0.04	2.76 ± 0.12	-33.82 ± 0.09	1.50 ± 0.20	0.51 ± 0.09	1.24 ± 0.54	8.38 ± 1.05
G148.24+00.41_7	-95.95, -238.17	-33.93 ± 0.03	2.77 ± 0.09	1.47 ± 0.10	–	–	–	–	–
G149.23+03.07_1	7.11, -188.49	2.83 ± 0.01	1.30 ± 0.02	4.45 ± 0.14	2.65 ± 0.12	1.00 ± 0.37	0.34 ± 0.09	0.20 ± 0.05	37.09 ± 12.36
G149.23+03.07_2	-158.24, -371.10	2.57 ± 0.02	1.04 ± 0.04	5.76 ± 0.36	–	–	–	–	–
G149.23+03.07_3	-44.41, 96.78	3.21 ± 0.01	1.19 ± 0.02	4.20 ± 0.13	3.23 ± 0.10	1.07 ± 0.19	0.42 ± 0.09	0.22 ± 0.05	28.31 ± 9.44
G149.23+03.07_4	-311.82, -133.32	2.87 ± 0.01	1.24 ± 0.03	3.97 ± 0.19	2.88 ± 0.12	0.90 ± 0.28	0.43 ± 0.13	0.24 ± 0.06	25.29 ± 8.43
G149.23+03.07_5	252.25, -14.61	3.06 ± 0.01	1.07 ± 0.02	4.29 ± 0.13	2.98 ± 0.15	1.10 ± 0.26	0.32 ± 0.10	0.20 ± 0.05	35.98 ± 11.99
G149.41+03.37_1	15.73, 42.72	3.28 ± 0.01	1.25 ± 0.02	4.27 ± 0.10	3.23 ± 0.06	1.11 ± 0.15	0.58 ± 0.08	0.30 ± 0.10	23.05 ± 7.68
G149.41+03.37_2	360.24, -134.24	3.36 ± 0.01	1.16 ± 0.03	4.48 ± 0.18	3.28 ± 0.09	1.00 ± 0.18	0.66 ± 0.14	0.49 ± 0.16	18.41 ± 6.14
G149.41+03.37_3	-375.32, 123.84	3.39 ± 0.02	1.28 ± 0.05	3.62 ± 0.25	–	–	–	–	–
G149.41+03.37_4	-139.98, -137.79	3.28 ± 0.01	1.02 ± 0.02	4.17 ± 0.12	3.04 ± 0.09	0.64 ± 0.31	0.33 ± 0.09	0.20 ± 0.05	33.91 ± 11.30
G149.41+03.37_5	-152.36, -373.20	3.12 ± 0.03	1.28 ± 0.09	2.82 ± 0.30	–	–	–	–	–
G149.41+03.37_6	282.50, 219.08	3.30 ± 0.02	1.13 ± 0.03	2.96 ± 0.15	3.15 ± 0.05	0.40 ± 0.08	0.87 ± 0.11	2.69 ± 0.56	7.94 ± 0.46
G149.41+03.37_7	263.32, -304.05	3.19 ± 0.02	1.20 ± 0.05	3.59 ± 0.27	–	–	–	–	–
G149.41+03.37_8	-267.72, 164.15	3.47 ± 0.02	1.15 ± 0.03	3.90 ± 0.20	–	–	–	–	–
G149.41+03.37_9	99.66, -365.07	3.09 ± 0.02	1.20 ± 0.04	2.97 ± 0.19	–	–	–	–	–
G149.41+03.37_10	244.83, -131.34	3.33 ± 0.01	1.17 ± 0.02	4.44 ± 0.15	3.22 ± 0.10	0.94 ± 0.20	0.52 ± 0.12	0.25 ± 0.06	26.84 ± 8.95
G149.52-01.23_1	-27.96, 8.55	-7.97 ± 0.01	2.34 ± 0.03	4.10 ± 0.11	-7.77 ± 0.06	1.60 ± 0.14	0.54 ± 0.06	0.25 ± 0.06	25.34 ± 8.45
G149.52-01.23_2	-13.74, 317.80	-8.01 ± 0.03	2.55 ± 0.06	2.57 ± 0.14	-7.67 ± 0.11	0.76 ± 0.38	0.38 ± 0.10	0.49 ± 0.16	10.85 ± 7.38
G149.52-01.23_3	-183.03, 368.15	-7.71 ± 0.03	1.53 ± 0.07	4.52 ± 0.38	–	–	–	–	–
G149.52-01.23_4	104.09, -390.24	-7.77 ± 0.04	1.44 ± 0.11	3.42 ± 0.33	–	–	–	–	–
G149.52-01.23_5	29.95, -206.06	-7.63 ± 0.01	1.73 ± 0.03	3.43 ± 0.12	-7.38 ± 0.11	1.54 ± 0.27	0.41 ± 0.09	0.26 ± 0.06	20.78 ± 6.93
G149.52-01.23_6	-134.43, -187.85	-8.21 ± 0.02	1.80 ± 0.05	3.10 ± 0.15	–	–	–	–	–
G149.52-01.23_7	179.51, -141.67	-8.19 ± 0.03	1.57 ± 0.11	1.98 ± 0.17	–	–	–	–	–
G149.58+03.45_1	-69.81, -9.11	3.44 ± 0.01	1.29 ± 0.02	4.26 ± 0.10	3.59 ± 0.04	0.92 ± 0.10	0.77 ± 0.08	1.05 ± 0.30	13.17 ± 1.17
G149.58+03.45_2	339.78, 68.55	3.36 ± 0.01	1.41 ± 0.03	3.94 ± 0.15	3.44 ± 0.06	1.14 ± 0.15	0.71 ± 0.10	1.03 ± 0.42	12.35 ± 1.62
G149.58+03.45_3	-405.46, 35.76	3.30 ± 0.03	1.57 ± 0.06	3.34 ± 0.27	2.86 ± 0.05	0.33 ± 0.07	0.78 ± 0.23	1.81 ± 1.04	9.34 ± 1.23
G149.58+03.45_4	-360.28, -132.96	3.16 ± 0.02	1.04 ± 0.04	3.67 ± 0.21	–	–	–	–	–
G149.58+03.45_5	126.13, 218.58	3.71 ± 0.02	1.54 ± 0.08	2.14 ± 0.13	3.66 ± 0.10	0.73 ± 0.23	0.38 ± 0.10	0.98 ± 0.79	6.95 ± 1.83
G149.58+03.45_6	-138.35, -256.72	3.05 ± 0.01	0.99 ± 0.03	3.16 ± 0.14	–	–	–	–	–
G149.65+03.54_1	-384.78, -105.36	3.48 ± 0.02	1.24 ± 0.04	5.24 ± 0.30	3.71 ± 0.05	0.58 ± 0.09	1.24 ± 0.20	1.87 ± 0.59	13.91 ± 1.09
G149.65+03.54_2	320.96, -110.65	3.16 ± 0.01	1.70 ± 0.02	3.51 ± 0.11	3.73 ± 0.04	0.46 ± 0.06	0.73 ± 0.08	1.46 ± 0.34	10.17 ± 0.63
G149.65+03.54_3	-115.54, -55.16	3.47 ± 0.01	1.31 ± 0.02	4.09 ± 0.10	3.61 ± 0.04	0.91 ± 0.17	0.58 ± 0.06	0.42 ± 0.25	18.48 ± 6.00
G149.65+03.54_4	57.01, -395.13	3.13 ± 0.02	1.49 ± 0.04	3.57 ± 0.19	–	–	–	–	–
G149.65+03.54_5	202.97, -273.05	3.37 ± 0.01	1.41 ± 0.03	3.64 ± 0.13	3.67 ± 0.04	0.33 ± 0.07	0.61 ± 0.06	0.85 ± 0.29	12.15 ± 1.57
G149.65+03.54_6	-391.16, 111.47	3.52 ± 0.05	1.26 ± 0.12	3.19 ± 0.46	–	–	–	–	–
G149.65+03.54_7	-199.86, -322.24	2.97 ± 0.01	0.99 ± 0.04	3.82 ± 0.20	–	–	–	–	–
G149.65+03.54_8	90.06, 87.63	3.46 ± 0.01	1.82 ± 0.03	2.56 ± 0.09	3.63 ± 0.11	1.72 ± 0.29	0.26 ± 0.05	0.22 ± 0.06	17.24 ± 5.75
G150.22+03.91_1	-23.00, 6.73	3.06 ± 0.01	1.47 ± 0.02	4.51 ± 0.10	3.31 ± 0.04	1.12 ± 0.11	0.92 ± 0.09	1.41 ± 0.32	12.89 ± 0.72
G150.22+03.91_2	-13.22, -401.13	3.04 ± 0.01	0.84 ± 0.03	6.85 ± 0.30	2.91 ± 0.03	0.33 ± 0.07	1.37 ± 0.25	1.34 ± 0.55	18.45 ± 2.09

TABLE 2—*Continued*

Name	Offset(R.A. DEC.)[a] (″ ″)	$V_{^{13}CO}$ km s^{-1}	$\Delta V_{^{13}CO}$ km s^{-1}	$T_{^{13}CO}$ K	$V_{C^{18}O}$ km s^{-1}	$\Delta V_{C^{18}O}$[b] km s^{-1}	$T_{C^{18}O}$ K	$\tau_{^{13}CO}$[c]	$T_{ex}(^{13}CO)$[d] K
G150.22+03.91_3	-377.18, -69.15	3.15 ± 0.02	1.27 ± 0.03	4.97 ± 0.24	3.33 ± 0.10	0.84 ± 0.18	0.71 ± 0.19	0.44 ± 0.15	21.56 ± 7.19
G150.22+03.91_4	184.92, -324.73	2.88 ± 0.01	1.01 ± 0.02	6.25 ± 0.18	2.83 ± 0.04	0.48 ± 0.10	1.31 ± 0.15	1.48 ± 0.36	16.77 ± 1.02
G150.22+03.91_5	377.23, -121.92	3.02 ± 0.01	1.10 ± 0.03	5.25 ± 0.25	3.14 ± 0.06	0.71 ± 0.13	1.13 ± 0.21	1.56 ± 0.61	14.37 ± 1.34
G150.22+03.91_6	-161.45, -234.68	2.96 ± 0.01	1.03 ± 0.02	5.21 ± 0.17	3.01 ± 0.08	0.90 ± 0.26	0.55 ± 0.11	0.22 ± 0.06	33.71 ± 11.24
G150.22+03.91_7	310.39, 77.93	3.24 ± 0.01	1.14 ± 0.02	4.03 ± 0.13	3.37 ± 0.11	1.00 ± 0.21	0.43 ± 0.12	0.23 ± 0.06	26.01 ± 8.67
G150.44+03.95_1	138.86, 228.10	3.00 ± 0.01	1.51 ± 0.03	4.56 ± 0.16	2.98 ± 0.12	1.09 ± 0.26	0.51 ± 0.12	0.24 ± 0.06	28.28 ± 9.43
G150.44+03.95_2	-133.88, -19.91	3.17 ± 0.01	1.10 ± 0.02	4.82 ± 0.14	3.17 ± 0.04	0.51 ± 0.09	1.09 ± 0.13	1.72 ± 0.39	13.14 ± 0.67
G150.44+03.95_3	-347.07, -208.30	3.37 ± 0.02	1.02 ± 0.03	5.45 ± 0.28	3.47 ± 0.02	0.33 ± 0.07	2.04 ± 0.23	3.82 ± 0.66	13.49 ± 0.61
G150.44+03.95_4	-345.49, 207.63	2.95 ± 0.02	0.95 ± 0.04	6.00 ± 0.36	2.94 ± 0.05	0.71 ± 0.12	1.99 ± 0.29	3.21 ± 0.75	14.69 ± 0.79
G150.44+03.95_5	-182.49, -302.29	3.31 ± 0.01	0.92 ± 0.03	5.64 ± 0.27	3.26 ± 0.07	0.55 ± 0.11	0.88 ± 0.20	0.65 ± 0.59	19.95 ± 7.84
G150.44+03.95_6	-217.43, 253.27	3.05 ± 0.02	1.26 ± 0.04	5.16 ± 0.24	3.17 ± 0.05	0.44 ± 0.16	1.52 ± 0.20	2.69 ± 0.57	13.16 ± 0.63
G150.44+03.95_7	134.82, -164.94	3.19 ± 0.01	1.11 ± 0.03	4.52 ± 0.17	3.18 ± 0.04	0.65 ± 0.10	0.86 ± 0.11	1.20 ± 0.40	13.40 ± 1.33
G151.08+04.46_1	-92.21, -144.30	3.18 ± 0.00	0.87 ± 0.01	5.92 ± 0.09	3.25 ± 0.02	0.69 ± 0.05	0.86 ± 0.06	0.48 ± 0.18	23.99 ± 4.54
G151.08+04.46_2	-246.08, 287.15	3.22 ± 0.01	1.02 ± 0.02	4.81 ± 0.16	3.25 ± 0.05	0.89 ± 0.11	0.83 ± 0.12	0.91 ± 0.40	15.32 ± 2.31
G151.08+04.46_3	-287.72, -274.61	3.28 ± 0.01	1.05 ± 0.03	5.56 ± 0.28	3.25 ± 0.07	0.85 ± 0.15	1.04 ± 0.19	1.14 ± 0.55	16.23 ± 2.42
G151.08+04.46_4	-83.33, 261.04	3.05 ± 0.01	0.92 ± 0.01	5.13 ± 0.11	3.05 ± 0.02	0.74 ± 0.06	0.99 ± 0.07	1.24 ± 0.22	14.83 ± 0.77
G151.08+04.46_5	-357.86, -72.17	3.27 ± 0.01	0.83 ± 0.02	5.73 ± 0.16	3.30 ± 0.03	0.53 ± 0.06	1.06 ± 0.11	1.11 ± 0.30	16.77 ± 1.41
G151.08+04.46_6	-397.47, 85.81	3.25 ± 0.01	0.70 ± 0.03	5.74 ± 0.28	3.16 ± 0.08	0.50 ± 0.10	1.01 ± 0.22	0.97 ± 0.61	17.48 ± 3.69
G151.08+04.46_7	-114.45, 31.17	3.32 ± 0.00	0.71 ± 0.01	6.06 ± 0.10	3.27 ± 0.01	0.53 ± 0.02	1.45 ± 0.06	1.91 ± 0.16	15.62 ± 0.33
G151.08+04.46_8	130.31, 233.01	3.00 ± 0.01	0.68 ± 0.01	4.62 ± 0.12	3.04 ± 0.04	0.56 ± 0.11	0.57 ± 0.08	0.20 ± 0.05	50.00 ± 5.00
G151.45+03.95_1	-34.86, -19.97	1.64 ± 0.01	2.16 ± 0.02	4.87 ± 0.09	1.57 ± 0.07	2.04 ± 0.14	0.51 ± 0.06	0.22 ± 0.06	31.81 ± 10.60
G151.45+03.95_2	-302.13, -104.53	1.70 ± 0.01	1.86 ± 0.02	4.76 ± 0.10	1.71 ± 0.06	1.30 ± 0.18	0.60 ± 0.08	0.20 ± 0.05	44.25 ± 14.75
G151.45+03.95_3	295.10, -9.87	1.08 ± 0.01	1.35 ± 0.02	4.56 ± 0.12	1.07 ± 0.12	0.85 ± 0.20	0.30 ± 0.09	0.20 ± 0.05	42.14 ± 14.05
G151.45+03.95_4	-284.99, 269.69	1.86 ± 0.03	1.88 ± 0.08	3.42 ± 0.27	–	–	–	–	–
G151.45+03.95_5	229.72, 320.75	1.94 ± 0.04	2.13 ± 0.09	2.79 ± 0.23	–	–	–	–	–
G151.45+03.95_6	194.37, 204.64	1.67 ± 0.01	1.88 ± 0.03	3.65 ± 0.11	–	–	–	–	–
G151.45+03.95_7	-402.90, 62.08	1.72 ± 0.03	1.58 ± 0.09	3.86 ± 0.36	–	–	–	–	–
G151.45+03.95_8	-31.57, 379.26	1.72 ± 0.02	1.68 ± 0.05	3.32 ± 0.20	–	–	–	–	–
G151.45+03.95_9	193.28, -188.74	1.12 ± 0.01	1.28 ± 0.02	5.30 ± 0.12	0.92 ± 0.13	0.98 ± 0.26	0.30 ± 0.10	0.20 ± 0.05	50.00 ± 5.00
G154.90+04.61_1	18.75, -112.68	3.52 ± 0.01	1.67 ± 0.01	4.77 ± 0.08	3.40 ± 0.08	1.21 ± 0.17	0.38 ± 0.07	0.20 ± 0.05	38.17 ± 12.72
G154.90+04.61_2	-146.87, 181.31	3.89 ± 0.01	1.43 ± 0.02	4.03 ± 0.08	3.61 ± 0.06	0.84 ± 0.17	0.40 ± 0.07	0.21 ± 0.05	27.46 ± 9.15
G154.90+04.61_3	361.89, 146.84	4.22 ± 0.03	1.06 ± 0.11	3.77 ± 0.32	4.36 ± 0.06	0.33 ± 0.07	1.00 ± 0.22	2.27 ± 0.89	10.15 ± 1.05
G154.90+04.61_4	353.02, -169.73	3.54 ± 0.03	1.73 ± 0.06	3.46 ± 0.26	3.41 ± 0.05	0.33 ± 0.07	0.77 ± 0.18	1.67 ± 0.81	9.79 ± 1.23
G154.90+04.61_5	211.89, -109.44	3.35 ± 0.01	1.45 ± 0.02	3.83 ± 0.12	3.36 ± 0.09	0.82 ± 0.20	0.34 ± 0.09	0.20 ± 0.05	28.17 ± 9.39
G154.90+04.61_6	140.98, 67.66	3.64 ± 0.01	1.71 ± 0.03	2.82 ± 0.10	–	–	–	–	–
G154.90+04.61_7	222.40, 291.67	4.25 ± 0.04	1.79 ± 0.09	1.99 ± 0.19	–	–	–	–	–
G156.04+06.03_1	-51.14, -40.45	5.66 ± 0.01	0.91 ± 0.03	3.31 ± 0.15	5.79 ± 0.03	0.33 ± 0.07	0.65 ± 0.09	1.26 ± 0.44	9.94 ± 1.02
G156.04+06.03_2	275.68, 72.82	4.58 ± 0.04	1.71 ± 0.19	1.63 ± 0.19	–	–	–	–	–
G156.04+06.03_3	-227.01, -78.60	5.36 ± 0.02	1.10 ± 0.03	3.39 ± 0.18	–	–	–	–	–
G156.20+05.26_1	11.86, -69.05	5.40 ± 0.01	0.77 ± 0.02	4.82 ± 0.17	5.36 ± 0.05	0.63 ± 0.12	0.51 ± 0.08	0.23 ± 0.06	31.18 ± 10.39
G156.20+05.26_2	-11.22, 162.33	5.31 ± 0.02	0.86 ± 0.05	3.70 ± 0.27	5.31 ± 0.09	0.54 ± 0.20	0.30 ± 0.09	0.20 ± 0.05	29.83 ± 9.94
G156.20+05.26_3	256.71, 223.02	5.69 ± 0.03	1.28 ± 0.07	1.90 ± 0.19	–	–	–	–	–
G157.25-01.00_1	-34.82, 90.25	5.20 ± 0.00	0.63 ± 0.01	7.17 ± 0.10	5.27 ± 0.01	0.43 ± 0.03	1.98 ± 0.05	2.43 ± 0.11	17.24 ± 0.23
G157.25-01.00_2	-59.65, -374.48	5.11 ± 0.01	0.52 ± 0.01	8.24 ± 0.24	5.11 ± 0.04	0.47 ± 0.08	1.20 ± 0.13	0.48 ± 0.27	31.93 ± 10.64

TABLE 2—*Continued*

Name	Offset(R.A. DEC.)[a] ($'' \; ''$)	$V_{^{13}CO}$ km s^{-1}	$\Delta V_{^{13}CO}$ km s^{-1}	$T_{^{13}CO}$ K	$V_{C^{18}O}$ km s^{-1}	$\Delta V_{C^{18}O}$[b] km s^{-1}	$T_{C^{18}O}$ K	$\tau_{^{13}CO}$[c]	$T_{ex}(^{13}CO)$[d] K
G157.25-01.00_3	-221.31, 330.33	5.33 ± 0.01	0.64 ± 0.02	6.96 ± 0.24	5.30 ± 0.04	0.41 ± 0.09	2.22 ± 0.18	3.04 ± 0.39	16.54 ± 0.50
G157.25-01.00_4	-389.39, 107.18	5.36 ± 0.01	0.47 ± 0.02	7.13 ± 0.24	–	–	–	–	–
G157.25-01.00_5	-89.22, -209.73	5.15 ± 0.00	0.54 ± 0.01	8.02 ± 0.12	5.15 ± 0.01	0.51 ± 0.04	1.60 ± 0.07	1.33 ± 0.13	20.86 ± 0.65
G157.25-01.00_6	-229.96, 224.53	5.33 ± 0.00	0.58 ± 0.01	7.46 ± 0.14	5.37 ± 0.02	0.41 ± 0.03	1.87 ± 0.10	2.08 ± 0.19	18.12 ± 0.40
G159.52+03.26_1	-38.49, -59.14	-15.09 ± 0.02	3.71 ± 0.05	2.26 ± 0.09	-14.89 ± 0.25	4.12 ± 0.69	0.28 ± 0.08	0.20 ± 0.05	17.53 ± 5.84
G159.52+03.26_2	-254.52, 263.96	-15.76 ± 0.04	2.92 ± 0.11	2.06 ± 0.18	–	–	–	–	–
G159.52+03.26_3	-144.78, 164.50	-15.67 ± 0.06	3.40 ± 0.13	1.39 ± 0.15	–	–	–	–	–
G159.52+03.26_4	47.42, -237.04	-15.71 ± 0.05	3.49 ± 0.12	1.32 ± 0.13	–	–	–	–	–
G159.52+03.26_5	-10.58, 245.45	-17.58 ± 0.03	2.44 ± 0.09	1.72 ± 0.13	-17.46 ± 0.19	1.19 ± 0.49	0.36 ± 0.10	1.59 ± 0.91	5.01 ± 0.72
G159.52+03.26_6	122.98, -26.10	-17.85 ± 0.05	3.33 ± 0.13	1.15 ± 0.12	–	–	–	–	–
G159.52+03.26_7	-236.46, 350.21	-16.31 ± 0.10	2.69 ± 0.24	2.01 ± 0.42	–	–	–	–	–
G159.52+03.26_8	-80.66, -208.37	-15.24 ± 0.04	2.24 ± 0.12	1.47 ± 0.15	-15.06 ± 0.09	0.44 ± 0.15	0.41 ± 0.11	2.66 ± 1.15	4.06 ± 0.44
G159.52+03.26_9	57.06, 114.38	-18.02 ± 0.05	2.85 ± 0.11	1.26 ± 0.13	–	–	–	–	–
G159.52+03.26_10	-146.82, 35.86	-15.09 ± 0.05	3.04 ± 0.17	1.45 ± 0.15	–	–	–	–	–
G162.79+01.34_1	-41.62, -156.53	0.55 ± 0.02	1.57 ± 0.04	3.14 ± 0.15	–	–	–	–	–
G162.79+01.34_2	-253.23, 243.72	0.45 ± 0.03	2.37 ± 0.09	2.27 ± 0.18	–	–	–	–	–
G162.79+01.34_3	-21.59, 195.16	1.06 ± 0.02	1.92 ± 0.05	2.58 ± 0.14	1.17 ± 0.08	0.82 ± 0.18	0.44 ± 0.09	0.89 ± 0.60	8.60 ± 2.06
G162.79+01.34_4	-240.65, 42.39	0.23 ± 0.02	1.59 ± 0.06	2.92 ± 0.17	–	–	–	–	–
G162.79+01.34_5	170.62, -167.84	0.45 ± 0.02	1.57 ± 0.05	2.80 ± 0.17	–	–	–	–	–
G169.14-01.13_1	-22.93, -72.14	-9.21 ± 0.01	2.29 ± 0.03	2.52 ± 0.09	-9.01 ± 0.14	2.27 ± 0.37	0.30 ± 0.07	0.20 ± 0.05	28.34 ± 9.45
G169.14-01.13_2	92.64, 114.74	-9.37 ± 0.02	2.28 ± 0.05	1.94 ± 0.10	–	–	–	–	–
G169.14-01.13_3	321.14, 247.88	-9.33 ± 0.06	2.27 ± 0.14	1.94 ± 0.24	–	–	–	–	–
G169.14-01.13_4	-254.76, -50.22	-9.41 ± 0.02	1.70 ± 0.06	2.02 ± 0.13	–	–	–	–	–
G169.14-01.13_5	369.46, 161.20	-9.79 ± 0.04	1.67 ± 0.11	1.92 ± 0.21	–	–	–	–	–
G169.14-01.13_6	-402.36, -113.17	-9.69 ± 0.11	1.80 ± 0.23	0.99 ± 0.28	–	–	–	–	–
G169.14-01.13_7	240.73, 6.62	-9.85 ± 0.02	1.33 ± 0.07	1.67 ± 0.12	–	–	–	–	–
G169.14-01.13_8	267.36, 201.66	-9.60 ± 0.03	1.84 ± 0.08	2.18 ± 0.17	–	–	–	–	–
G169.14-01.13_9	-206.07, -204.61	-9.27 ± 0.03	0.92 ± 0.09	1.90 ± 0.23	–	–	–	–	–
G169.14-01.13_10	-325.27, -150.34	-9.27 ± 0.04	0.65 ± 0.10	2.17 ± 0.35	–	–	–	–	–
G169.14-01.13_11	358.17, 233.01	-9.60 ± 0.07	2.58 ± 0.19	2.01 ± 0.33	–	–	–	–	–
G169.14-01.13_12	116.21, -172.91	-7.96 ± 0.03	1.21 ± 0.09	1.80 ± 0.18	–	–	–	–	–
G171.03+02.66_1	60.74, -97.74	-20.53 ± 0.02	3.26 ± 0.05	2.21 ± 0.10	-20.77 ± 0.17	2.59 ± 0.30	0.29 ± 0.08	0.33 ± 0.11	11.62 ± 3.87
G171.03+02.66_2	-114.61, 78.99	-20.68 ± 0.03	3.38 ± 0.06	1.82 ± 0.11	-21.53 ± 0.15	1.57 ± 0.36	0.34 ± 0.09	1.27 ± 0.82	5.55 ± 1.00
G171.03+02.66_3	107.90, -341.83	-19.57 ± 0.03	1.56 ± 0.09	2.46 ± 0.17	-19.63 ± 0.07	0.58 ± 0.13	0.55 ± 0.12	1.82 ± 0.79	6.92 ± 0.77
G171.03+02.66_4	-126.96, 376.55	-20.67 ± 0.06	1.95 ± 0.12	1.96 ± 0.27	-20.83 ± 0.08	0.83 ± 0.17	0.78 ± 0.17	4.34 ± 1.58	5.15 ± 0.73
G171.03+02.66_5	-136.02, -225.22	-20.26 ± 0.05	2.89 ± 0.11	1.36 ± 0.13	–	–	–	–	–
G171.03+02.66_6	-42.06, 302.53	-20.94 ± 0.04	2.20 ± 0.09	1.56 ± 0.16	-21.11 ± 0.12	0.88 ± 0.29	0.42 ± 0.13	2.48 ± 1.28	4.30 ± 0.50
G171.03+02.66_7	363.50, -159.41	-19.96 ± 0.06	2.03 ± 0.17	1.35 ± 0.20	–	–	–	–	–
G171.03+02.66_8	-260.40, 168.75	-19.49 ± 0.02	0.91 ± 0.06	2.22 ± 0.20	-19.61 ± 0.11	0.38 ± 0.13	0.63 ± 0.14	2.67 ± 1.00	5.97 ± 0.64
G171.34+02.59_1	-48.97, -284.73	-19.38 ± 0.02	2.14 ± 0.03	3.33 ± 0.12	-19.60 ± 0.17	2.18 ± 0.49	0.32 ± 0.09	0.21 ± 0.05	23.34 ± 7.78
G171.34+02.59_2	5.41, 43.14	-19.36 ± 0.01	2.54 ± 0.03	2.89 ± 0.09	-19.34 ± 0.14	2.35 ± 0.32	0.38 ± 0.08	0.32 ± 0.11	15.41 ± 5.14
G171.34+02.59_3	-9.28, 412.73	-19.08 ± 0.03	1.82 ± 0.09	2.34 ± 0.21	–	–	–	–	–
G171.34+02.59_4	-160.03, 316.04	-19.25 ± 0.04	2.26 ± 0.09	1.72 ± 0.14	–	–	–	–	–
G171.34+02.59_5	103.67, -387.54	-19.25 ± 0.03	1.96 ± 0.08	3.03 ± 0.25	-19.59 ± 0.11	0.67 ± 0.22	0.68 ± 0.20	1.84 ± 1.03	8.49 ± 1.13

TABLE 2—*Continued*

Name	Offset(R.A. DEC.)[a] (″ ″)	$V_{^{13}CO}$ km s^{-1}	$\Delta V_{^{13}CO}$ km s^{-1}	$T_{^{13}CO}$ K	$V_{C^{18}O}$ km s^{-1}	$\Delta V_{C^{18}O}$[b] km s^{-1}	$T_{C^{18}O}$ K	$\tau_{^{13}CO}$[c]	$T_{ex}(^{13}CO)$[d] K
G171.34+02.59_6	191.60, 313.73	-18.86 ± 0.08	3.88 ± 0.16	1.02 ± 0.14	–	–	–	–	–
G171.34+02.59_7	220.80, 54.02	-20.49 ± 0.04	1.30 ± 0.09	2.51 ± 0.27	–	–	–	–	–
G172.85+02.27_1	26.84, -84.80	-17.12 ± 0.01	3.49 ± 0.03	4.86 ± 0.11	-17.24 ± 0.06	2.30 ± 0.15	0.80 ± 0.08	0.88 ± 0.27	15.62 ± 1.70
G172.85+02.27_2	310.61, -47.49	-16.98 ± 0.02	3.49 ± 0.04	4.08 ± 0.12	-17.22 ± 0.16	3.09 ± 0.32	0.37 ± 0.08	0.20 ± 0.05	29.66 ± 9.89
G172.85+02.27_3	-215.17, 232.74	-16.70 ± 0.02	3.68 ± 0.05	3.50 ± 0.14	-16.67 ± 0.17	2.76 ± 0.42	0.42 ± 0.11	0.20 ± 0.05	39.32 ± 13.11
G172.85+02.27_4	115.71, 289.66	-17.01 ± 0.04	4.05 ± 0.09	2.47 ± 0.16	–	–	–	–	–
G172.85+02.27_5	241.12, -312.57	-16.68 ± 0.05	4.08 ± 0.12	3.09 ± 0.29	–	–	–	–	–
G172.85+02.27_6	91.74, -331.98	-17.00 ± 0.03	3.83 ± 0.07	2.96 ± 0.18	–	–	–	–	–
G172.85+02.27_7	174.71, 123.09	-17.18 ± 0.03	4.07 ± 0.07	2.57 ± 0.14	–	–	–	–	–
G175.20+01.28_1	-110.37, 126.07	-6.01 ± 0.02	1.89 ± 0.03	3.03 ± 0.12	-5.92 ± 0.11	1.24 ± 0.21	0.38 ± 0.09	0.20 ± 0.05	23.30 ± 7.77
G175.20+01.28_2	231.59, -122.36	-5.39 ± 0.03	2.30 ± 0.06	2.11 ± 0.12	–	–	–	–	–
G175.20+01.28_3	-262.29, 78.09	-5.65 ± 0.03	1.95 ± 0.06	2.06 ± 0.15	–	–	–	–	–
G175.20+01.28_4	338.95, -232.58	-5.86 ± 0.04	1.68 ± 0.08	2.87 ± 0.28	-5.96 ± 0.11	0.78 ± 0.21	0.69 ± 0.21	2.07 ± 1.14	7.92 ± 1.09
G175.20+01.28_5	-53.42, -51.13	-5.39 ± 0.02	1.48 ± 0.05	1.78 ± 0.11	–	–	–	–	–
G175.53+01.34_1	-69.75, -54.34	-6.92 ± 0.03	1.99 ± 0.06	1.86 ± 0.12	–	–	–	–	–
G175.53+01.34_2	-228.62, 226.74	-6.33 ± 0.04	1.46 ± 0.08	1.60 ± 0.17	–	–	–	–	–
G175.53+01.34_3	32.85, 15.06	-6.76 ± 0.04	2.25 ± 0.08	1.32 ± 0.12	–	–	–	–	–
G175.53+01.34_4	317.70, -243.43	-7.68 ± 0.04	1.59 ± 0.09	2.07 ± 0.23	–	–	–	–	–
G175.53+01.34_5	149.04, -258.08	-7.51 ± 0.03	1.30 ± 0.09	1.44 ± 0.15	–	–	–	–	–
G175.53+01.34_6	-2.23, 284.13	-6.59 ± 0.04	1.28 ± 0.09	1.33 ± 0.15	–	–	–	–	–
G176.17-02.10_1	54.04, -40.41	-20.45 ± 0.01	1.12 ± 0.02	3.35 ± 0.09	-20.35 ± 0.03	0.69 ± 0.06	0.78 ± 0.07	2.18 ± 0.33	9.13 ± 0.33
G176.17-02.10_2	148.21, -301.14	-20.62 ± 0.01	1.18 ± 0.03	3.03 ± 0.14	-20.47 ± 0.09	0.69 ± 0.18	0.42 ± 0.11	0.61 ± 0.20	11.62 ± 5.46
G176.17-02.10_3	-344.67, -228.43	-20.65 ± 0.04	1.12 ± 0.11	2.45 ± 0.31	–	–	–	–	–
G176.17-02.10_4	-267.29, 91.06	-20.38 ± 0.03	1.37 ± 0.06	1.78 ± 0.14	–	–	–	–	–
G176.17-02.10_5	-84.83, -327.04	-21.04 ± 0.02	0.85 ± 0.06	2.28 ± 0.21	–	–	–	–	–
G176.17-02.10_6	-117.24, -61.62	-20.73 ± 0.01	0.98 ± 0.02	2.83 ± 0.10	-20.74 ± 0.10	0.61 ± 0.16	0.25 ± 0.07	0.20 ± 0.05	21.44 ± 7.15
G176.17-02.10_7	319.82, -258.70	-20.71 ± 0.03	0.92 ± 0.06	2.19 ± 0.22	–	–	–	–	–
G176.17-02.10_8	-120.28, 150.69	-20.70 ± 0.02	1.18 ± 0.05	1.87 ± 0.14	–	–	–	–	–
G176.17-02.10_9	-322.08, -145.39	-20.75 ± 0.05	1.26 ± 0.13	1.40 ± 0.20	–	–	–	–	–
G176.35+01.92_1	-7.20, 49.29	-9.45 ± 0.02	1.95 ± 0.04	2.43 ± 0.10	-9.41 ± 0.10	1.69 ± 0.20	0.36 ± 0.07	0.59 ± 0.49	9.51 ± 3.56
G176.35+01.92_2	-82.45, -236.29	-9.01 ± 0.02	1.60 ± 0.05	2.72 ± 0.17	-9.20 ± 0.12	1.36 ± 0.22	0.42 ± 0.10	0.71 ± 0.67	9.79 ± 3.69
G176.35+01.92_3	-97.29, -387.61	-8.56 ± 0.07	1.57 ± 0.15	1.90 ± 0.37	–	–	–	–	–
G176.35+01.92_4	-21.53, -111.46	-9.28 ± 0.03	1.62 ± 0.07	1.66 ± 0.14	–	–	–	–	–
G176.35+01.92_5	-265.93, 201.13	-9.91 ± 0.05	1.21 ± 0.13	1.48 ± 0.24	–	–	–	–	–
G176.35+01.92_6	-174.75, 117.70	-10.02 ± 0.03	1.27 ± 0.08	1.43 ± 0.13	–	–	–	–	–
G176.94+04.63_1	2.13, 89.50	-17.53 ± 0.01	2.12 ± 0.03	3.21 ± 0.11	-17.63 ± 0.12	1.77 ± 0.24	0.45 ± 0.10	0.48 ± 0.16	13.64 ± 7.74
G176.94+04.63_2	-250.59, -275.72	-17.51 ± 0.07	3.73 ± 0.13	1.76 ± 0.22	–	–	–	–	–
G176.94+04.63_3	-33.67, -146.13	-18.23 ± 0.03	2.69 ± 0.07	2.02 ± 0.14	–	–	–	–	–
G176.94+04.63_4	-247.15, -131.90	-17.20 ± 0.05	3.21 ± 0.11	1.69 ± 0.18	–	–	–	–	–
G176.94+04.63_5	-162.05, -24.08	-17.29 ± 0.02	2.49 ± 0.06	2.44 ± 0.13	–	–	–	–	–
G176.94+04.63_6	-63.35, -301.82	-18.89 ± 0.07	2.11 ± 0.17	1.31 ± 0.20	-15.96 ± 0.05	0.33 ± 0.07	0.58 ± 0.17	5.07 ± 2.34	3.59 ± 0.45
G176.94+04.63_7	-155.71, 131.29	-16.58 ± 0.04	2.28 ± 0.10	1.51 ± 0.15	–	–	–	–	–
G176.94+04.63_8	148.22, 37.28	-17.48 ± 0.04	2.12 ± 0.11	1.39 ± 0.12	–	–	–	–	–
G176.94+04.63_9	-174.47, -227.61	-17.68 ± 0.07	3.35 ± 0.15	1.76 ± 0.24	–	–	–	–	–

TABLE 2—*Continued*

Name	Offset(R.A. DEC.)[a] ($''$ $''$)	$V_{^{13}CO}$ km s^{-1}	$\Delta V_{^{13}CO}$ km s^{-1}	$T_{^{13}CO}$ K	$V_{C^{18}O}$ km s^{-1}	$\Delta V_{C^{18}O}$[b] km s^{-1}	$T_{C^{18}O}$ K	$\tau_{^{13}CO}$[c]	$T_{ex}(^{13}CO)$[d] K
G176.94+04.63_10	34.81, -361.74	-19.35 ± 0.06	1.45 ± 0.17	1.60 ± 0.27	–	–	–	–	–
G176.94+04.63_11	5.03, -45.19	-18.07 ± 0.02	2.01 ± 0.05	2.60 ± 0.14	-18.26 ± 0.31	1.61 ± 0.32	0.43 ± 0.12	0.93 ± 0.79	8.55 ± 2.42
G176.94+04.63_12	-195.85, -359.94	–	–	–	–	–	–	–	–
G176.94+04.63_13	101.24, 265.44	-16.86 ± 0.08	2.69 ± 0.18	1.02 ± 0.17	–	–	–	–	–
G177.09+02.85_1	16.63, -15.01	-10.68 ± 0.03	2.12 ± 0.06	1.59 ± 0.11	–	–	–	–	–
G177.09+02.85_2	-224.74, -2.96	-9.49 ± 0.04	2.16 ± 0.10	1.30 ± 0.14	–	–	–	–	–
G177.09+02.85_3	-5.52, 370.03	-9.49 ± 0.05	1.66 ± 0.11	1.28 ± 0.15	-9.85 ± 0.15	0.37 ± 0.07	0.47 ± 0.12	4.28 ± 1.69	3.54 ± 0.34
G177.09+02.85_4	13.07, 168.95	-10.03 ± 0.05	2.37 ± 0.12	1.05 ± 0.12	–	–	–	–	–
G177.09+02.85_5	-274.40, 300.94	-9.56 ± 0.12	1.53 ± 0.28	1.40 ± 0.41	–	–	–	–	–
G177.09+02.85_6	-422.75, -9.48	-9.31 ± 0.11	1.65 ± 0.27	1.26 ± 0.38	–	–	–	–	–
G177.09+02.85_7	-254.17, 190.38	-9.18 ± 0.07	1.79 ± 0.17	0.92 ± 0.16	–	–	–	–	–
G177.14-01.21_1	9.64, 10.99	-17.10 ± 0.01	2.12 ± 0.02	4.10 ± 0.10	-17.08 ± 0.04	1.53 ± 0.09	0.81 ± 0.06	1.63 ± 0.24	11.50 ± 0.45
G177.14-01.21_2	-21.89, -390.28	-16.85 ± 0.02	1.51 ± 0.04	4.89 ± 0.22	–	–	–	–	–
G177.14-01.21_3	-30.93, 184.63	-17.48 ± 0.01	1.56 ± 0.03	3.44 ± 0.12	-17.42 ± 0.07	0.99 ± 0.17	0.50 ± 0.09	0.76 ± 0.45	11.99 ± 2.69
G177.14-01.21_4	-37.98, -282.83	-16.65 ± 0.01	1.55 ± 0.03	3.49 ± 0.15	-16.68 ± 0.17	2.00 ± 0.41	0.35 ± 0.10	0.22 ± 0.05	23.69 ± 7.90
G177.14-01.21_5	-100.97, -174.86	-16.46 ± 0.02	1.75 ± 0.05	2.25 ± 0.14	–	–	–	–	–
G177.14-01.21_6	-157.09, -56.37	-16.82 ± 0.02	1.42 ± 0.04	2.58 ± 0.14	-17.17 ± 0.08	0.72 ± 0.20	0.39 ± 0.08	0.84 ± 0.59	8.79 ± 2.28
G177.14-01.21_7	149.99, -90.78	-16.63 ± 0.02	1.44 ± 0.04	2.52 ± 0.11	–	–	–	–	–
G177.86+01.04_1	-44.31, -7.43	-18.29 ± 0.02	2.23 ± 0.04	2.26 ± 0.10	-18.15 ± 0.12	2.22 ± 0.24	0.35 ± 0.07	0.89 ± 0.54	7.56 ± 1.59
G177.86+01.04_2	-189.83, 191.81	-17.44 ± 0.02	1.74 ± 0.05	2.41 ± 0.12	-17.46 ± 0.12	1.06 ± 0.19	0.30 ± 0.09	0.40 ± 0.13	11.35 ± 3.78
G177.86+01.04_3	-387.22, 52.55	-18.20 ± 0.05	1.69 ± 0.11	2.20 ± 0.29	-18.59 ± 0.04	0.33 ± 0.07	0.82 ± 0.18	4.27 ± 1.54	5.78 ± 0.78
G177.86+01.04_4	162.92, -119.18	-19.76 ± 0.11	3.17 ± 0.30	0.60 ± 0.13	-16.71 ± 0.11	0.78 ± 0.23	0.26 ± 0.08	5.27 ± 2.83	2.33 ± 0.21
G178.28-00.61_1	208.29, 338.14	-0.48 ± 0.02	2.25 ± 0.04	4.64 ± 0.18	-0.49 ± 0.13	1.68 ± 0.26	0.71 ± 0.17	0.66 ± 0.64	16.69 ± 6.66
G178.28-00.61_2	42.10, 47.53	-0.53 ± 0.01	2.38 ± 0.02	3.57 ± 0.09	-0.85 ± 0.11	1.69 ± 0.26	0.51 ± 0.09	0.47 ± 0.44	15.28 ± 7.16
G178.28-00.61_3	191.12, 236.39	-0.74 ± 0.01	2.25 ± 0.03	4.30 ± 0.14	-0.93 ± 0.14	2.14 ± 0.28	0.57 ± 0.13	0.30 ± 0.10	23.13 ± 7.71
G178.28-00.61_4	218.57, 368.92	-0.30 ± 0.02	2.05 ± 0.04	5.53 ± 0.26	–	–	–	–	–
G178.28-00.61_5	52.71, -343.57	-0.50 ± 0.02	1.41 ± 0.05	2.42 ± 0.14	–	–	–	–	–
G178.28-00.61_6	-163.19, -135.99	-0.12 ± 0.02	1.71 ± 0.05	2.09 ± 0.13	–	–	–	–	–

[a]The absolute coordinate of each source is listed in Table 1.

[b]**If the linewidth of $C^{18}O$ is less than two velocity channels (or two times velocity resolution), the Gaussian fitting will produce a linewidth of $0.33 \pm 0.07\,km\,s^{-1}$.**

[c]**The optical depth with $\tau_{^{13}CO} < 0.20$ is unreliable, therefore we set them as $\tau_{^{13}CO} = 0.20 \pm 0.05$.**

[d]**The excitation temperature with $T_{ex}(^{13}CO) > 50.00\,K$ is unreliable, therefore we set them as $T_{ex}(^{13}CO) = 50.00 \pm 5.00\,K$.**

Table 3

Derived parameters of extracted CO clumps

Name	FWHM[a] $''$	$R_{\rm eff}$[b] pc	$\sigma_{\rm C^{18}O}$ km s^{-1}	$N_{\rm H_2}^{\rm ^{13}CO}$ 10^{21} cm^{-2}	$n_{\rm H_2}^{\rm ^{13}CO}$ 10^{3} cm^{-3}	$\Sigma^{\rm ^{13}CO}$ g cm^{-2}	$M_{\rm H_2}^{\rm ^{13}CO}$ $M_\odot$	$M_{\rm vir}$ $M_\odot$	$\alpha_{\rm vir}$
G098.50-03.24_1	162.0	0.75	0.39 ± 0.08	7.7 ± 2.0	4.2 ± 1.1	0.089 ± 0.023	240.8 ± 61.4	87.8 ± 17.5	0.36 ± 0.12
G098.50-03.24_2	128.4	0.59	0.25 ± 0.05	7.0 ± 1.3	4.0 ± 0.8	0.068 ± 0.013	114.4 ± 21.7	44.5 ± 9.1	0.39 ± 0.11
G108.85-00.80_1	166.3	1.55	0.85 ± 0.08	41.5 ± 7.0	10.9 ± 1.8	0.488 ± 0.082	5630.1 ± 945.5	392.1 ± 36.8	0.07 ± 0.01
G108.85-00.80_2	106.8	1.00	0.64 ± 0.06	68.3 ± 12.6	27.5 ± 5.1	0.788 ± 0.145	3749.7 ± 690.7	190.6 ± 18.8	0.05 ± 0.01
G108.85-00.80_3	164.5	1.53	1.04 ± 0.13	25.5 ± 7.0	4.9 ± 1.4	0.217 ± 0.060	2440.1 ± 671.5	474.2 ± 59.7	0.19 ± 0.06
G108.85-00.80_4	170.7	1.59	0.66 ± 0.09	21.5 ± 4.3	4.3 ± 0.9	0.196 ± 0.039	2379.7 ± 475.9	311.5 ± 40.8	0.13 ± 0.03
G110.65+09.65_1	240.7	0.58	0.44 ± 0.02	40.3 ± 2.4	18.4 ± 1.1	0.303 ± 0.018	479.9 ± 28.1	74.9 ± 3.2	0.16 ± 0.01
G110.65+09.65_2	218.2	0.52	0.49 ± 0.06	12.8 ± 2.6	8.2 ± 1.6	0.122 ± 0.024	159.7 ± 31.9	75.6 ± 9.8	0.47 ± 0.11
G110.65+09.65_3	217.4	0.52	0.47 ± 0.04	20.8 ± 2.2	10.5 ± 1.1	0.156 ± 0.017	201.4 ± 21.7	73.1 ± 5.4	0.36 ± 0.05
G110.65+09.65_4	237.2	0.57	0.43 ± 0.03	23.2 ± 2.2	10.7 ± 1.0	0.173 ± 0.016	266.1 ± 25.0	72.4 ± 4.9	0.27 ± 0.03
G112.52+08.38_1	176.1	0.40	0.49 ± 0.15	11.8 ± 2.8	10.2 ± 2.4	0.116 ± 0.027	88.6 ± 20.8	58.6 ± 17.7	0.66 ± 0.25
G112.52+08.38_2	319.1	0.72	–	–	–	–	–	–	–
G112.52+08.38_3	124.7	0.28	–	–	–	–	–	–	–
G112.52+08.38_4	193.4	0.44	0.14 ± 0.03	8.8 ± 1.8	5.8 ± 1.2	0.073 ± 0.015	66.7 ± 13.3	18.4 ± 3.7	0.28 ± 0.08
G112.52+08.38_5	206.2	0.47	–	–	–	–	–	–	–
G112.60+08.53_1	312.3	0.71	0.77 ± 0.06	12.3 ± 2.5	4.7 ± 0.9	0.095 ± 0.019	226.9 ± 45.4	161.5 ± 13.5	0.71 ± 0.15
G112.60+08.53_2	120.1	0.27	0.93 ± 0.22	11.8 ± 2.4	22.2 ± 4.4	0.173 ± 0.035	61.4 ± 12.3	75.0 ± 17.9	1.22 ± 0.38
G112.60+08.53_3	230.0	0.52	0.78 ± 0.12	7.6 ± 1.5	3.7 ± 0.7	0.056 ± 0.011	72.1 ± 14.4	121.0 ± 19.2	1.68 ± 0.43
G112.60+08.53_4	210.6	0.48	0.84 ± 0.16	10.5 ± 2.1	5.9 ± 1.2	0.081 ± 0.016	87.7 ± 17.5	119.0 ± 21.9	1.36 ± 0.37
G112.60+08.53_5	228.7	0.52	0.63 ± 0.07	9.9 ± 2.0	5.2 ± 1.0	0.077 ± 0.015	98.5 ± 19.7	96.3 ± 11.1	0.98 ± 0.23
G112.60+08.53_6	72.1	0.16	0.14 ± 0.03	13.7 ± 2.7	54.8 ± 11.0	0.256 ± 0.051	32.5 ± 6.5	6.8 ± 1.4	0.21 ± 0.06
G112.60+08.53_7	160.5	0.36	–	–	–	–	–	–	–
G112.60+08.53_8	202.0	0.46	–	–	–	–	–	–	–
G115.92+09.46_1	196.8	0.42	0.44 ± 0.09	10.3 ± 2.1	6.4 ± 1.3	0.078 ± 0.016	65.8 ± 13.2	55.3 ± 11.7	0.84 ± 0.24
G115.92+09.46_2	158.5	0.34	0.16 ± 0.04	5.6 ± 1.1	4.6 ± 0.9	0.045 ± 0.008	24.6 ± 4.6	15.9 ± 4.1	0.64 ± 0.21
G115.92+09.46_3	165.5	0.35	0.14 ± 0.03	3.3 ± 0.7	2.4 ± 0.5	0.025 ± 0.005	14.7 ± 2.9	14.9 ± 3.0	1.01 ± 0.29
G115.92+09.46_4	131.0	0.28	–	–	–	–	–	–	–
G115.92+09.46_5	128.7	0.28	–	–	–	–	–	–	–
G115.92+09.46_6	112.2	0.24	–	–	–	–	–	–	–
G115.92+09.46_7	132.8	0.28	0.14 ± 0.03	2.3 ± 0.5	2.1 ± 0.4	0.017 ± 0.003	6.7 ± 1.3	11.9 ± 2.4	1.78 ± 0.50
G116.08-02.38_1	312.4	0.66	0.64 ± 0.07	11.2 ± 2.3	4.7 ± 1.0	0.088 ± 0.018	183.8 ± 38.0	125.7 ± 12.9	0.68 ± 0.16
G116.08-02.38_2	195.2	0.41	0.31 ± 0.08	9.8 ± 3.1	6.1 ± 2.0	0.072 ± 0.023	58.8 ± 19.0	38.1 ± 9.4	0.65 ± 0.26
G116.08-02.38_3	182.7	0.38	–	–	–	–	–	–	–
G116.08-02.38_4	216.2	0.46	0.37 ± 0.15	8.8 ± 2.6	5.3 ± 1.6	0.070 ± 0.020	69.4 ± 20.2	50.2 ± 19.7	0.72 ± 0.35
G116.08-02.38_5	153.5	0.32	0.46 ± 0.12	6.6 ± 0.7	5.6 ± 0.6	0.052 ± 0.005	25.9 ± 2.6	43.8 ± 11.1	1.69 ± 0.46
G116.08-02.38_6	132.9	0.28	0.42 ± 0.11	7.9 ± 1.6	7.3 ± 1.5	0.059 ± 0.012	21.9 ± 4.4	34.6 ± 9.3	1.58 ± 0.53
G116.08-02.38_7	142.8	0.30	–	–	–	–	–	–	–
G116.12+08.98_1	166.5	0.36	0.25 ± 0.08	6.9 ± 1.4	5.0 ± 1.0	0.051 ± 0.010	30.9 ± 6.2	26.1 ± 8.7	0.84 ± 0.33
G116.12+08.98_2	152.8	0.33	–	–	–	–	–	–	–
G116.12+08.98_3	166.6	0.36	–	–	–	–	–	–	–
G116.12+08.98_4	116.0	0.25	–	–	–	–	–	–	–
G116.12+08.98_5	103.4	0.22	–	–	–	–	–	–	–
G120.16+03.09_1	254.7	0.95	0.95 ± 0.03	50.2 ± 3.6	14.6 ± 1.0	0.396 ± 0.028	1701.0 ± 121.0	266.9 ± 8.6	0.16 ± 0.01
G120.16+03.09_2	120.1	0.32	0.71 ± 0.06	50.7 ± 7.1	55.2 ± 7.8	0.509 ± 0.072	252.8 ± 35.6	67.9 ± 6.1	0.27 ± 0.04

TABLE 3—*Continued*

Name	FWHM[a] $''$	$R_{\rm eff}$[b] pc	$\sigma_{\rm C^{18}O}$ km s^{-1}	$N_{\rm H_2}^{\rm 13CO}$ 10^{21} cm^{-2}	$n_{\rm H_2}^{\rm 13CO}$ 10^{3} cm^{-3}	$\Sigma^{\rm 13CO}$ g cm^{-2}	$M_{\rm H_2}^{\rm 13CO}$ $M_\odot$	$M_{\rm vir}$ $M_\odot$	$\alpha_{\rm vir}$
G120.16+03.09_3	217.2	0.58	0.90 ± 0.05	32.0 ± 3.3	14.3 ± 1.5	0.239 ± 0.024	391.1 ± 39.9	156.4 ± 8.8	0.40 ± 0.05
G120.16+03.09_4	196.2	0.53	1.07 ± 0.12	25.5 ± 5.1	12.3 ± 2.5	0.187 ± 0.037	250.2 ± 50.0	168.4 ± 18.7	0.67 ± 0.15
G120.16+03.09_5	238.5	0.90	0.82 ± 0.03	39.1 ± 3.1	12.6 ± 1.0	0.326 ± 0.026	1273.0 ± 101.5	220.0 ± 8.2	0.17 ± 0.02
G120.16+03.09_6	112.6	0.43	0.52 ± 0.09	21.2 ± 4.5	22.5 ± 4.8	0.278 ± 0.060	248.6 ± 53.2	66.9 ± 11.3	0.27 ± 0.07
G120.67+02.66_1	252.5	0.66	0.61 ± 0.07	26.8 ± 5.4	11.0 ± 2.2	0.208 ± 0.042	436.8 ± 87.4	120.8 ± 13.0	0.28 ± 0.06
G120.67+02.66_2	241.2	0.63	0.93 ± 0.08	19.8 ± 4.0	8.0 ± 1.6	0.145 ± 0.029	278.7 ± 55.7	174.6 ± 14.7	0.63 ± 0.14
G120.67+02.66_3	164.0	0.43	0.90 ± 0.12	15.3 ± 3.1	11.7 ± 2.3	0.144 ± 0.029	126.5 ± 25.3	114.1 ± 15.0	0.90 ± 0.22
G120.67+02.66_4	175.7	0.47	–	–	–	–	–	–	–
G120.67+02.66_5	75.9	0.20	–	–	–	–	–	–	–
G120.67+02.66_6	146.2	0.41	0.66 ± 0.07	15.0 ± 0.9	10.0 ± 0.6	0.118 ± 0.007	97.3 ± 5.8	80.6 ± 8.6	0.83 ± 0.10
G120.67+02.66_7	181.2	0.49	0.67 ± 0.20	11.8 ± 2.4	6.2 ± 1.2	0.087 ± 0.017	98.9 ± 19.8	96.4 ± 28.3	0.97 ± 0.35
G120.67+02.66_8	138.0	0.36	–	–	–	–	–	–	–
G120.98+02.66_1	230.2	0.62	0.56 ± 0.04	16.7 ± 1.2	7.5 ± 0.6	0.132 ± 0.010	239.0 ± 17.6	102.6 ± 8.1	0.43 ± 0.05
G120.98+02.66_2	159.6	0.43	0.29 ± 0.05	23.0 ± 5.9	16.7 ± 4.3	0.205 ± 0.053	180.0 ± 46.1	37.3 ± 6.4	0.21 ± 0.06
G120.98+02.66_3	228.9	0.61	–	–	–	–	–	–	–
G120.98+02.66_4	87.6	0.23	–	–	–	–	–	–	–
G120.98+02.66_5	147.0	0.39	–	–	–	–	–	–	–
G120.98+02.66_6	139.2	0.37	–	–	–	–	–	–	–
G120.98+02.66_7	82.2	0.22	–	–	–	–	–	–	–
G120.98+02.66_8	81.9	0.22	–	–	–	–	–	–	–
G120.98+02.66_9	144.0	0.38	–	–	–	–	–	–	–
G120.98+02.66_10	140.2	0.37	–	–	–	–	–	–	–
G121.35+03.39_1	302.1	0.62	0.41 ± 0.03	22.7 ± 2.1	9.9 ± 0.9	0.176 ± 0.016	323.2 ± 29.6	75.1 ± 4.9	0.23 ± 0.03
G121.35+03.39_2	278.7	0.57	0.67 ± 0.10	7.1 ± 1.4	3.2 ± 0.6	0.053 ± 0.011	82.8 ± 16.6	113.0 ± 17.4	1.36 ± 0.34
G121.35+03.39_3	110.2	0.23	0.72 ± 0.11	18.0 ± 4.8	34.0 ± 9.1	0.220 ± 0.059	53.4 ± 14.4	48.0 ± 7.6	0.90 ± 0.28
G121.35+03.39_4	127.6	0.27	0.45 ± 0.10	13.1 ± 3.9	16.5 ± 5.0	0.128 ± 0.039	45.1 ± 13.6	36.3 ± 8.3	0.81 ± 0.30
G121.35+03.39_5	197.9	0.41	0.38 ± 0.04	15.2 ± 2.3	10.1 ± 1.6	0.117 ± 0.018	92.3 ± 14.2	45.6 ± 5.4	0.49 ± 0.10
G121.35+03.39_6	102.8	0.21	–	–	–	–	–	–	–
G121.35+03.39_7	245.5	0.50	0.53 ± 0.19	3.8 ± 0.8	1.9 ± 0.4	0.027 ± 0.005	33.2 ± 6.6	78.6 ± 27.6	2.37 ± 0.96
G121.35+03.39_8	211.8	0.43	–	–	–	–	–	–	–
G121.90-01.54_1	226.2	0.39	0.42 ± 0.07	9.3 ± 1.9	7.3 ± 1.5	0.081 ± 0.016	57.9 ± 11.6	48.1 ± 8.4	0.83 ± 0.22
G121.90-01.54_2	154.0	0.41	0.34 ± 0.07	10.0 ± 2.3	6.9 ± 1.6	0.082 ± 0.019	66.1 ± 15.2	41.7 ± 8.6	0.63 ± 0.20
G121.90-01.54_3	137.7	0.23	0.24 ± 0.11	6.8 ± 1.4	8.4 ± 1.7	0.055 ± 0.011	13.9 ± 2.8	16.0 ± 7.8	1.15 ± 0.60
G121.90-01.54_4	177.4	0.30	–	–	–	–	–	–	–
G121.90-01.54_5	227.5	0.38	0.29 ± 0.04	7.9 ± 1.1	6.7 ± 0.9	0.073 ± 0.010	49.3 ± 6.9	32.5 ± 4.0	0.66 ± 0.12
G121.90-01.54_6	152.1	0.27	0.14 ± 0.03	11.2 ± 3.0	10.6 ± 2.8	0.082 ± 0.022	28.1 ± 7.4	11.3 ± 2.3	0.40 ± 0.13
G121.90-01.54_7	94.8	0.16	–	–	–	–	–	–	–
G121.90-01.54_8	134.7	0.23	0.30 ± 0.07	7.6 ± 1.5	8.8 ± 1.7	0.058 ± 0.011	14.6 ± 2.8	20.1 ± 4.6	1.38 ± 0.41
G121.92-01.71_1	287.1	0.49	0.60 ± 0.07	9.8 ± 2.0	5.3 ± 1.1	0.074 ± 0.015	84.5 ± 16.9	86.8 ± 10.2	1.03 ± 0.24
G121.92-01.71_2	84.5	0.14	0.18 ± 0.05	18.2 ± 5.3	58.3 ± 17.0	0.235 ± 0.069	22.4 ± 6.5	7.6 ± 2.1	0.34 ± 0.14
G121.92-01.71_3	102.5	0.27	0.48 ± 0.07	10.1 ± 2.5	11.1 ± 2.7	0.087 ± 0.021	31.2 ± 7.6	39.4 ± 5.4	1.26 ± 0.35
G121.92-01.71_4	167.2	0.28	0.50 ± 0.06	15.1 ± 2.4	16.4 ± 2.6	0.133 ± 0.021	50.3 ± 8.0	41.5 ± 5.1	0.82 ± 0.17
G121.92-01.71_5	86.5	0.15	–	–	–	–	–	–	–
G121.92-01.71_6	152.5	0.24	0.45 ± 0.13	6.4 ± 1.3	7.6 ± 1.5	0.053 ± 0.011	15.0 ± 3.0	32.1 ± 9.4	2.14 ± 0.76

TABLE 3—*Continued*

Name	FWHM[a] $''$	$R_{\rm eff}$[b] pc	$\sigma_{\rm C^{18}O}$ km s^{-1}	$N_{\rm H_2}^{\rm 13CO}$ 10^{21} cm^{-2}	$n_{\rm H_2}^{\rm 13CO}$ 10^{3} cm^{-3}	$\Sigma^{\rm 13CO}$ g cm^{-2}	$M_{\rm H_2}^{\rm 13CO}$ $M_\odot$	$M_{\rm vir}$ $M_\odot$	$\alpha_{\rm vir}$
G121.92-01.71_7	69.7	0.19	–	–	–	–	–	–	–
G121.92-01.71_8	111.3	0.18	0.46 ± 0.11	7.6 ± 1.5	11.4 ± 2.3	0.060 ± 0.012	9.4 ± 1.9	25.0 ± 5.8	2.65 ± 0.82
G121.92-01.71_9	138.1	0.24	–	–	–	–	–	–	–
G121.92-01.71_10	131.7	0.35	0.19 ± 0.06	5.4 ± 1.1	4.3 ± 0.9	0.043 ± 0.009	25.6 ± 5.1	19.9 ± 6.3	0.78 ± 0.29
G125.66-00.55_1	269.7	0.48	–	–	–	–	–	–	–
G125.66-00.55_2	115.6	0.20	–	–	–	–	–	–	–
G125.66-00.55_3	181.8	0.48	0.69 ± 0.11	29.7 ± 8.8	16.2 ± 4.8	0.224 ± 0.067	251.0 ± 74.4	99.4 ± 15.8	0.40 ± 0.13
G125.66-00.55_4	221.2	0.38	0.65 ± 0.15	20.4 ± 5.9	17.0 ± 5.0	0.187 ± 0.054	130.7 ± 38.2	74.0 ± 17.1	0.57 ± 0.21
G125.66-00.55_5	127.3	0.34	–	–	–	–	–	–	–
G125.66-00.55_6	137.8	0.37	0.41 ± 0.10	15.3 ± 3.1	10.7 ± 2.1	0.114 ± 0.023	75.3 ± 15.1	45.5 ± 10.8	0.60 ± 0.19
G125.66-00.55_7	156.6	0.42	–	–	–	–	–	–	–
G125.66-00.55_8	145.0	0.52	–	–	–	–	–	–	–
G125.66-00.55_9	57.7	0.10	–	–	–	–	–	–	–
G125.66-00.55_10	71.2	0.19	–	–	–	–	–	–	–
G126.49-01.30_1	132.8	0.36	0.64 ± 0.13	22.6 ± 7.2	23.2 ± 7.4	0.239 ± 0.076	148.4 ± 47.3	68.5 ± 14.3	0.46 ± 0.18
G126.49-01.30_2	156.5	0.27	0.61 ± 0.13	21.2 ± 5.8	25.4 ± 7.0	0.200 ± 0.055	72.6 ± 19.9	50.1 ± 10.9	0.69 ± 0.24
G126.49-01.30_3	288.6	0.50	0.61 ± 0.04	18.6 ± 2.0	11.7 ± 1.3	0.168 ± 0.018	201.7 ± 21.7	90.0 ± 5.5	0.45 ± 0.06
G126.49-01.30_4	84.7	0.15	0.26 ± 0.05	29.5 ± 8.0	66.9 ± 18.1	0.287 ± 0.078	30.8 ± 8.4	11.7 ± 2.4	0.38 ± 0.13
G126.49-01.30_5	116.4	0.20	0.14 ± 0.03	17.3 ± 3.5	37.3 ± 7.5	0.217 ± 0.043	42.6 ± 8.5	8.5 ± 1.7	0.20 ± 0.06
G126.49-01.30_6	201.1	0.35	0.67 ± 0.25	7.4 ± 1.5	5.9 ± 1.2	0.060 ± 0.012	35.2 ± 7.0	70.3 ± 26.5	2.00 ± 0.85
G126.49-01.30_7	71.8	0.13	0.20 ± 0.08	28.4 ± 6.3	116.2 ± 25.8	0.421 ± 0.094	32.2 ± 7.2	7.5 ± 3.1	0.23 ± 0.11
G126.49-01.30_8	149.8	0.26	0.74 ± 0.10	12.6 ± 3.7	12.7 ± 3.7	0.096 ± 0.028	31.5 ± 9.1	57.6 ± 7.8	1.83 ± 0.58
G126.49-01.30_9	220.3	0.38	0.86 ± 0.12	11.0 ± 2.2	8.2 ± 1.6	0.090 ± 0.018	62.3 ± 12.5	97.5 ± 13.0	1.57 ± 0.38
G126.49-01.30_10	200.6	0.35	0.30 ± 0.04	7.6 ± 1.4	5.6 ± 1.0	0.056 ± 0.010	33.4 ± 6.2	31.6 ± 4.3	0.94 ± 0.22
G126.95-01.06_1	384.9	0.67	0.53 ± 0.09	8.5 ± 1.5	3.2 ± 0.6	0.062 ± 0.011	135.4 ± 24.3	105.2 ± 17.7	0.78 ± 0.19
G126.95-01.06_2	176.5	0.31	–	–	–	–	–	–	–
G126.95-01.06_3	205.6	0.36	–	–	–	–	–	–	–
G126.95-01.06_4	199.7	0.54	0.29 ± 0.09	6.9 ± 1.4	4.5 ± 0.9	0.070 ± 0.014	98.1 ± 19.6	46.1 ± 13.9	0.47 ± 0.17
G126.95-01.06_5	151.2	0.26	–	–	–	–	–	–	–
G126.95-01.06_6	162.7	0.30	–	–	–	–	–	–	–
G127.22-02.25_1	205.1	0.52	–	–	–	–	–	–	–
G127.22-02.25_2	196.3	0.53	–	–	–	–	–	–	–
G127.22-02.25_3	137.2	0.15	–	–	–	–	–	–	–
G127.22-02.25_4	142.0	0.37	–	–	–	–	–	–	–
G127.22-02.25_5	139.0	0.21	–	–	–	–	–	–	–
G127.22-02.25_6	91.2	0.23	–	–	–	–	–	–	–
G127.22-02.25_7	88.0	0.24	–	–	–	–	–	–	–
G127.22-02.25_8	90.0	0.10	–	–	–	–	–	–	–
G127.22-02.25_9	77.2	0.12	–	–	–	–	–	–	–
G127.22-02.25_10	65.2	0.17	–	–	–	–	–	–	–
G127.22-02.25_11	76.7	0.21	–	–	–	–	–	–	–
G127.88+02.66_1	283.1	0.73	0.46 ± 0.05	15.8 ± 3.2	5.5 ± 1.1	0.116 ± 0.023	298.4 ± 59.7	100.1 ± 11.6	0.34 ± 0.08
G127.88+02.66_2	229.3	0.60	0.47 ± 0.04	15.6 ± 1.6	7.0 ± 0.7	0.120 ± 0.012	204.5 ± 21.1	83.5 ± 7.3	0.41 ± 0.06
G127.88+02.66_3	162.3	0.42	0.34 ± 0.04	15.8 ± 1.3	9.6 ± 0.8	0.116 ± 0.009	99.3 ± 7.9	42.1 ± 4.6	0.42 ± 0.06

TABLE 3—*Continued*

Name	FWHM[a] $''$	$R_{\rm eff}$[b] pc	$\sigma_{\rm C^{18}O}$ km s^{-1}	$N_{\rm H_2}^{\rm 13CO}$ 10^{21}cm^{-2}	$n_{\rm H_2}^{\rm 13CO}$ 10^{3}cm^{-3}	$\Sigma^{\rm 13CO}$ g cm^{-2}	$M_{\rm H_2}^{\rm 13CO}$ $M_\odot$	$M_{\rm vir}$ $M_\odot$	$\alpha_{\rm vir}$
G127.88+02.66_4	188.3	0.49	–	–	–	–	–	–	–
G128.95-00.18_1	269.9	0.72	0.36 ± 0.08	9.3 ± 1.9	3.3 ± 0.7	0.069 ± 0.014	172.6 ± 34.9	76.2 ± 17.4	0.44 ± 0.13
G128.95-00.18_2	258.9	0.69	0.33 ± 0.06	8.2 ± 2.2	3.2 ± 0.9	0.064 ± 0.017	146.1 ± 39.6	67.4 ± 13.1	0.46 ± 0.15
G128.95-00.18_3	218.0	0.58	0.29 ± 0.05	11.5 ± 1.8	7.7 ± 1.2	0.128 ± 0.020	208.4 ± 31.9	49.6 ± 8.0	0.24 ± 0.05
G128.95-00.18_4	73.7	0.20	–	–	–	–	–	–	–
G128.95-00.18_5	114.1	0.30	0.25 ± 0.05	9.1 ± 2.1	8.2 ± 1.9	0.072 ± 0.017	31.9 ± 7.3	22.5 ± 4.6	0.71 ± 0.22
G128.95-00.18_6	109.0	0.29	0.33 ± 0.06	10.7 ± 2.6	9.4 ± 2.3	0.078 ± 0.019	31.5 ± 7.7	28.4 ± 5.2	0.90 ± 0.27
G128.95-00.18_7	124.8	0.33	–	–	–	–	–	–	–
G128.95-00.18_8	149.8	0.40	0.34 ± 0.05	8.5 ± 1.4	5.5 ± 0.9	0.063 ± 0.011	48.3 ± 8.2	40.6 ± 6.4	0.84 ± 0.19
G128.95-00.18_9	115.7	0.31	–	–	–	–	–	–	–
G131.72+09.70_1	262.4	0.43	0.38 ± 0.06	8.4 ± 1.7	4.9 ± 1.0	0.061 ± 0.012	55.3 ± 11.1	48.4 ± 7.5	0.87 ± 0.22
G131.72+09.70_2	150.8	0.25	0.14 ± 0.03	11.4 ± 2.8	11.9 ± 2.9	0.085 ± 0.021	25.4 ± 6.1	10.5 ± 2.1	0.41 ± 0.13
G131.72+09.70_3	149.0	0.25	0.29 ± 0.05	10.3 ± 2.1	11.5 ± 2.3	0.081 ± 0.016	23.5 ± 4.7	20.8 ± 3.5	0.89 ± 0.23
G131.72+09.70_4	138.2	0.23	–	–	–	–	–	–	–
G131.72+09.70_5	135.7	0.22	0.26 ± 0.05	12.2 ± 2.3	15.0 ± 2.9	0.097 ± 0.018	23.3 ± 4.4	17.6 ± 3.2	0.76 ± 0.20
G131.72+09.70_6	112.2	0.19	–	–	–	–	–	–	–
G131.72+09.70_7	60.5	0.10	–	–	–	–	–	–	–
G131.72+09.70_8	179.9	0.30	–	–	–	–	–	–	–
G131.72+09.70_9	152.9	0.25	–	–	–	–	–	–	–
G131.72+09.70_10	118.2	0.20	–	–	–	–	–	–	–
G131.72+09.70_11	101.9	0.17	–	–	–	–	–	–	–
G131.72+09.70_12	113.4	0.19	–	–	–	–	–	–	–
G132.07+08.80_1	280.4	0.48	0.35 ± 0.06	9.1 ± 1.8	5.3 ± 1.1	0.073 ± 0.015	80.6 ± 16.1	49.4 ± 9.0	0.61 ± 0.17
G132.07+08.80_2	162.5	0.28	0.35 ± 0.13	9.0 ± 1.8	10.8 ± 2.2	0.086 ± 0.017	31.5 ± 6.3	29.1 ± 10.9	0.92 ± 0.39
G132.07+08.80_3	170.2	0.29	–	–	–	–	–	–	–
G132.07+08.80_4	185.2	0.32	–	–	–	–	–	–	–
G132.07+08.80_5	128.3	0.22	–	–	–	–	–	–	–
G132.07+08.80_6	63.9	0.11	–	–	–	–	–	–	–
G132.03+08.95_1	239.6	0.41	–	–	–	–	–	–	–
G132.03+08.95_2	116.9	0.20	0.37 ± 0.08	13.4 ± 2.7	43.7 ± 8.7	0.253 ± 0.051	49.4 ± 9.9	22.3 ± 5.0	0.45 ± 0.14
G132.03+08.95_3	98.2	0.17	–	–	–	–	–	–	–
G132.03+08.95_4	203.5	0.35	–	–	–	–	–	–	–
G132.03+08.95_5	222.8	0.38	–	–	–	–	–	–	–
G132.03+08.95_6	88.1	0.15	–	–	–	–	–	–	–
G132.03+08.95_7	122.6	0.21	0.44 ± 0.12	7.7 ± 1.5	19.8 ± 4.0	0.120 ± 0.024	25.7 ± 5.1	27.7 ± 7.5	1.08 ± 0.36
G133.28+08.81_1	208.3	0.35	0.66 ± 0.14	12.5 ± 2.5	9.8 ± 2.0	0.098 ± 0.020	58.1 ± 11.6	68.5 ± 14.3	1.18 ± 0.34
G133.28+08.81_2	293.5	0.49	0.42 ± 0.14	5.8 ± 1.2	3.0 ± 0.6	0.043 ± 0.009	49.6 ± 9.9	61.4 ± 19.8	1.24 ± 0.47
G133.28+08.81_3	170.9	0.29	–	–	–	–	–	–	–
G133.28+08.81_4	92.5	0.16	0.23 ± 0.09	23.5 ± 4.7	40.6 ± 8.1	0.182 ± 0.036	21.1 ± 4.2	10.5 ± 4.2	0.50 ± 0.22
G133.28+08.81_5	116.1	0.20	–	–	–	–	–	–	–
G133.28+08.81_6	95.4	0.16	–	–	–	–	–	–	–
G133.28+08.81_7	161.0	0.27	0.14 ± 0.03	10.7 ± 2.1	11.6 ± 2.3	0.090 ± 0.018	32.0 ± 6.4	11.7 ± 2.3	0.36 ± 0.10
G133.28+08.81_8	97.2	0.16	–	–	–	–	–	–	–
G133.28+08.81_9	141.4	0.24	–	–	–	–	–	–	–

TABLE 3—*Continued*

Name	FWHM[a] $''$	$R_{\rm eff}$[b] pc	$\sigma_{\rm C^{18}O}$ km s^{-1}	$N_{\rm H_2}^{\rm 13CO}$ 10^{21}cm^{-2}	$n_{\rm H_2}^{\rm 13CO}$ 10^{3}cm^{-3}	$\Sigma^{\rm 13CO}$ g cm^{-2}	$M_{\rm H_2}^{\rm 13CO}$ $M_\odot$	$M_{\rm vir}$ $M_\odot$	$\alpha_{\rm vir}$
G133.48+09.02_1	248.5	0.44	1.11 ± 0.05	66.8 ± 7.9	47.3 ± 5.6	0.596 ± 0.070	550.7 ± 64.7	144.7 ± 6.6	0.26 ± 0.03
G133.48+09.02_2	201.3	0.36	1.58 ± 0.17	22.6 ± 6.7	17.7 ± 5.2	0.181 ± 0.053	109.8 ± 32.4	166.8 ± 17.5	1.52 ± 0.48
G133.48+09.02_3	210.1	0.37	0.70 ± 0.12	25.6 ± 6.3	18.0 ± 4.4	0.191 ± 0.047	124.3 ± 30.5	77.1 ± 13.7	0.62 ± 0.19
G133.48+09.02_4	156.8	0.28	–	–	–	–	–	–	–
G133.48+09.02_5	194.2	0.34	1.05 ± 0.16	13.9 ± 1.8	10.8 ± 1.4	0.106 ± 0.013	58.9 ± 7.4	106.1 ± 16.2	1.80 ± 0.36
G136.31-01.77_1	237.3	0.35	0.51 ± 0.07	8.4 ± 2.1	7.8 ± 2.0	0.079 ± 0.020	47.7 ± 12.1	54.2 ± 7.2	1.14 ± 0.33
G136.31-01.77_2	82.0	0.12	–	–	–	–	–	–	–
G136.31-01.77_3	145.8	0.22	–	–	–	–	–	–	–
G136.31-01.77_4	134.4	0.20	–	–	–	–	–	–	–
G136.31-01.77_5	274.5	0.42	–	–	–	–	–	–	–
G136.31-01.77_6	74.9	0.12	–	–	–	–	–	–	–
G136.31-01.77_7	141.5	0.21	–	–	–	–	–	–	–
G140.49+06.07_1	306.7	1.10	0.84 ± 0.12	10.9 ± 2.2	2.5 ± 0.5	0.080 ± 0.016	461.6 ± 92.3	273.2 ± 39.9	0.59 ± 0.15
G140.49+06.07_2	108.6	0.41	0.23 ± 0.05	12.2 ± 2.4	10.0 ± 2.0	0.116 ± 0.023	91.5 ± 18.3	27.5 ± 5.5	0.30 ± 0.09
G140.49+06.07_3	146.7	0.50	0.30 ± 0.10	9.0 ± 1.0	5.2 ± 0.6	0.075 ± 0.008	91.5 ± 10.2	44.3 ± 14.5	0.48 ± 0.17
G140.49+06.07_4	190.1	0.69	0.49 ± 0.12	9.5 ± 1.9	3.6 ± 0.7	0.071 ± 0.014	161.7 ± 32.3	100.3 ± 25.0	0.62 ± 0.20
G140.49+06.07_5	131.8	0.46	0.49 ± 0.16	7.5 ± 1.5	4.5 ± 0.9	0.059 ± 0.012	60.2 ± 12.0	66.9 ± 21.3	1.11 ± 0.42
G140.49+06.07_6	193.1	0.70	–	–	–	–	–	–	–
G140.77+05.00_1	188.4	0.31	0.50 ± 0.04	10.6 ± 0.2	9.4 ± 0.1	0.083 ± 0.001	37.3 ± 0.5	45.1 ± 3.2	1.21 ± 0.09
G140.77+05.00_2	114.1	0.19	0.52 ± 0.14	17.5 ± 3.5	31.2 ± 6.2	0.166 ± 0.033	27.4 ± 5.5	28.6 ± 7.7	1.04 ± 0.35
G140.77+05.00_3	162.5	0.26	0.33 ± 0.09	5.6 ± 1.1	5.7 ± 1.1	0.044 ± 0.009	14.6 ± 2.9	26.0 ± 7.4	1.78 ± 0.62
G140.77+05.00_4	164.3	0.27	0.46 ± 0.08	8.8 ± 1.8	8.6 ± 1.7	0.066 ± 0.013	22.5 ± 4.5	36.8 ± 6.1	1.63 ± 0.42
G140.77+05.00_5	114.3	0.19	–	–	–	–	–	–	–
G140.77+05.00_6	148.9	0.24	0.39 ± 0.13	5.0 ± 1.0	5.6 ± 1.1	0.039 ± 0.008	11.1 ± 2.2	28.1 ± 9.5	2.53 ± 0.99
G140.77+05.00_7	115.6	0.19	0.17 ± 0.03	5.2 ± 1.0	7.4 ± 1.5	0.040 ± 0.008	6.8 ± 1.4	9.6 ± 1.9	1.40 ± 0.40
G142.49+07.48_1	226.4	0.36	0.41 ± 0.14	4.7 ± 0.9	3.4 ± 0.7	0.035 ± 0.007	22.4 ± 4.5	44.4 ± 15.0	1.98 ± 0.78
G142.49+07.48_2	232.7	0.37	–	–	–	–	–	–	–
G142.49+07.48_3	81.0	0.13	–	–	–	–	–	–	–
G142.49+07.48_4	138.1	0.22	0.18 ± 0.08	8.3 ± 2.2	10.4 ± 2.7	0.066 ± 0.017	15.5 ± 4.1	12.1 ± 4.9	0.78 ± 0.38
G142.49+07.48_5	111.5	0.18	0.14 ± 0.03	9.3 ± 1.9	13.4 ± 2.7	0.069 ± 0.014	10.6 ± 2.1	7.5 ± 1.5	0.71 ± 0.20
G142.49+07.48_6	96.5	0.16	–	–	–	–	–	–	–
G142.49+07.48_7	136.9	0.22	–	–	–	–	–	–	–
G142.49+07.48_8	80.7	0.13	–	–	–	–	–	–	–
G142.49+07.48_9	113.2	0.18	–	–	–	–	–	–	–
G142.49+07.48_10	127.3	0.20	–	–	–	–	–	–	–
G142.49+07.48_11	56.8	0.09	–	–	–	–	–	–	–
G142.49+07.48_12	102.5	0.17	0.14 ± 0.03	4.9 ± 1.0	9.0 ± 1.8	0.043 ± 0.009	5.6 ± 1.1	6.9 ± 1.4	1.24 ± 0.35
G142.62+07.29_1	173.8	0.28	0.21 ± 0.04	4.7 ± 1.0	6.7 ± 1.4	0.053 ± 0.011	19.1 ± 4.0	17.3 ± 3.5	0.91 ± 0.27
G142.62+07.29_2	67.7	0.11	–	–	–	–	–	–	–
G142.62+07.29_3	143.8	0.23	0.29 ± 0.09	3.3 ± 0.7	4.5 ± 0.9	0.029 ± 0.006	7.4 ± 1.5	19.5 ± 5.9	2.65 ± 0.96
G142.62+07.29_4	127.5	0.20	–	–	–	–	–	–	–
G142.62+07.29_5	117.6	0.19	–	–	–	–	–	–	–
G142.62+07.29_6	104.4	0.17	–	–	–	–	–	–	–
G142.62+07.29_7	98.6	0.16	–	–	–	–	–	–	–

TABLE 3—*Continued*

Name	FWHM[a] $''$	$R_{\rm eff}$[b] pc	$\sigma_{\rm C^{18}O}$ km s^{-1}	$N_{\rm H_2}^{\rm 13CO}$ 10^{21} cm^{-2}	$n_{\rm H_2}^{\rm 13CO}$ 10^{3} cm^{-3}	$\Sigma^{\rm 13CO}$ g cm^{-2}	$M_{\rm H_2}^{\rm 13CO}$ $M_\odot$	$M_{\rm vir}$ $M_\odot$	$\alpha_{\rm vir}$
G142.62+07.29_8	63.7	0.10	–	–	–	–	–	–	–
G144.84+00.76_1	237.6	1.52	–	–	–	–	–	–	–
G144.84+00.76_2	189.3	1.21	–	–	–	–	–	–	–
G144.84+00.76_3	212.6	1.35	–	–	–	–	–	–	–
G144.84+00.76_4	105.2	0.67	–	–	–	–	–	–	–
G144.84+00.76_5	75.1	0.48	–	–	–	–	–	–	–
G144.84+00.76_6	94.7	0.60	–	–	–	–	–	–	–
G144.84+00.76_7	88.5	0.56	–	–	–	–	–	–	–
G144.84+00.76_8	76.7	0.49	–	–	–	–	–	–	–
G144.84+00.76_9	146.4	0.94	–	–	–	–	–	–	–
G144.84+00.76_10	105.8	0.68	–	–	–	–	–	–	–
G144.84+00.76_11	102.5	0.65	–	–	–	–	–	–	–
G144.84+00.76_12	83.2	0.53	–	–	–	–	–	–	–
G144.84+00.76_13	119.5	0.77	–	–	–	–	–	–	–
G144.84+00.76_14	115.1	0.73	–	–	–	–	–	–	–
G146.11+07.80_1	247.2	0.38	0.40 ± 0.04	8.9 ± 1.2	6.5 ± 0.9	0.070 ± 0.010	47.3 ± 6.5	44.9 ± 4.5	0.95 ± 0.16
G146.11+07.80_2	165.7	0.25	–	–	–	–	–	–	–
G146.11+07.80_3	128.4	0.20	0.32 ± 0.05	9.0 ± 1.7	13.2 ± 2.5	0.074 ± 0.014	13.5 ± 2.6	18.3 ± 2.8	1.36 ± 0.34
G146.11+07.80_4	202.0	0.31	–	–	–	–	–	–	–
G146.11+07.80_5	135.6	0.21	0.30 ± 0.06	3.6 ± 0.7	5.0 ± 1.0	0.029 ± 0.006	6.0 ± 1.2	18.1 ± 3.9	3.02 ± 0.89
G146.11+07.80_6	91.8	0.14	–	–	–	–	–	–	–
G146.71+02.05_1	277.7	0.38	0.33 ± 0.06	6.7 ± 1.3	4.6 ± 0.9	0.050 ± 0.010	34.0 ± 6.8	37.3 ± 7.2	1.10 ± 0.30
G146.71+02.05_2	222.4	0.30	0.34 ± 0.14	5.0 ± 1.0	4.5 ± 0.9	0.039 ± 0.008	17.3 ± 3.5	30.5 ± 12.3	1.77 ± 0.80
G146.71+02.05_3	189.2	0.26	–	–	–	–	–	–	–
G146.71+02.05_4	144.8	0.20	–	–	–	–	–	–	–
G146.71+02.05_5	81.1	0.11	–	–	–	–	–	–	–
G146.71+02.05_6	140.2	0.19	–	–	–	–	–	–	–
G146.71+02.05_7	223.9	0.30	–	–	–	–	–	–	–
G146.71+02.05_8	191.3	0.26	0.14 ± 0.03	4.1 ± 0.8	4.1 ± 0.8	0.031 ± 0.006	10.0 ± 2.0	11.0 ± 2.2	1.10 ± 0.31
G147.01+03.39_1	155.8	0.23	0.29 ± 0.07	4.7 ± 0.9	5.3 ± 1.1	0.034 ± 0.007	8.3 ± 1.7	19.4 ± 4.7	2.33 ± 0.73
G148.00+00.09_1	106.3	0.67	0.77 ± 0.22	21.2 ± 4.2	11.8 ± 2.4	0.224 ± 0.045	474.8 ± 95.0	152.9 ± 43.9	0.32 ± 0.11
G148.00+00.09_2	207.1	1.30	0.91 ± 0.09	11.2 ± 2.2	2.3 ± 0.5	0.084 ± 0.017	679.5 ± 135.9	348.5 ± 34.0	0.51 ± 0.11
G148.00+00.09_3	74.3	0.47	–	–	–	–	–	–	–
G148.00+00.09_4	224.2	1.41	0.50 ± 0.05	13.9 ± 2.1	2.5 ± 0.4	0.103 ± 0.015	972.1 ± 146.4	207.0 ± 22.7	0.21 ± 0.04
G148.00+00.09_5	112.1	0.70	0.32 ± 0.08	14.5 ± 4.0	6.0 ± 1.7	0.121 ± 0.033	285.4 ± 78.6	67.1 ± 17.3	0.24 ± 0.09
G148.00+00.09_6	211.6	1.33	0.43 ± 0.10	6.7 ± 1.3	1.3 ± 0.3	0.051 ± 0.010	428.6 ± 85.7	170.9 ± 38.8	0.40 ± 0.12
G148.00+00.09_7	155.5	0.97	–	–	–	–	–	–	–
G148.00+00.09_8	157.6	0.99	–	–	–	–	–	–	–
G148.00+00.09_9	122.9	0.77	–	–	–	–	–	–	–
G148.00+00.09_10	94.3	0.59	0.26 ± 0.05	30.4 ± 6.6	16.8 ± 3.6	0.285 ± 0.062	475.3 ± 102.9	46.0 ± 9.3	0.10 ± 0.03
G148.00+00.09_11	120.9	0.76	–	–	–	–	–	–	–
G148.00+00.09_12	52.3	0.33	0.61 ± 0.10	34.9 ± 7.0	27.2 ± 5.4	0.255 ± 0.051	130.5 ± 26.1	58.7 ± 10.2	0.45 ± 0.12
G148.00+00.09_13	148.6	0.93	–	–	–	–	–	–	–
G148.24+00.41_1	152.3	0.96	0.32 ± 0.06	33.8 ± 7.0	11.3 ± 2.4	0.312 ± 0.065	1379.4 ± 286.4	91.7 ± 18.2	0.07 ± 0.02

TABLE 3—*Continued*

Name	FWHM[a] $''$	$R_{\rm eff}$[b] pc	$\sigma_{\rm C^{18}O}$ km s^{-1}	$N_{\rm H_2}^{\rm 13CO}$ 10^{21} cm^{-2}	$n_{\rm H_2}^{\rm 13CO}$ 10^{3} cm^{-3}	$\Sigma^{\rm 13CO}$ g cm^{-2}	$M_{\rm H_2}^{\rm 13CO}$ $M_\odot$	$M_{\rm vir}$ $M_\odot$	$\alpha_{\rm vir}$
G148.24+00.41_2	180.7	1.14	0.74 ± 0.06	23.1 ± 3.5	6.4 ± 1.0	0.209 ± 0.031	1302.9 ± 194.6	250.8 ± 19.0	0.19 ± 0.03
G148.24+00.41_3	169.0	1.07	0.78 ± 0.17	9.6 ± 1.3	3.5 ± 0.5	0.107 ± 0.015	584.4 ± 79.5	245.1 ± 53.2	0.42 ± 0.11
G148.24+00.41_4	247.8	1.57	0.50 ± 0.05	11.8 ± 1.8	2.0 ± 0.3	0.088 ± 0.013	1035.0 ± 157.4	230.1 ± 24.1	0.22 ± 0.04
G148.24+00.41_5	132.1	0.83	–	–	–	–	–	–	–
G148.24+00.41_6	136.4	0.86	0.64 ± 0.08	12.3 ± 3.2	4.0 ± 1.1	0.099 ± 0.026	352.3 ± 92.1	162.7 ± 21.5	0.46 ± 0.14
G148.24+00.41_7	185.3	1.17	–	–	–	–	–	–	–
G149.23+03.07_1	266.7	0.36	0.42 ± 0.16	13.9 ± 2.8	9.9 ± 2.0	0.103 ± 0.021	65.4 ± 13.1	45.6 ± 17.0	0.70 ± 0.30
G149.23+03.07_2	90.6	0.12	–	–	–	–	–	–	–
G149.23+03.07_3	287.0	0.39	0.45 ± 0.08	10.0 ± 2.0	7.3 ± 1.5	0.082 ± 0.016	59.8 ± 12.0	52.5 ± 9.2	0.88 ± 0.23
G149.23+03.07_4	349.7	0.48	0.38 ± 0.12	9.3 ± 1.9	6.0 ± 1.2	0.082 ± 0.016	88.7 ± 17.7	54.1 ± 16.6	0.61 ± 0.22
G149.23+03.07_5	234.9	0.32	0.47 ± 0.11	10.7 ± 2.1	8.8 ± 1.8	0.080 ± 0.016	39.4 ± 7.9	44.5 ± 10.5	1.13 ± 0.35
G149.41+03.37_1	340.2	0.46	0.47 ± 0.06	10.1 ± 2.0	6.9 ± 1.4	0.091 ± 0.018	93.3 ± 18.7	64.5 ± 8.7	0.69 ± 0.17
G149.41+03.37_2	133.6	0.18	0.42 ± 0.07	10.2 ± 2.0	17.9 ± 3.6	0.093 ± 0.019	14.7 ± 2.9	22.9 ± 4.0	1.55 ± 0.41
G149.41+03.37_3	105.9	0.14	–	–	–	–	–	–	–
G149.41+03.37_4	224.8	0.31	0.27 ± 0.13	9.5 ± 1.9	9.4 ± 1.9	0.082 ± 0.016	36.7 ± 7.3	24.8 ± 11.9	0.68 ± 0.35
G149.41+03.37_5	94.4	0.13	–	–	–	–	–	–	–
G149.41+03.37_6	186.5	0.25	0.17 ± 0.03	12.6 ± 2.2	14.1 ± 2.4	0.103 ± 0.018	31.6 ± 5.5	12.8 ± 2.6	0.41 ± 0.11
G149.41+03.37_7	68.9	0.09	–	–	–	–	–	–	–
G149.41+03.37_8	145.3	0.20	–	–	–	–	–	–	–
G149.41+03.37_9	139.1	0.19	–	–	–	–	–	–	–
G149.41+03.37_10	152.5	0.21	0.40 ± 0.08	10.5 ± 2.1	19.6 ± 3.9	0.117 ± 0.023	24.0 ± 4.8	24.7 ± 5.2	1.03 ± 0.30
G149.52-01.23_1	244.2	0.36	0.68 ± 0.06	18.3 ± 3.7	13.1 ± 2.6	0.136 ± 0.027	86.0 ± 17.2	73.3 ± 6.4	0.85 ± 0.19
G149.52-01.23_2	206.4	0.31	0.32 ± 0.16	8.8 ± 0.9	7.4 ± 0.8	0.065 ± 0.007	29.3 ± 3.1	29.4 ± 14.6	1.01 ± 0.51
G149.52-01.23_3	68.4	0.10	–	–	–	–	–	–	–
G149.52-01.23_4	79.6	0.12	–	–	–	–	–	–	–
G149.52-01.23_5	166.0	0.25	0.66 ± 0.11	9.8 ± 2.0	10.3 ± 2.1	0.073 ± 0.015	21.2 ± 4.2	47.9 ± 8.4	2.26 ± 0.60
G149.52-01.23_6	151.0	0.23	–	–	–	–	–	–	–
G149.52-01.23_7	124.2	0.19	–	–	–	–	–	–	–
G149.58+03.45_1	338.0	0.46	0.39 ± 0.04	13.2 ± 1.9	9.9 ± 1.4	0.130 ± 0.019	130.9 ± 18.8	53.2 ± 5.7	0.41 ± 0.07
G149.58+03.45_2	253.8	0.34	0.48 ± 0.06	12.6 ± 2.5	10.5 ± 2.1	0.104 ± 0.021	59.2 ± 11.9	49.5 ± 6.6	0.84 ± 0.20
G149.58+03.45_3	78.0	0.11	0.14 ± 0.03	15.4 ± 3.1	99.9 ± 20.0	0.304 ± 0.061	16.3 ± 3.3	4.4 ± 0.9	0.27 ± 0.08
G149.58+03.45_4	119.3	0.16	–	–	–	–	–	–	–
G149.58+03.45_5	222.7	0.30	0.31 ± 0.10	5.1 ± 1.0	4.6 ± 0.9	0.040 ± 0.008	17.4 ± 3.5	27.8 ± 8.7	1.60 ± 0.59
G149.58+03.45_6	221.9	0.30	–	–	–	–	–	–	–
G149.65+03.54_1	99.6	0.14	0.24 ± 0.04	24.9 ± 5.6	84.3 ± 19.0	0.327 ± 0.074	28.6 ± 6.5	9.8 ± 1.6	0.34 ± 0.09
G149.65+03.54_2	218.4	0.30	0.19 ± 0.02	15.5 ± 2.3	14.1 ± 2.1	0.120 ± 0.018	50.5 ± 7.5	17.1 ± 2.1	0.34 ± 0.07
G149.65+03.54_3	308.3	0.42	0.39 ± 0.07	9.7 ± 0.3	6.0 ± 0.2	0.072 ± 0.002	60.7 ± 1.8	48.2 ± 9.0	0.79 ± 0.15
G149.65+03.54_4	97.9	0.13	–	–	–	–	–	–	–
G149.65+03.54_5	219.6	0.30	0.14 ± 0.03	10.2 ± 1.4	8.8 ± 1.2	0.075 ± 0.010	32.0 ± 4.4	12.5 ± 2.5	0.39 ± 0.10
G149.65+03.54_6	73.0	0.10	–	–	–	–	–	–	–
G149.65+03.54_7	134.5	0.18	–	–	–	–	–	–	–
G149.65+03.54_8	246.2	0.33	0.73 ± 0.12	6.3 ± 1.3	5.0 ± 1.0	0.048 ± 0.010	25.6 ± 5.1	72.5 ± 12.3	2.83 ± 0.74
G150.22+03.91_1	343.6	0.46	0.48 ± 0.05	19.4 ± 2.7	11.9 ± 1.6	0.156 ± 0.022	158.4 ± 21.9	65.1 ± 6.3	0.41 ± 0.07
G150.22+03.91_2	106.3	0.14	0.14 ± 0.03	20.0 ± 4.6	48.7 ± 11.2	0.199 ± 0.046	19.3 ± 4.4	6.0 ± 1.2	0.31 ± 0.09

TABLE 3—*Continued*

Name	FWHM[a] $''$	$R_{\rm eff}$[b] pc	$\sigma_{\rm C^{18}O}$ km s^{-1}	$N_{\rm H_2}^{\rm 13CO}$ 10^{21}cm^{-2}	$n_{\rm H_2}^{\rm 13CO}$ 10^{3}cm^{-3}	$\Sigma^{\rm 13CO}$ g cm^{-2}	$M_{\rm H_2}^{\rm 13CO}$ $M_\odot$	$M_{\rm vir}$ $M_\odot$	$\alpha_{\rm vir}$
G150.22+03.91_3	130.5	0.17	0.36 ± 0.08	13.1 ± 2.6	13.3 ± 2.7	0.066 ± 0.013	9.7 ± 1.9	18.6 ± 3.9	1.92 ± 0.56
G150.22+03.91_4	162.5	0.22	0.20 ± 0.04	22.4 ± 3.3	36.5 ± 5.4	0.228 ± 0.034	51.7 ± 7.6	13.2 ± 2.7	0.25 ± 0.06
G150.22+03.91_5	96.8	0.13	0.30 ± 0.06	19.5 ± 4.9	80.1 ± 20.2	0.298 ± 0.075	23.9 ± 6.0	11.6 ± 2.2	0.48 ± 0.15
G150.22+03.91_6	315.6	0.42	0.38 ± 0.11	12.6 ± 2.5	8.1 ± 1.6	0.099 ± 0.020	84.3 ± 16.9	47.8 ± 14.1	0.57 ± 0.20
G150.22+03.91_7	237.3	0.32	0.42 ± 0.09	8.8 ± 1.8	7.6 ± 1.5	0.069 ± 0.014	33.4 ± 6.7	39.9 ± 8.5	1.20 ± 0.35
G150.44+03.95_1	370.1	0.50	0.46 ± 0.11	14.4 ± 2.9	8.8 ± 1.8	0.126 ± 0.025	147.6 ± 29.5	68.0 ± 16.2	0.46 ± 0.14
G150.44+03.95_2	304.8	0.41	0.21 ± 0.04	18.3 ± 2.9	11.9 ± 1.9	0.139 ± 0.022	111.0 ± 17.6	26.0 ± 4.5	0.23 ± 0.06
G150.44+03.95_3	88.3	0.12	0.14 ± 0.03	39.5 ± 6.2	114.9 ± 18.1	0.389 ± 0.061	25.9 ± 4.1	5.0 ± 1.0	0.19 ± 0.05
G150.44+03.95_4	88.9	0.12	0.30 ± 0.05	35.8 ± 7.3	74.7 ± 15.2	0.255 ± 0.052	17.3 ± 3.5	10.6 ± 1.8	0.61 ± 0.16
G150.44+03.95_5	164.3	0.22	0.23 ± 0.05	12.3 ± 2.5	16.6 ± 3.4	0.104 ± 0.021	24.1 ± 4.9	15.3 ± 3.0	0.63 ± 0.18
G150.44+03.95_6	153.9	0.21	0.19 ± 0.07	32.9 ± 5.8	58.9 ± 10.5	0.348 ± 0.062	70.6 ± 12.5	11.5 ± 4.1	0.16 ± 0.06
G150.44+03.95_7	384.9	0.51	0.28 ± 0.04	13.3 ± 2.4	6.8 ± 1.2	0.101 ± 0.018	127.9 ± 23.3	42.2 ± 6.4	0.33 ± 0.08
G151.08+04.46_1	228.4	0.30	0.29 ± 0.02	12.0 ± 0.3	12.8 ± 0.3	0.112 ± 0.003	49.8 ± 1.1	26.3 ± 1.9	0.53 ± 0.04
G151.08+04.46_2	133.5	0.18	0.38 ± 0.05	11.9 ± 2.2	22.2 ± 4.0	0.113 ± 0.021	17.2 ± 3.1	19.9 ± 2.6	1.16 ± 0.26
G151.08+04.46_3	85.4	0.11	0.36 ± 0.06	16.9 ± 4.1	65.9 ± 16.1	0.215 ± 0.052	13.3 ± 3.2	12.2 ± 2.2	0.92 ± 0.28
G151.08+04.46_4	258.8	0.35	0.32 ± 0.02	13.7 ± 1.3	11.8 ± 1.2	0.117 ± 0.011	66.9 ± 6.5	32.4 ± 2.5	0.48 ± 0.06
G151.08+04.46_5	160.6	0.21	0.22 ± 0.03	13.8 ± 1.8	16.5 ± 2.2	0.101 ± 0.013	22.3 ± 2.9	14.3 ± 1.7	0.64 ± 0.11
G151.08+04.46_6	81.9	0.11	0.21 ± 0.04	11.0 ± 2.9	31.1 ± 8.3	0.097 ± 0.026	5.6 ± 1.5	6.9 ± 1.4	1.25 ± 0.42
G151.08+04.46_7	172.1	0.23	0.22 ± 0.01	17.8 ± 1.1	24.1 ± 1.4	0.158 ± 0.009	39.8 ± 2.4	15.2 ± 0.7	0.38 ± 0.03
G151.08+04.46_8	197.7	0.26	0.24 ± 0.05	7.0 ± 1.4	7.9 ± 1.6	0.059 ± 0.012	19.8 ± 4.0	18.6 ± 3.8	0.94 ± 0.27
G151.45+03.95_1	335.9	0.45	0.87 ± 0.06	23.6 ± 4.7	15.4 ± 3.1	0.199 ± 0.040	194.7 ± 38.9	116.2 ± 7.8	0.60 ± 0.13
G151.45+03.95_2	247.9	0.33	0.55 ± 0.08	24.3 ± 4.9	19.3 ± 3.9	0.185 ± 0.037	98.5 ± 19.7	54.8 ± 7.6	0.56 ± 0.14
G151.45+03.95_3	244.4	0.33	0.36 ± 0.08	16.2 ± 3.2	12.8 ± 2.6	0.121 ± 0.024	63.1 ± 12.6	35.4 ± 8.2	0.56 ± 0.17
G151.45+03.95_4	98.0	0.13	–	–	–	–	–	–	–
G151.45+03.95_5	98.1	0.13	–	–	–	–	–	–	–
G151.45+03.95_6	196.4	0.26	–	–	–	–	–	–	–
G151.45+03.95_7	69.9	0.09	–	–	–	–	–	–	–
G151.45+03.95_8	121.2	0.16	–	–	–	–	–	–	–
G151.45+03.95_9	197.2	0.27	0.42 ± 0.11	18.1 ± 3.6	17.5 ± 3.5	0.134 ± 0.027	45.3 ± 9.1	33.0 ± 8.7	0.73 ± 0.24
G154.90+04.61_1	210.4	0.28	0.51 ± 0.07	19.7 ± 3.9	21.4 ± 4.3	0.170 ± 0.034	62.5 ± 12.5	42.2 ± 5.8	0.67 ± 0.16
G154.90+04.61_2	219.2	0.29	0.36 ± 0.07	11.3 ± 2.3	10.8 ± 2.2	0.090 ± 0.018	35.8 ± 7.2	30.5 ± 6.3	0.85 ± 0.25
G154.90+04.61_3	111.2	0.15	0.14 ± 0.03	15.0 ± 4.7	48.3 ± 15.1	0.203 ± 0.063	20.8 ± 6.5	6.1 ± 1.2	0.30 ± 0.11
G154.90+04.61_4	102.1	0.13	0.14 ± 0.03	16.9 ± 3.4	48.3 ± 9.7	0.186 ± 0.037	16.2 ± 3.2	5.7 ± 1.1	0.35 ± 0.10
G154.90+04.61_5	230.4	0.30	0.35 ± 0.09	10.8 ± 2.2	9.1 ± 1.8	0.079 ± 0.016	34.9 ± 7.0	31.6 ± 7.8	0.90 ± 0.29
G154.90+04.61_6	186.2	0.25	–	–	–	–	–	–	–
G154.90+04.61_7	118.0	0.16	–	–	–	–	–	–	–
G156.04+06.03_1	224.4	0.27	0.14 ± 0.03	6.9 ± 1.4	6.5 ± 1.3	0.051 ± 0.010	18.2 ± 3.7	11.5 ± 2.3	0.63 ± 0.18
G156.04+06.03_2	170.9	0.21	–	–	–	–	–	–	–
G156.04+06.03_3	150.9	0.18	–	–	–	–	–	–	–
G156.20+05.26_1	262.0	0.33	0.27 ± 0.05	8.2 ± 1.6	7.0 ± 1.4	0.067 ± 0.013	35.3 ± 7.1	26.4 ± 4.9	0.75 ± 0.20
G156.20+05.26_2	232.6	0.30	0.23 ± 0.08	6.4 ± 1.3	5.7 ± 1.1	0.048 ± 0.010	20.1 ± 4.0	20.2 ± 7.4	1.00 ± 0.42
G156.20+05.26_3	208.4	0.26	–	–	–	–	–	–	–
G157.25-01.00_1	331.9	0.44	0.18 ± 0.01	24.1 ± 0.9	15.0 ± 0.5	0.191 ± 0.007	180.3 ± 6.6	23.9 ± 1.8	0.13 ± 0.01
G157.25-01.00_2	154.2	0.21	0.20 ± 0.03	12.1 ± 2.4	25.8 ± 5.2	0.153 ± 0.031	31.2 ± 6.2	12.1 ± 2.1	0.39 ± 0.10

TABLE 3—*Continued*

Name	FWHM[a] $''$	$R_{\rm eff}$[b] pc	$\sigma_{\rm C^{18}O}$ km s^{-1}	$N_{\rm H_2}^{\rm 13CO}$ 10^{21}cm^{-2}	$n_{\rm H_2}^{\rm 13CO}$ 10^{3}cm^{-3}	$\Sigma^{\rm 13CO}$ g cm^{-2}	$M_{\rm H_2}^{\rm 13CO}$ $M_\odot$	$M_{\rm vir}$ $M_\odot$	$\alpha_{\rm vir}$
G157.25-01.00_3	94.0	0.13	0.17 ± 0.04	28.5 ± 3.1	71.9 ± 7.9	0.259 ± 0.029	19.7 ± 2.2	6.5 ± 1.4	0.33 ± 0.08
G157.25-01.00_4	83.7	0.11	–	–	–	–	–	–	–
G157.25-01.00_5	266.8	0.36	0.22 ± 0.01	16.0 ± 0.8	13.4 ± 0.7	0.137 ± 0.007	83.9 ± 4.4	22.9 ± 1.6	0.27 ± 0.02
G157.25-01.00_6	139.3	0.19	0.18 ± 0.01	20.8 ± 1.4	46.6 ± 3.2	0.249 ± 0.017	41.5 ± 2.8	9.7 ± 0.6	0.23 ± 0.02
G159.52+03.26_1	149.9	0.86	1.75 ± 0.30	11.0 ± 2.2	3.5 ± 0.7	0.086 ± 0.017	304.2 ± 60.8	446.5 ± 75.3	1.47 ± 0.38
G159.52+03.26_2	150.9	0.87	–	–	–	–	–	–	–
G159.52+03.26_3	147.2	0.85	–	–	–	–	–	–	–
G159.52+03.26_4	134.5	0.77	–	–	–	–	–	–	–
G159.52+03.26_5	128.2	0.75	0.50 ± 0.21	8.0 ± 1.6	3.1 ± 0.6	0.067 ± 0.013	180.4 ± 36.1	112.2 ± 46.0	0.62 ± 0.28
G159.52+03.26_6	134.9	0.79	–	–	–	–	–	–	–
G159.52+03.26_7	52.3	0.30	–	–	–	–	–	–	–
G159.52+03.26_8	101.0	0.58	0.19 ± 0.06	9.3 ± 1.9	5.2 ± 1.0	0.086 ± 0.017	138.9 ± 27.8	32.3 ± 10.8	0.23 ± 0.09
G159.52+03.26_9	104.6	0.61	–	–	–	–	–	–	–
G159.52+03.26_10	108.3	0.62	–	–	–	–	–	–	–
G162.79+01.34_1	268.5	0.35	–	–	–	–	–	–	–
G162.79+01.34_2	215.8	0.28	–	–	–	–	–	–	–
G162.79+01.34_3	262.5	0.34	0.35 ± 0.08	8.1 ± 2.5	6.8 ± 2.1	0.067 ± 0.021	37.9 ± 11.8	35.3 ± 7.7	0.93 ± 0.36
G162.79+01.34_4	174.0	0.23	–	–	–	–	–	–	–
G162.79+01.34_5	221.4	0.29	–	–	–	–	–	–	–
G169.14-01.13_1	178.4	0.97	0.97 ± 0.16	10.4 ± 2.1	2.9 ± 0.6	0.080 ± 0.016	363.4 ± 72.7	278.6 ± 45.3	0.77 ± 0.20
G169.14-01.13_2	200.6	1.09	–	–	–	–	–	–	–
G169.14-01.13_3	73.1	0.40	–	–	–	–	–	–	–
G169.14-01.13_4	127.2	0.69	–	–	–	–	–	–	–
G169.14-01.13_5	64.4	0.35	–	–	–	–	–	–	–
G169.14-01.13_6	66.7	0.36	–	–	–	–	–	–	–
G169.14-01.13_7	134.3	0.73	–	–	–	–	–	–	–
G169.14-01.13_8	87.7	0.48	–	–	–	–	–	–	–
G169.14-01.13_9	72.0	0.39	–	–	–	–	–	–	–
G169.14-01.13_10	73.3	0.40	–	–	–	–	–	–	–
G169.14-01.13_11	52.3	0.28	–	–	–	–	–	–	–
G169.14-01.13_12	73.6	0.40	–	–	–	–	–	–	–
G171.03+02.66_1	249.6	1.32	1.10 ± 0.13	8.4 ± 1.7	1.6 ± 0.3	0.062 ± 0.012	515.5 ± 103.1	432.3 ± 49.7	0.84 ± 0.19
G171.03+02.66_2	225.0	1.19	0.67 ± 0.15	10.3 ± 2.1	2.2 ± 0.4	0.077 ± 0.015	522.3 ± 104.5	236.8 ± 54.6	0.45 ± 0.14
G171.03+02.66_3	190.5	1.00	0.25 ± 0.06	9.5 ± 3.0	2.8 ± 0.9	0.081 ± 0.026	388.9 ± 125.0	73.4 ± 16.5	0.19 ± 0.07
G171.03+02.66_4	101.7	0.54	0.35 ± 0.07	18.2 ± 6.0	7.9 ± 2.6	0.123 ± 0.040	170.9 ± 56.3	56.1 ± 11.9	0.33 ± 0.13
G171.03+02.66_5	197.5	1.04	–	–	–	–	–	–	–
G171.03+02.66_6	151.1	0.80	0.38 ± 0.12	9.2 ± 1.8	4.2 ± 0.8	0.096 ± 0.019	296.4 ± 59.3	89.4 ± 29.7	0.30 ± 0.12
G171.03+02.66_7	113.7	0.60	–	–	–	–	–	–	–
G171.03+02.66_8	164.2	0.86	0.16 ± 0.06	6.5 ± 2.1	2.0 ± 0.6	0.050 ± 0.016	177.4 ± 56.5	41.1 ± 14.6	0.23 ± 0.11
G171.34+02.59_1	265.6	1.38	0.93 ± 0.21	12.1 ± 2.4	2.3 ± 0.5	0.092 ± 0.018	833.8 ± 166.8	378.8 ± 84.6	0.45 ± 0.14
G171.34+02.59_2	264.6	1.37	1.00 ± 0.14	10.4 ± 2.1	2.1 ± 0.4	0.082 ± 0.016	739.2 ± 147.8	406.9 ± 55.7	0.55 ± 0.13
G171.34+02.59_3	86.7	0.45	–	–	–	–	–	–	–
G171.34+02.59_4	205.8	1.07	–	–	–	–	–	–	–
G171.34+02.59_5	71.3	0.37	0.28 ± 0.10	16.7 ± 3.3	21.5 ± 4.3	0.228 ± 0.046	149.7 ± 29.9	31.0 ± 10.4	0.21 ± 0.08

TABLE 3—*Continued*

Name	FWHM[a] $''$	$R_{\rm eff}$[b] pc	$\sigma_{\rm C^{18}O}$ km s^{-1}	$N_{\rm H_2}^{\rm 13CO}$ 10^{21} cm^{-2}	$n_{\rm H_2}^{\rm 13CO}$ 10^{3} cm^{-3}	$\Sigma^{\rm 13CO}$ g cm^{-2}	$M_{\rm H_2}^{\rm 13CO}$ $M_\odot$	$M_{\rm vir}$ $M_\odot$	$\alpha_{\rm vir}$
G171.34+02.59_6	184.9	0.96	–	–	–	–	–	–	–
G171.34+02.59_7	153.8	0.81	–	–	–	–	–	–	–
G172.85+02.27_1	224.9	1.12	0.98 ± 0.07	40.7 ± 5.0	10.0 ± 1.2	0.320 ± 0.039	1920.6 ± 236.8	324.6 ± 21.7	0.17 ± 0.02
G172.85+02.27_2	250.9	1.25	1.31 ± 0.14	29.1 ± 5.8	6.0 ± 1.2	0.213 ± 0.043	1592.1 ± 318.4	485.6 ± 50.6	0.30 ± 0.07
G172.85+02.27_3	252.6	1.26	1.17 ± 0.18	31.0 ± 6.2	6.3 ± 1.3	0.227 ± 0.045	1716.7 ± 343.3	436.5 ± 66.5	0.25 ± 0.06
G172.85+02.27_4	194.4	0.97	–	–	–	–	–	–	–
G172.85+02.27_5	96.3	0.48	–	–	–	–	–	–	–
G172.85+02.27_6	166.6	0.83	–	–	–	–	–	–	–
G172.85+02.27_7	136.4	0.68	–	–	–	–	–	–	–
G175.20+01.28_1	135.9	0.67	0.53 ± 0.09	9.4 ± 1.9	3.7 ± 0.7	0.071 ± 0.014	152.6 ± 30.5	104.5 ± 17.8	0.68 ± 0.18
G175.20+01.28_2	177.5	0.87	–	–	–	–	–	–	–
G175.20+01.28_3	131.6	0.65	–	–	–	–	–	–	–
G175.20+01.28_4	62.5	0.31	0.33 ± 0.09	14.3 ± 2.9	13.3 ± 2.7	0.117 ± 0.023	52.7 ± 10.5	30.0 ± 8.2	0.57 ± 0.19
G175.20+01.28_5	188.0	0.92	–	–	–	–	–	–	–
G175.53+01.34_1	141.2	0.69	–	–	–	–	–	–	–
G175.53+01.34_2	156.0	0.77	–	–	–	–	–	–	–
G175.53+01.34_3	129.0	0.63	–	–	–	–	–	–	–
G175.53+01.34_4	91.3	0.45	–	–	–	–	–	–	–
G175.53+01.34_5	165.0	0.81	–	–	–	–	–	–	–
G175.53+01.34_6	150.0	0.74	–	–	–	–	–	–	–
G176.17-02.10_1	173.9	2.51	0.29 ± 0.03	12.8 ± 1.5	1.4 ± 0.2	0.098 ± 0.012	2969.4 ± 349.9	217.2 ± 20.0	0.07 ± 0.01
G176.17-02.10_2	181.4	2.62	0.29 ± 0.08	5.6 ± 0.6	0.7 ± 0.1	0.054 ± 0.005	1766.7 ± 174.1	228.6 ± 60.8	0.13 ± 0.04
G176.17-02.10_3	63.1	0.91	–	–	–	–	–	–	–
G176.17-02.10_4	170.2	2.46	–	–	–	–	–	–	–
G176.17-02.10_5	108.7	1.57	–	–	–	–	–	–	–
G176.17-02.10_6	172.9	2.50	0.26 ± 0.07	4.3 ± 0.9	0.5 ± 0.1	0.033 ± 0.007	980.1 ± 196.0	193.3 ± 50.4	0.20 ± 0.06
G176.17-02.10_7	67.0	0.97	–	–	–	–	–	–	–
G176.17-02.10_8	111.9	1.62	–	–	–	–	–	–	–
G176.17-02.10_9	112.6	1.63	–	–	–	–	–	–	–
G176.35+01.92_1	114.1	0.56	0.72 ± 0.08	6.4 ± 1.5	2.9 ± 0.7	0.047 ± 0.011	71.0 ± 16.3	120.4 ± 14.2	1.69 ± 0.44
G176.35+01.92_2	128.0	0.63	0.58 ± 0.09	6.7 ± 1.3	3.1 ± 0.6	0.056 ± 0.011	107.3 ± 21.5	108.4 ± 17.6	1.01 ± 0.26
G176.35+01.92_3	76.6	0.38	–	–	–	–	–	–	–
G176.35+01.92_4	99.7	0.49	–	–	–	–	–	–	–
G176.35+01.92_5	67.7	0.33	–	–	–	–	–	–	–
G176.35+01.92_6	120.5	0.60	–	–	–	–	–	–	–
G176.94+04.63_1	164.4	0.85	0.75 ± 0.10	10.6 ± 1.3	4.0 ± 0.5	0.097 ± 0.012	337.6 ± 40.3	189.7 ± 26.1	0.56 ± 0.10
G176.94+04.63_2	124.7	0.65	–	–	–	–	–	–	–
G176.94+04.63_3	176.4	0.92	–	–	–	–	–	–	–
G176.94+04.63_4	133.6	0.69	–	–	–	–	–	–	–
G176.94+04.63_5	135.7	0.70	–	–	–	–	–	–	–
G176.94+04.63_6	86.8	0.46	0.14 ± 0.03	14.2 ± 2.8	8.2 ± 1.6	0.107 ± 0.021	105.8 ± 21.2	19.1 ± 3.8	0.18 ± 0.05
G176.94+04.63_7	118.5	0.61	–	–	–	–	–	–	–
G176.94+04.63_8	130.9	0.68	–	–	–	–	–	–	–
G176.94+04.63_9	72.2	0.37	–	–	–	–	–	–	–

TABLE 3—*Continued*

Name	FWHM[a] $''$	$R_{\rm eff}$[b] pc	$\sigma_{\rm C^{18}O}$ km s^{-1}	$N_{\rm H_2}^{\rm 13CO}$ 10^{21}cm^{-2}	$n_{\rm H_2}^{\rm 13CO}$ 10^{3}cm^{-3}	$\Sigma^{\rm 13CO}$ g cm^{-2}	$M_{\rm H_2}^{\rm 13CO}$ $M_\odot$	$M_{\rm vir}$ $M_\odot$	$\alpha_{\rm vir}$
G176.94+04.63_10	113.0	0.60	–	–	–	–	–	–	–
G176.94+04.63_11	76.8	0.40	0.68 ± 0.14	8.7 ± 1.7	5.7 ± 1.1	0.065 ± 0.013	49.9 ± 10.0	81.0 ± 16.2	1.62 ± 0.46
G176.94+04.63_12	52.3	0.27	–	–	–	–	–	–	–
G176.94+04.63_13	115.0	0.59	–	–	–	–	–	–	–
G177.09+02.85_1	167.6	2.43	–	–	–	–	–	–	–
G177.09+02.85_2	162.1	2.35	–	–	–	–	–	–	–
G177.09+02.85_3	157.7	2.28	0.16 ± 0.03	9.2 ± 1.8	1.0 ± 0.2	0.069 ± 0.014	1717.1 ± 343.4	107.5 ± 21.5	0.06 ± 0.02
G177.09+02.85_4	143.7	2.08	–	–	–	–	–	–	–
G177.09+02.85_5	70.7	1.02	–	–	–	–	–	–	–
G177.09+02.85_6	66.3	0.96	–	–	–	–	–	–	–
G177.09+02.85_7	137.2	0.68	–	–	–	–	–	–	–
G177.14-01.21_1	175.9	2.56	0.65 ± 0.04	26.7 ± 2.7	2.7 ± 0.3	0.195 ± 0.020	6132.0 ± 612.9	494.5 ± 30.3	0.08 ± 0.01
G177.14-01.21_2	106.7	1.55	–	–	–	–	–	–	–
G177.14-01.21_3	136.5	1.99	0.42 ± 0.07	9.9 ± 2.1	1.3 ± 0.3	0.073 ± 0.016	1380.8 ± 297.9	248.3 ± 41.8	0.18 ± 0.05
G177.14-01.21_4	152.0	2.21	0.85 ± 0.18	9.4 ± 1.9	1.2 ± 0.2	0.073 ± 0.015	1712.2 ± 342.4	557.6 ± 115.4	0.33 ± 0.09
G177.14-01.21_5	126.6	1.84	–	–	–	–	–	–	–
G177.14-01.21_6	144.0	2.10	0.31 ± 0.08	5.8 ± 1.8	0.7 ± 0.2	0.045 ± 0.014	941.7 ± 289.5	190.6 ± 51.5	0.20 ± 0.08
G177.14-01.21_7	168.4	2.45	–	–	–	–	–	–	–
G177.86+01.04_1	221.4	3.21	0.94 ± 0.10	7.6 ± 2.2	0.7 ± 0.2	0.068 ± 0.019	3344.8 ± 960.5	899.0 ± 96.0	0.27 ± 0.08
G177.86+01.04_2	225.2	3.27	0.45 ± 0.08	5.2 ± 1.0	0.5 ± 0.1	0.044 ± 0.009	2274.1 ± 454.8	435.5 ± 79.9	0.19 ± 0.05
G177.86+01.04_3	87.3	1.27	0.14 ± 0.03	18.4 ± 6.0	4.3 ± 1.4	0.156 ± 0.051	1197.5 ± 389.0	53.3 ± 10.7	0.04 ± 0.02
G177.86+01.04_4	141.1	2.05	0.33 ± 0.10	13.7 ± 2.7	1.7 ± 0.3	0.101 ± 0.020	2032.1 ± 406.4	200.9 ± 58.3	0.10 ± 0.03
G178.28-00.61_1	100.8	0.28	0.71 ± 0.11	22.1 ± 5.6	24.5 ± 6.2	0.198 ± 0.050	75.7 ± 19.1	59.7 ± 9.2	0.79 ± 0.23
G178.28-00.61_2	293.2	0.82	0.72 ± 0.11	14.2 ± 1.6	4.9 ± 0.6	0.116 ± 0.013	374.0 ± 42.5	174.7 ± 26.5	0.47 ± 0.09
G178.28-00.61_3	117.4	0.33	0.91 ± 0.12	18.4 ± 3.7	16.1 ± 3.2	0.152 ± 0.030	78.8 ± 15.8	88.8 ± 11.4	1.13 ± 0.27
G178.28-00.61_4	52.3	0.15	–	–	–	–	–	–	–
G178.28-00.61_5	172.1	0.48	–	–	–	–	–	–	–
G178.28-00.61_6	158.1	0.44	–	–	–	–	–	–	–

[a]The extracted clump sizes with *Gaussclumps* procedure (see Section 3.2).

[b]The clump effective radius $R_{\rm eff}$ = FWHM/$(2\sqrt{\ln 2})$. The uncertainties of $R_{\rm eff}$ are ∼10%, which will cause additional uncertainty of around 21% in the derived masses.

Table 4

Observed parameters of extracted 850 μm cores

Name	Offset(R.A. DEC.)[a] ($''$ $''$)	$V_{^{13}CO}$ km s^{-1}	$\Delta V_{^{13}CO}$ km s^{-1}	$T_{^{13}CO}$ K	$V_{C^{18}O}$ km s^{-1}	$\Delta V_{C^{18}O}$ km s^{-1}	$T_{C^{18}O}$ K	$\tau_{^{13}CO}$	$T_{ex}(^{13}CO)$ K
G108.85-00.80_1	78.42, 89.09	-49.46 ± 0.02	3.06 ± 0.05	6.26 ± 0.29	-49.53 ± 0.10	2.01 ± 0.23	1.22 ± 0.23	1.36 ± 0.57	17.12 ± 1.95
G108.85-00.80_2	-49.32, -80.21	-49.99 ± 0.03	3.17 ± 0.07	4.95 ± 0.32	-49.84 ± 0.16	2.84 ± 0.34	0.94 ± 0.22	1.29 ± 0.70	14.25 ± 2.19
G108.85-00.80_3	64.49, 46.21	-49.43 ± 0.02	2.76 ± 0.05	6.44 ± 0.30	-49.50 ± 0.08	1.79 ± 0.18	1.41 ± 0.21	1.72 ± 0.51	16.68 ± 1.22
G108.85-00.80_4	107.96, 184.14	-49.51 ± 0.03	3.14 ± 0.08	4.07 ± 0.29	–	–	–	–	–
G108.85-00.80_5	-49.38, -113.27	-49.76 ± 0.04	3.22 ± 0.09	3.76 ± 0.32	-48.72 ± 0.13	1.19 ± 0.33	1.08 ± 0.26	2.71 ± 1.03	9.96 ± 0.92
G108.85-00.80_6	-102.54, -65.87	-51.07 ± 0.03	2.37 ± 0.07	5.57 ± 0.36	–	–	–	–	–
G108.85-00.80_7	-68.94, -67.74	-50.71 ± 0.03	2.80 ± 0.06	5.46 ± 0.28	-50.72 ± 0.14	2.52 ± 0.27	1.07 ± 0.22	1.37 ± 0.65	15.26 ± 1.89
G108.85-00.80_8	49.32, 93.62	-49.48 ± 0.03	3.14 ± 0.07	4.72 ± 0.31	–	–	–	–	–
G108.85-00.80_9	99.78, 144.00	-49.39 ± 0.03	3.00 ± 0.06	4.70 ± 0.26	–	–	–	–	–
G110.65+09.65_1	-52.08, -54.56	-4.27 ± 0.02	1.59 ± 0.04	6.07 ± 0.27	-4.34 ± 0.04	0.95 ± 0.09	2.16 ± 0.19	3.54 ± 0.51	14.75 ± 0.56
G110.65+09.65_2	-80.41, -12.92	-4.11 ± 0.02	1.57 ± 0.04	5.82 ± 0.25	-4.21 ± 0.04	1.00 ± 0.09	1.83 ± 0.17	2.96 ± 0.45	14.42 ± 0.57
G110.65+09.65_3	-20.50, -54.79	-4.32 ± 0.01	1.58 ± 0.03	6.93 ± 0.26	-4.31 ± 0.04	1.22 ± 0.12	1.92 ± 0.17	2.44 ± 0.38	16.80 ± 0.63
G110.65+09.65_4	-97.79, -38.93	-4.12 ± 0.02	1.58 ± 0.04	5.46 ± 0.27	-4.23 ± 0.04	0.97 ± 0.10	1.88 ± 0.19	3.38 ± 0.54	13.58 ± 0.60
G110.65+09.65_5	-101.10, 1.14	-4.18 ± 0.02	1.69 ± 0.04	5.70 ± 0.27	-4.34 ± 0.05	1.03 ± 0.14	1.40 ± 0.19	1.99 ± 0.49	14.77 ± 0.88
G120.16+03.09_1	-94.01, -156.23	-19.72 ± 0.02	2.53 ± 0.05	5.89 ± 0.29	-19.61 ± 0.08	2.04 ± 0.16	1.38 ± 0.19	1.87 ± 0.49	15.31 ± 1.01
G120.16+03.09_2	98.68, -37.56	-19.35 ± 0.02	2.47 ± 0.04	6.67 ± 0.26	-19.57 ± 0.09	2.45 ± 0.20	1.26 ± 0.18	1.20 ± 0.44	18.59 ± 2.05
G120.16+03.09_3	56.72, -19.18	-19.33 ± 0.01	2.36 ± 0.03	7.55 ± 0.23	-19.31 ± 0.05	1.62 ± 0.10	1.85 ± 0.17	2.02 ± 0.34	18.36 ± 0.71
G120.16+03.09_4	-30.74, 37.40	-19.61 ± 0.01	2.77 ± 0.03	7.09 ± 0.22	-19.81 ± 0.06	1.98 ± 0.13	1.76 ± 0.17	2.07 ± 0.37	17.44 ± 0.68
G120.16+03.09_5	-136.23, -95.98	-19.40 ± 0.02	2.68 ± 0.05	5.84 ± 0.29	-19.61 ± 0.09	2.31 ± 0.20	1.34 ± 0.20	1.80 ± 0.51	15.30 ± 1.09
G120.16+03.09_6	-13.81, -40.29	-19.55 ± 0.02	2.73 ± 0.04	6.29 ± 0.23	-19.55 ± 0.07	2.21 ± 0.15	1.42 ± 0.17	1.75 ± 0.41	16.32 ± 0.92
G120.16+03.09_7	-114.20, -144.07	-19.70 ± 0.02	2.47 ± 0.04	6.28 ± 0.29	-19.81 ± 0.08	1.99 ± 0.16	1.57 ± 0.21	2.10 ± 0.50	15.85 ± 0.88
G120.16+03.09_8	2.85, 20.11	-19.53 ± 0.02	2.60 ± 0.03	7.36 ± 0.25	-19.56 ± 0.05	1.96 ± 0.10	2.12 ± 0.18	2.63 ± 0.38	17.45 ± 0.57
G120.67+02.66_1	-41.96, 40.25	-18.17 ± 0.02	2.13 ± 0.05	4.79 ± 0.24	-18.36 ± 0.12	1.36 ± 0.26	0.78 ± 0.19	0.76 ± 0.65	16.28 ± 5.41
G120.67+02.66_2	50.42, -37.75	-18.09 ± 0.01	1.91 ± 0.03	6.53 ± 0.22	-18.10 ± 0.10	1.42 ± 0.21	0.99 ± 0.18	0.59 ± 0.47	23.57 ± 7.86
G120.67+02.66_3	5.12, 89.33	-16.95 ± 0.02	1.66 ± 0.04	6.16 ± 0.26	-16.92 ± 0.05	0.64 ± 0.12	1.32 ± 0.21	1.56 ± 0.51	16.40 ± 1.33
G120.67+02.66_4	22.35, 71.66	-16.97 ± 0.02	1.81 ± 0.04	6.24 ± 0.25	-16.89 ± 0.06	0.82 ± 0.39	1.13 ± 0.19	1.06 ± 0.49	18.23 ± 2.71
G120.67+02.66_5	-282.20, 15.44	-17.31 ± 0.03	1.71 ± 0.07	6.26 ± 0.43	–	–	–	–	–
G120.67+02.66_6	-44.65, 68.48	-17.67 ± 0.02	2.47 ± 0.05	4.53 ± 0.25	–	–	–	–	–
G120.67+02.66_7	-24.19, -88.27	-17.89 ± 0.02	1.77 ± 0.06	4.54 ± 0.25	-17.89 ± 0.10	0.74 ± 0.24	0.80 ± 0.22	0.98 ± 0.78	14.25 ± 3.67
G120.67+02.66_8	240.16, -98.69	-17.96 ± 0.02	1.93 ± 0.05	4.53 ± 0.24	-18.12 ± 0.11	1.15 ± 0.24	1.03 ± 0.24	1.75 ± 0.78	12.41 ± 1.19
G120.67+02.66_9	-144.25, 122.45	-17.36 ± 0.02	1.72 ± 0.05	5.40 ± 0.30	-17.09 ± 0.12	1.08 ± 0.29	0.85 ± 0.22	0.67 ± 0.22	18.95 ± 6.32
G120.67+02.66_10	-6.00, 67.61	-17.13 ± 0.02	1.96 ± 0.04	6.05 ± 0.22	-17.04 ± 0.07	1.12 ± 0.24	1.13 ± 0.18	1.15 ± 0.46	17.38 ± 2.10
G120.67+02.66_11	211.56, -81.82	-17.89 ± 0.02	1.84 ± 0.04	4.89 ± 0.25	-18.17 ± 0.12	1.60 ± 0.23	0.84 ± 0.19	0.92 ± 0.64	15.49 ± 3.66
G120.67+02.66_12	-326.07, 54.02	-17.23 ± 0.03	1.77 ± 0.09	5.97 ± 0.53	–	–	–	–	–
G120.67+02.66_13	88.02, 40.50	-17.29 ± 0.01	1.80 ± 0.04	5.70 ± 0.22	-17.13 ± 0.08	0.98 ± 0.20	0.87 ± 0.18	0.61 ± 0.53	20.69 ± 6.90
G120.67+02.66_14	-256.25, -6.76	-17.36 ± 0.02	1.61 ± 0.06	6.43 ± 0.44	-17.43 ± 0.09	0.70 ± 0.18	1.19 ± 0.28	1.12 ± 0.69	18.38 ± 3.64
G120.98+02.66_1	-43.04, -31.36	-17.26 ± 0.02	1.48 ± 0.04	6.15 ± 0.33	-17.24 ± 0.07	0.86 ± 0.20	1.46 ± 0.21	1.89 ± 0.51	15.82 ± 1.10
G120.98+02.66_2	-1.94, 17.24	-17.28 ± 0.02	1.56 ± 0.03	6.36 ± 0.28	-17.28 ± 0.08	1.59 ± 0.22	1.27 ± 0.20	1.34 ± 0.49	17.38 ± 1.76
G120.98+02.66_3	30.68, 18.80	-17.25 ± 0.02	1.61 ± 0.04	6.00 ± 0.28	-17.29 ± 0.07	1.43 ± 0.17	1.35 ± 0.20	1.72 ± 0.50	15.77 ± 1.13
G120.98+02.66_4	-11.20, -16.42	-17.13 ± 0.02	1.57 ± 0.04	6.04 ± 0.28	-17.05 ± 0.10	1.46 ± 0.23	1.05 ± 0.21	0.94 ± 0.56	18.39 ± 3.79
G120.98+02.66_5	83.86, 127.76	-17.31 ± 0.02	1.68 ± 0.06	4.31 ± 0.28	–	–	–	–	–
G121.35+03.39_1	103.71, -12.44	-5.47 ± 0.02	1.26 ± 0.05	3.95 ± 0.26	-5.46 ± 0.05	0.74 ± 0.12	1.60 ± 0.21	4.27 ± 0.88	10.19 ± 0.63
G121.35+03.39_2	138.21, 9.95	-5.31 ± 0.02	1.23 ± 0.05	3.56 ± 0.25	-5.42 ± 0.07	0.90 ± 0.14	1.25 ± 0.23	3.48 ± 1.00	9.32 ± 0.67
G121.35+03.39_3	-218.01, 197.83	-5.17 ± 0.04	1.27 ± 0.11	3.17 ± 0.42	-4.89 ± 0.06	0.62 ± 0.17	1.52 ± 0.28	5.44 ± 1.79	8.26 ± 1.07

TABLE 4—*Continued*

Name	Offset(R.A. DEC.)[a] ($'' \; ''$)	$V_{^{13}CO}$ km s^{-1}	$\Delta V_{^{13}CO}$ km s^{-1}	$T_{^{13}CO}$ K	$V_{C^{18}O}$ km s^{-1}	$\Delta V_{C^{18}O}$ km s^{-1}	$T_{C^{18}O}$ K	$\tau_{^{13}CO}$	$T_{ex}(^{13}CO)$ K
G121.35+03.39_4	210.50, -68.00	-5.49 ± 0.04	1.61 ± 0.09	2.66 ± 0.30	-5.51 ± 0.12	1.12 ± 0.26	0.83 ± 0.24	2.94 ± 1.35	7.10 ± 0.89
G125.66-00.55_1	-39.93, -51.55	-12.18 ± 0.04	5.14 ± 0.11	5.53 ± 0.27	-9.50 ± 0.07	1.09 ± 0.18	1.21 ± 0.20	1.61 ± 0.55	14.92 ± 1.27
G127.88+02.66_1	5.46, -194.55	-11.39 ± 0.01	1.52 ± 0.03	6.08 ± 0.23	-11.30 ± 0.10	1.35 ± 0.24	0.79 ± 0.17	0.22 ± 0.05	39.83 ± 13.28
G127.88+02.66_2	-58.05, -41.68	-11.18 ± 0.01	1.43 ± 0.03	5.77 ± 0.21	-11.11 ± 0.09	1.47 ± 0.24	0.78 ± 0.15	0.31 ± 0.10	29.71 ± 9.90
G128.95-00.18_1	148.40, 32.49	-14.30 ± 0.06	1.03 ± 0.15	2.81 ± 0.61	–	–	–	–	–
G128.95-00.18_2	218.98, -137.36	-14.02 ± 0.06	1.72 ± 0.13	2.96 ± 0.48	-13.82 ± 0.16	0.39 ± 0.08	1.13 ± 0.33	3.96 ± 1.89	7.77 ± 1.31
G128.95-00.18_3	-59.94, 29.72	-14.74 ± 0.02	1.19 ± 0.04	4.21 ± 0.24	–	–	–	–	–
G128.95-00.18_4	-181.56, 140.20	-14.75 ± 0.02	0.95 ± 0.05	4.58 ± 0.34	–	–	–	–	–
G128.95-00.18_5	-207.77, 143.75	-14.74 ± 0.02	0.98 ± 0.04	4.46 ± 0.29	-14.81 ± 0.06	0.45 ± 0.14	1.60 ± 0.25	3.62 ± 0.87	11.42 ± 0.70
G128.95-00.18_6	196.46, -126.91	-14.07 ± 0.04	1.34 ± 0.12	4.21 ± 0.52	-13.78 ± 0.10	0.80 ± 0.21	1.20 ± 0.32	2.58 ± 1.18	11.08 ± 1.47
G131.72+09.70_1	3.93, 4.10	-8.25 ± 0.02	1.21 ± 0.04	4.78 ± 0.30	-8.30 ± 0.10	0.71 ± 0.20	0.87 ± 0.23	1.05 ± 0.78	14.60 ± 3.39
G133.28+08.81_1	133.54, 62.77	-10.99 ± 0.03	1.81 ± 0.08	3.15 ± 0.26	-11.02 ± 0.05	1.04 ± 0.13	1.81 ± 0.22	7.16 ± 1.70	8.20 ± 0.67
G133.48+09.02_1	-15.21, 7.76	-16.10 ± 0.03	2.81 ± 0.07	7.86 ± 0.52	-16.15 ± 0.08	2.15 ± 0.19	1.97 ± 0.27	2.08 ± 0.53	18.85 ± 1.38
G133.48+09.02_2	-36.17, -43.86	-16.02 ± 0.03	2.82 ± 0.06	7.76 ± 0.43	-15.92 ± 0.11	2.43 ± 0.28	1.59 ± 0.27	1.41 ± 0.54	20.06 ± 2.22
G133.48+09.02_3	6.96, 80.12	-16.28 ± 0.03	2.79 ± 0.07	7.32 ± 0.44	-15.93 ± 0.18	3.44 ± 0.38	1.23 ± 0.29	0.85 ± 0.67	22.35 ± 6.80
G133.48+09.02_4	57.56, 167.15	-16.02 ± 0.05	2.98 ± 0.12	5.26 ± 0.55	–	–	–	–	–
G133.48+09.02_5	-2.64, 188.38	-15.74 ± 0.05	2.91 ± 0.10	4.84 ± 0.47	–	–	–	–	–
G133.48+09.02_6	-76.99, -64.32	-15.62 ± 0.03	2.25 ± 0.07	6.87 ± 0.51	-15.67 ± 0.11	2.20 ± 0.23	1.47 ± 0.28	1.55 ± 0.64	17.90 ± 2.12
G133.48+09.02_7	-41.23, -107.16	-15.68 ± 0.04	3.05 ± 0.09	6.05 ± 0.47	-15.42 ± 0.15	2.91 ± 0.33	1.42 ± 0.30	1.85 ± 0.76	15.68 ± 1.64
G133.48+09.02_8	-39.78, 3.63	-16.10 ± 0.03	2.81 ± 0.07	7.86 ± 0.52	-16.15 ± 0.08	2.15 ± 0.19	1.97 ± 0.27	2.08 ± 0.53	18.85 ± 1.38
G133.48+09.02_9	3.63, -35.19	-16.19 ± 0.03	3.05 ± 0.07	7.35 ± 0.47	-16.22 ± 0.10	2.51 ± 0.23	1.78 ± 0.27	1.95 ± 0.57	18.08 ± 1.40
G133.48+09.02_10	23.43, 42.34	-16.45 ± 0.04	2.85 ± 0.09	6.89 ± 0.47	-16.50 ± 0.14	2.03 ± 0.50	1.45 ± 0.29	1.50 ± 0.66	18.07 ± 2.21
G133.48+09.02_11	30.49, -76.31	-16.20 ± 0.04	3.21 ± 0.08	6.54 ± 0.49	-15.96 ± 0.14	2.92 ± 0.28	1.41 ± 0.30	1.57 ± 0.70	17.17 ± 2.11
G133.48+09.02_12	-44.38, -186.60	-15.56 ± 0.08	3.36 ± 0.22	3.94 ± 0.60	–	–	–	–	–
G133.48+09.02_13	-14.52, -163.97	-15.34 ± 0.05	3.23 ± 0.11	4.69 ± 0.48	-15.07 ± 0.17	2.50 ± 0.52	1.00 ± 0.27	1.54 ± 0.89	13.10 ± 2.18
G133.48+09.02_14	-30.17, 53.49	-16.34 ± 0.03	3.11 ± 0.07	7.54 ± 0.46	-16.17 ± 0.12	2.92 ± 0.25	1.49 ± 0.27	1.30 ± 0.57	20.01 ± 2.67
G133.48+09.02_15	-42.99, -69.29	-15.76 ± 0.03	2.47 ± 0.07	6.89 ± 0.48	-15.75 ± 0.08	1.72 ± 0.18	1.97 ± 0.29	2.57 ± 0.66	16.64 ± 1.13
G133.48+09.02_16	78.95, -120.55	-15.35 ± 0.05	3.01 ± 0.13	4.71 ± 0.48	-14.91 ± 0.08	1.09 ± 0.15	1.59 ± 0.28	3.30 ± 0.98	12.02 ± 1.16
G133.48+09.02_17	-0.87, 228.32	-15.25 ± 0.07	2.91 ± 0.17	3.45 ± 0.50	–	–	–	–	–
G133.48+09.02_18	75.47, 10.28	-16.58 ± 0.04	3.02 ± 0.10	5.66 ± 0.51	-16.87 ± 0.15	2.16 ± 0.37	1.31 ± 0.28	1.80 ± 0.76	14.92 ± 1.77
G140.49+06.07_1	-10.57, -29.18	-16.44 ± 0.02	1.55 ± 0.06	4.93 ± 0.31	–	–	–	–	–
G146.11+07.80_1	22.23, 162.29	-12.00 ± 0.02	1.33 ± 0.03	3.98 ± 0.19	-11.90 ± 0.06	1.02 ± 0.13	0.96 ± 0.14	1.94 ± 0.53	10.88 ± 0.72
G146.11+07.80_2	-287.12, 163.10	–	–	–	–	–	–	–	–
G147.01+03.39_1	-18.45, -7.03	-4.78 ± 0.01	0.64 ± 0.03	4.54 ± 0.29	-4.79 ± 0.06	0.59 ± 0.11	1.12 ± 0.21	2.02 ± 0.70	12.17 ± 1.03
G148.00+00.09_1	328.39, 11.29	-33.20 ± 0.03	2.16 ± 0.07	4.26 ± 0.29	–	–	–	–	–
G148.00+00.09_2	308.72, 25.02	-33.68 ± 0.03	1.88 ± 0.08	4.06 ± 0.33	–	–	–	–	–
G148.00+00.09_3	109.39, 15.81	-33.87 ± 0.02	1.66 ± 0.08	4.55 ± 0.29	-34.02 ± 0.10	0.81 ± 0.20	0.94 ± 0.24	1.55 ± 0.83	12.73 ± 1.64
G148.00+00.09_4	311.01, -123.54	-32.88 ± 0.05	2.24 ± 0.12	3.47 ± 0.37	–	–	–	–	–
G148.00+00.09_5	-43.82, -104.35	-34.34 ± 0.02	1.75 ± 0.05	4.15 ± 0.27	-34.33 ± 0.13	1.48 ± 0.24	0.84 ± 0.21	1.50 ± 0.80	11.80 ± 1.56
G149.52-01.23_1	38.82, 40.64	-7.71 ± 0.02	2.07 ± 0.04	5.40 ± 0.24	-7.41 ± 0.08	1.12 ± 0.19	0.83 ± 0.14	0.61 ± 0.45	19.71 ± 6.53
G149.52-01.23_2	-26.98, -72.05	-7.81 ± 0.01	1.81 ± 0.03	6.12 ± 0.23	-7.65 ± 0.05	1.10 ± 0.13	1.41 ± 0.15	1.79 ± 0.39	15.91 ± 0.87
G156.04+06.03_1	-169.13, -12.63	5.53 ± 0.04	0.90 ± 0.08	3.16 ± 0.47	–	–	–	–	–
G156.20+05.26_1	-11.33, 24.10	5.31 ± 0.01	0.66 ± 0.03	5.70 ± 0.36	–	–	–	–	–
G156.20+05.26_2	-239.84, 223.72	–	–	–	–	–	–	–	–

TABLE 4—*Continued*

Name	Offset(R.A. DEC.)[a] ($''$ $''$)	$V_{^{13}CO}$ km s^{-1}	$\Delta V_{^{13}CO}$ km s^{-1}	$T_{^{13}CO}$ K	$V_{C^{18}O}$ km s^{-1}	$\Delta V_{C^{18}O}$ km s^{-1}	$T_{C^{18}O}$ K	$\tau_{^{13}CO}$	$T_{ex}(^{13}CO)$ K
G159.52+03.26_1	8.45, 0.25	-14.93 ± 0.05	3.81 ± 0.10	3.06 ± 0.26	-14.46 ± 0.21	3.62 ± 0.54	0.72 ± 0.20	1.98 ± 1.00	8.48 ± 1.04
G159.52+03.26_2	14.94, -28.95	-14.83 ± 0.05	3.56 ± 0.12	2.98 ± 0.29	-14.64 ± 0.20	2.70 ± 0.63	0.64 ± 0.19	1.67 ± 1.00	8.48 ± 1.36
G169.14-01.13_1	-223.23, 15.61	-9.29 ± 0.03	1.58 ± 0.08	3.13 ± 0.30	-9.29 ± 0.10	1.04 ± 0.23	0.75 ± 0.19	2.05 ± 0.95	8.62 ± 1.11
G171.34+02.59_1	-44.85, -140.46	-19.31 ± 0.02	2.00 ± 0.04	3.85 ± 0.18	-19.39 ± 0.12	1.26 ± 0.24	0.66 ± 0.17	0.99 ± 0.72	12.24 ± 2.82
G171.34+02.59_2	-51.01, 68.72	-19.08 ± 0.02	1.75 ± 0.06	3.37 ± 0.21	-18.90 ± 0.09	0.95 ± 0.22	0.79 ± 0.18	1.96 ± 0.80	9.31 ± 0.87
G172.85+02.27_1	-8.94, 2.00	-17.35 ± 0.02	3.35 ± 0.06	6.79 ± 0.31	-17.27 ± 0.11	2.34 ± 0.31	1.30 ± 0.23	1.32 ± 0.53	18.39 ± 2.08
G172.85+02.27_2	-36.58, 9.24	-17.21 ± 0.03	3.28 ± 0.07	6.69 ± 0.32	-17.24 ± 0.09	2.17 ± 0.23	1.42 ± 0.22	1.64 ± 0.53	17.34 ± 1.41
G172.85+02.27_3	7.84, -31.33	-17.15 ± 0.03	3.34 ± 0.06	6.56 ± 0.33	-17.25 ± 0.10	1.95 ± 0.23	1.22 ± 0.22	1.23 ± 0.55	18.19 ± 2.40
G172.85+02.27_4	-18.96, 30.70	-17.39 ± 0.02	3.25 ± 0.06	6.66 ± 0.29	-17.48 ± 0.07	1.92 ± 0.15	1.58 ± 0.20	2.01 ± 0.46	16.70 ± 0.91
G172.85+02.27_5	24.01, -52.54	-16.99 ± 0.03	3.35 ± 0.07	5.68 ± 0.35	-16.71 ± 0.17	2.59 ± 0.38	0.88 ± 0.23	0.72 ± 0.69	19.27 ± 7.65
G172.85+02.27_6	267.97, 59.03	-17.58 ± 0.04	3.29 ± 0.08	5.57 ± 0.41	–	–	–	–	–
G172.85+02.27_7	-25.62, -25.13	-17.15 ± 0.03	3.12 ± 0.06	6.15 ± 0.33	-17.06 ± 0.07	1.49 ± 0.17	1.58 ± 0.24	2.29 ± 0.59	15.42 ± 0.91
G175.20+01.28_1	-1.87, -8.20	-6.12 ± 0.03	2.05 ± 0.07	3.97 ± 0.31	–	–	–	–	–
G176.17-02.10_1	23.54, 4.78	-20.37 ± 0.02	1.18 ± 0.04	4.30 ± 0.26	-20.32 ± 0.04	0.50 ± 0.07	1.76 ± 0.19	4.89 ± 0.85	10.97 ± 0.61
G176.94+04.63_1	110.26, 108.72	-17.61 ± 0.02	1.97 ± 0.05	4.49 ± 0.22	-17.60 ± 0.18	1.41 ± 0.41	0.73 ± 0.20	0.87 ± 0.76	14.64 ± 4.44
G176.94+04.63_2	80.64, 79.53	-17.53 ± 0.02	2.06 ± 0.04	4.71 ± 0.20	-17.78 ± 0.11	1.46 ± 0.23	0.79 ± 0.18	0.95 ± 0.64	14.86 ± 3.32
G177.14-01.21_1	-5.41, 26.68	-17.45 ± 0.02	2.29 ± 0.05	5.58 ± 0.26	-17.34 ± 0.05	1.28 ± 0.12	1.69 ± 0.19	3.23 ± 0.55	13.86 ± 0.59
G177.14-01.21_2	-8.46, 67.26	-17.36 ± 0.02	2.23 ± 0.05	5.14 ± 0.27	-17.30 ± 0.06	1.23 ± 0.17	1.40 ± 0.20	2.77 ± 0.61	13.09 ± 0.69
G177.14-01.21_3	7.97, -4.93	-17.23 ± 0.02	2.39 ± 0.05	5.58 ± 0.27	-17.31 ± 0.09	1.72 ± 0.30	1.14 ± 0.19	1.73 ± 0.56	14.85 ± 1.15
G178.28-00.61_1	-7.66, 35.90	-0.52 ± 0.02	2.05 ± 0.05	5.23 ± 0.27	-0.62 ± 0.09	1.53 ± 0.21	1.13 ± 0.21	1.63 ± 0.62	14.22 ± 1.30
G178.28-00.61_2	6.42, -3.54	-0.80 ± 0.02	1.95 ± 0.06	4.95 ± 0.26	-1.11 ± 0.07	0.82 ± 0.19	1.20 ± 0.23	2.01 ± 0.70	13.12 ± 0.97
G178.28-00.61_3	14.82, -60.69	-0.89 ± 0.02	1.83 ± 0.05	4.65 ± 0.23	-1.12 ± 0.05	1.02 ± 0.11	1.68 ± 0.21	3.71 ± 0.70	11.82 ± 0.55
G178.28-00.61_4	7.58, 128.09	-0.30 ± 0.02	1.96 ± 0.05	4.57 ± 0.26	-0.47 ± 0.09	0.91 ± 0.24	1.06 ± 0.24	1.86 ± 0.77	12.39 ± 1.10
G178.28-00.61_5	143.47, 216.17	-0.84 ± 0.03	2.30 ± 0.07	4.74 ± 0.35	–	–	–	–	–
G178.28-00.61_6	96.32, -84.03	-1.02 ± 0.02	1.72 ± 0.05	4.69 ± 0.28	-1.17 ± 0.12	1.09 ± 0.31	0.71 ± 0.20	0.62 ± 0.21	17.28 ± 5.76
G178.28-00.61_7	-3.90, -97.24	-0.68 ± 0.03	2.62 ± 0.07	3.72 ± 0.24	-1.19 ± 0.08	1.29 ± 0.22	1.39 ± 0.22	3.89 ± 0.95	9.67 ± 0.61
G178.28-00.61_8	31.89, -7.08	-0.87 ± 0.02	1.72 ± 0.04	5.79 ± 0.24	-0.98 ± 0.07	1.02 ± 0.13	1.34 ± 0.22	1.85 ± 0.57	15.12 ± 0.98
G178.28-00.61_9	32.82, -57.09	-0.90 ± 0.02	1.74 ± 0.05	5.20 ± 0.25	-1.10 ± 0.08	1.28 ± 0.20	1.08 ± 0.20	1.50 ± 0.60	14.37 ± 1.42
G178.28-00.61_10	-15.63, 102.99	-0.24 ± 0.02	1.91 ± 0.05	5.02 ± 0.28	-0.35 ± 0.15	1.29 ± 0.36	0.81 ± 0.25	0.77 ± 0.26	16.88 ± 7.07

[a]The absolute coordinate of each source is listed in Table 1.

TABLE 5

DERIVED PARAMETERS OF EXTRACTED 850 μM CORES

Name	FWHM[a] $''$	$R_{\rm eff}$[b] pc	$\sigma_{\rm C^{18}O}$ km s^{-1}	S_{850} Jy	$N_{\rm H_2}^{850\mu{\rm m}}$ 10^{22}cm^{-2}	$n_{\rm H_2}^{850\mu{\rm m}}$ 10^{4}cm^{-3}	$\Sigma^{850\mu{\rm m}}$ g cm^{-2}	$M_{\rm H_2}^{850\mu{\rm m}}$ $M_\odot$	$\alpha_{\rm vir}$	Infrared[c] WISE
G108.85-00.80_1	30.2	0.28	0.85 ± 0.10	2.19	6.4 ± 1.5	5.0 ± 0.9	0.403 ± 0.072	154.0 ± 27.6	0.46 ± 0.10	yes
G108.85-00.80_2	26.5	0.25	1.21 ± 0.14	1.43	4.6 ± 1.4	6.5 ± 1.7	0.464 ± 0.122	135.9 ± 35.7	0.65 ± 0.19	no
G108.85-00.80_3	30.7	0.29	0.76 ± 0.08	1.55	7.0 ± 1.4	3.5 ± 0.4	0.289 ± 0.034	113.8 ± 13.3	0.57 ± 0.09	no
G108.85-00.80_4	18.7	0.17	–	0.53	18.8 ± 0.8	12.4 ± 1.6	0.621 ± 0.081	90.5 ± 11.8	–	no
G108.85-00.80_5	16.3	0.15	0.51 ± 0.14	0.37	5.3 ± 1.7	14.1 ± 2.7	0.615 ± 0.118	68.2 ± 13.1	0.33 ± 0.11	no
G108.85-00.80_6	20.0	0.19	–	0.69	22.5 ± 0.8	8.0 ± 0.7	0.428 ± 0.039	71.0 ± 6.5	–	yes
G108.85-00.80_7	17.6	0.16	1.07 ± 0.11	0.38	4.9 ± 1.4	5.4 ± 1.1	0.253 ± 0.052	32.3 ± 6.6	1.60 ± 0.37	yes
G108.85-00.80_8	22.8	0.21	–	0.77	23.4 ± 0.9	7.6 ± 0.8	0.465 ± 0.049	101.2 ± 10.7	–	no
G108.85-00.80_9	17.8	0.17	–	0.39	22.2 ± 0.7	8.2 ± 0.7	0.394 ± 0.035	52.2 ± 4.7	–	no
G110.65+09.65_1	23.8	0.06	0.40 ± 0.04	2.17	6.7 ± 0.9	50.6 ± 3.2	0.823 ± 0.052	12.7 ± 0.8	0.53 ± 0.06	yes
G110.65+09.65_2	29.1	0.07	0.42 ± 0.04	2.52	5.3 ± 0.7	33.2 ± 2.2	0.663 ± 0.045	15.3 ± 1.0	0.57 ± 0.06	yes
G110.65+09.65_3	26.4	0.06	0.52 ± 0.05	0.81	5.8 ± 0.7	11.2 ± 0.7	0.202 ± 0.012	3.9 ± 0.2	2.52 ± 0.29	no
G110.65+09.65_4	31.1	0.07	0.41 ± 0.04	1.36	5.5 ± 0.8	16.2 ± 1.3	0.346 ± 0.027	9.1 ± 0.7	0.99 ± 0.12	no
G110.65+09.65_5	23.3	0.06	0.44 ± 0.06	0.60	4.0 ± 0.7	14.9 ± 1.5	0.237 ± 0.024	3.5 ± 0.4	2.05 ± 0.35	no
G120.16+03.09_1	18.7	0.07	0.87 ± 0.07	1.13	6.0 ± 1.1	31.9 ± 3.5	0.652 ± 0.071	15.9 ± 1.7	1.15 ± 0.16	yes
G120.16+03.09_2	20.2	0.07	1.04 ± 0.08	1.03	5.3 ± 1.0	17.8 ± 3.0	0.373 ± 0.063	9.6 ± 1.6	2.36 ± 0.44	yes
G120.16+03.09_3	30.8	0.11	0.69 ± 0.04	2.34	8.4 ± 1.0	11.7 ± 0.7	0.374 ± 0.022	22.0 ± 1.3	1.03 ± 0.09	yes
G120.16+03.09_4	34.0	0.13	0.84 ± 0.05	1.19	9.2 ± 1.2	4.6 ± 0.3	0.167 ± 0.010	13.1 ± 0.8	2.43 ± 0.21	yes
G120.16+03.09_5	19.1	0.07	0.98 ± 0.08	0.37	6.1 ± 1.2	10.2 ± 1.2	0.204 ± 0.024	4.8 ± 0.6	4.27 ± 0.62	yes
G120.16+03.09_6	29.8	0.11	0.94 ± 0.07	0.87	6.8 ± 1.1	5.6 ± 0.5	0.179 ± 0.016	10.6 ± 1.0	2.93 ± 0.34	no
G120.16+03.09_7	24.2	0.09	0.85 ± 0.07	0.68	7.0 ± 1.2	8.3 ± 0.8	0.220 ± 0.020	9.0 ± 0.8	2.58 ± 0.31	no
G120.16+03.09_8	32.8	0.12	0.83 ± 0.04	0.92	11.0 ± 1.3	4.0 ± 0.2	0.140 ± 0.007	9.9 ± 0.5	3.03 ± 0.22	yes
G120.67+02.66_1	22.5	0.07	0.58 ± 0.11	2.33	2.3 ± 0.6	42.3 ± 22.6	0.842 ± 0.450	19.4 ± 10.4	0.61 ± 0.35	no
G120.67+02.66_2	21.2	0.06	0.60 ± 0.09	1.54	3.2 ± 0.6	19.6 ± 9.2	0.360 ± 0.168	7.1 ± 3.3	1.62 ± 0.80	yes
G120.67+02.66_3	27.2	0.07	0.27 ± 0.05	2.19	3.7 ± 0.8	25.3 ± 3.3	0.532 ± 0.069	13.7 ± 1.8	0.43 ± 0.10	yes
G120.67+02.66_4	20.3	0.05	0.35 ± 0.17	0.79	3.3 ± 0.7	18.9 ± 4.3	0.295 ± 0.067	4.2 ± 1.0	1.35 ± 0.72	no
G120.67+02.66_5	16.7	0.04	–	0.43	19.1 ± 0.8	25.8 ± 2.3	0.322 ± 0.029	2.9 ± 0.3	–	yes
G120.67+02.66_6	23.5	0.06	–	0.87	17.3 ± 0.6	30.2 ± 2.8	0.534 ± 0.049	9.7 ± 0.9	–	yes
G120.67+02.66_7	20.6	0.06	0.31 ± 0.10	0.57	1.9 ± 0.4	17.9 ± 7.9	0.306 ± 0.135	5.2 ± 2.3	1.07 ± 0.58	yes
G120.67+02.66_8	21.1	0.06	0.49 ± 0.10	0.52	3.0 ± 0.9	19.3 ± 3.4	0.342 ± 0.060	6.2 ± 1.1	1.43 ± 0.39	yes
G120.67+02.66_9	23.1	0.06	0.46 ± 0.12	0.68	2.2 ± 0.4	10.5 ± 5.3	0.183 ± 0.092	3.2 ± 1.6	2.56 ± 1.46	yes
G120.67+02.66_10	20.6	0.05	0.48 ± 0.10	0.64	3.6 ± 0.7	15.9 ± 3.0	0.249 ± 0.047	3.5 ± 0.7	2.18 ± 0.62	no
G120.67+02.66_11	21.1	0.06	0.68 ± 0.10	0.59	2.2 ± 0.6	14.9 ± 5.8	0.261 ± 0.101	4.6 ± 1.8	2.65 ± 1.10	no
G120.67+02.66_12	14.1	0.04	–	0.21	18.6 ± 1.0	21.9 ± 2.6	0.234 ± 0.028	1.6 ± 0.2	–	no
G120.67+02.66_13	14.1	0.04	0.42 ± 0.09	0.21	2.4 ± 0.5	12.6 ± 6.1	0.132 ± 0.065	0.9 ± 0.4	5.31 ± 2.82	yes
G120.67+02.66_14	18.0	0.05	0.30 ± 0.08	0.37	3.2 ± 0.9	12.8 ± 3.9	0.173 ± 0.052	1.8 ± 0.6	2.25 ± 0.90	yes
G120.98+02.66_1	22.5	0.06	0.36 ± 0.09	1.23	3.8 ± 0.7	27.0 ± 3.0	0.465 ± 0.053	8.1 ± 0.9	0.81 ± 0.21	yes
G120.98+02.66_2	27.6	0.07	0.68 ± 0.10	1.77	3.3 ± 0.7	18.4 ± 2.9	0.384 ± 0.061	9.8 ± 1.5	1.50 ± 0.32	yes
G120.98+02.66_3	27.7	0.07	0.61 ± 0.07	1.21	3.7 ± 0.7	14.4 ± 1.7	0.305 ± 0.035	8.0 ± 0.9	1.67 ± 0.28	no
G120.98+02.66_4	35.7	0.10	0.62 ± 0.10	1.11	2.6 ± 0.6	4.8 ± 1.5	0.132 ± 0.042	5.7 ± 1.8	3.04 ± 1.07	yes
G120.98+02.66_5	23.8	0.06	–	0.44	11.0 ± 0.5	15.8 ± 1.8	0.286 ± 0.032	5.5 ± 0.6	–	no
G121.35+03.39_1	25.4	0.05	0.31 ± 0.05	1.20	3.4 ± 0.6	53.2 ± 6.7	0.793 ± 0.100	10.3 ± 1.3	0.47 ± 0.10	yes
G121.35+03.39_2	25.9	0.05	0.38 ± 0.06	0.89	2.3 ± 0.6	44.6 ± 7.0	0.678 ± 0.106	9.1 ± 1.4	0.66 ± 0.15	no
G121.35+03.39_3	17.4	0.04	0.27 ± 0.07	0.39	3.1 ± 0.9	84.8 ± 25.8	0.865 ± 0.263	5.2 ± 1.6	0.53 ± 0.22	yes

TABLE 5—*Continued*

Name	FWHM[a] $''$	$R_{\rm eff}$[b] pc	$\sigma_{\rm C^{18}O}$ km s^{-1}	S_{850} Jy	$N_{\rm H_2}^{850\mu m}$ 10^{22}cm^{-2}	$n_{\rm H_2}^{850\mu m}$ 10^{4}cm^{-3}	$\Sigma^{850\mu m}$ g cm^{-2}	$M_{\rm H_2}^{850\mu m}$ $M_\odot$	$\alpha_{\rm vir}$	Infrared[c] WISE
G121.35+03.39_4	19.5	0.04	0.48 ± 0.11	0.33	1.6 ± 0.3	73.9 ± 24.5	0.848 ± 0.281	6.5 ± 2.1	0.87 ± 0.35	no
G125.66-00.55_1	18.0	0.03	0.46 ± 0.08	0.26	10.1 ± 2.3	18.5 ± 2.6	0.170 ± 0.024	0.8 ± 0.1	5.28 ± 1.16	no
G127.88+02.66_1	14.1	0.04	0.57 ± 0.10	0.21	2.5 ± 0.5	5.5 ± 2.2	0.057 ± 0.023	0.4 ± 0.1	16.99 ± 7.58	no
G127.88+02.66_2	17.2	0.04	0.62 ± 0.10	0.32	1.9 ± 0.4	6.5 ± 2.8	0.083 ± 0.036	0.8 ± 0.3	10.54 ± 4.91	yes
G128.95-00.18_1	22.2	0.06	–	0.69	3.5 ± 0.6	74.6 ± 41.4	1.269 ± 0.703	21.4 ± 11.8	–	no
G128.95-00.18_2	14.1	0.04	0.17 ± 0.03	0.19	2.7 ± 0.5	70.0 ± 28.9	0.751 ± 0.310	5.0 ± 2.1	0.37 ± 0.17	yes
G128.95-00.18_3	19.5	0.05	–	0.39	7.5 ± 0.3	26.1 ± 2.7	0.392 ± 0.040	5.1 ± 0.5	–	yes
G128.95-00.18_4	18.6	0.05	–	0.36	6.8 ± 0.4	24.3 ± 3.0	0.347 ± 0.043	4.1 ± 0.5	–	no
G128.95-00.18_5	17.0	0.05	0.19 ± 0.06	0.28	2.7 ± 0.6	25.0 ± 2.9	0.327 ± 0.038	3.3 ± 0.4	0.80 ± 0.26	no
G128.95-00.18_6	14.1	0.04	0.34 ± 0.09	0.17	2.5 ± 0.5	28.0 ± 7.2	0.301 ± 0.078	2.0 ± 0.5	1.86 ± 0.69	no
G131.72+09.70_1	15.4	0.03	0.30 ± 0.09	0.40	1.5 ± 0.3	49.8 ± 19.5	0.363 ± 0.142	1.1 ± 0.4	2.03 ± 0.98	yes
G133.28+08.81_1	25.4	0.04	0.44 ± 0.06	0.76	5.7 ± 1.2	65.7 ± 12.6	0.808 ± 0.155	7.1 ± 1.4	0.79 ± 0.18	yes
G133.48+09.02_1	37.8	0.07	0.91 ± 0.08	10.43	10.8 ± 2.0	55.5 ± 6.2	1.062 ± 0.118	22.6 ± 2.5	0.80 ± 0.11	yes
G133.48+09.02_2	27.4	0.05	1.03 ± 0.12	4.00	8.3 ± 1.8	51.0 ± 8.3	0.706 ± 0.116	7.9 ± 1.3	1.88 ± 0.37	yes
G133.48+09.02_3	29.4	0.05	1.46 ± 0.16	4.53	6.0 ± 1.5	39.7 ± 17.2	0.592 ± 0.257	7.7 ± 3.3	2.94 ± 1.32	no
G133.48+09.02_4	18.7	0.03	–	1.74	26.1 ± 1.5	140.1 ± 21.7	1.327 ± 0.206	6.9 ± 1.1	–	yes
G133.48+09.02_5	22.8	0.04	–	1.68	22.6 ± 1.3	86.0 ± 13.3	0.988 ± 0.153	7.6 ± 1.2	–	yes
G133.48+09.02_6	23.0	0.04	0.93 ± 0.10	1.44	5.9 ± 1.5	36.7 ± 6.7	0.427 ± 0.078	3.3 ± 0.6	3.35 ± 0.70	no
G133.48+09.02_7	27.3	0.05	1.23 ± 0.14	2.66	7.5 ± 2.1	50.4 ± 8.6	0.695 ± 0.119	7.7 ± 1.3	2.29 ± 0.47	no
G133.48+09.02_8	20.6	0.04	0.91 ± 0.08	1.19	10.8 ± 2.0	38.8 ± 4.3	0.405 ± 0.045	2.6 ± 0.3	3.83 ± 0.54	no
G133.48+09.02_9	39.2	0.07	1.07 ± 0.10	3.59	10.2 ± 2.1	18.2 ± 2.2	0.361 ± 0.043	8.3 ± 1.0	2.64 ± 0.40	no
G133.48+09.02_10	34.2	0.06	0.86 ± 0.21	2.89	7.3 ± 1.9	22.0 ± 4.1	0.382 ± 0.072	6.7 ± 1.3	2.31 ± 0.71	yes
G133.48+09.02_11	38.9	0.07	1.24 ± 0.12	3.15	7.9 ± 2.2	17.6 ± 3.4	0.348 ± 0.067	7.9 ± 1.5	3.20 ± 0.69	yes
G133.48+09.02_12	19.3	0.03	–	0.73	19.2 ± 1.8	87.2 ± 24.8	0.848 ± 0.241	4.7 ± 1.3	–	yes
G133.48+09.02_13	18.4	0.03	1.06 ± 0.22	0.59	4.8 ± 1.0	48.8 ± 14.5	0.455 ± 0.135	2.3 ± 0.7	4.44 ± 1.61	yes
G133.48+09.02_14	32.3	0.06	1.24 ± 0.11	1.87	8.4 ± 1.9	14.6 ± 2.9	0.239 ± 0.047	3.7 ± 0.7	5.65 ± 1.22	yes
G133.48+09.02_15	22.9	0.04	0.73 ± 0.08	0.95	9.4 ± 1.9	27.6 ± 3.0	0.319 ± 0.035	2.5 ± 0.3	3.52 ± 0.53	yes
G133.48+09.02_16	24.9	0.04	0.46 ± 0.07	1.02	8.3 ± 2.1	40.6 ± 7.3	0.510 ± 0.092	4.7 ± 0.8	1.28 ± 0.29	no
G133.48+09.02_17	26.6	0.05	–	1.03	13.5 ± 1.3	61.0 ± 18.6	0.820 ± 0.250	8.6 ± 2.6	–	no
G133.48+09.02_18	18.1	0.03	0.92 ± 0.16	0.43	6.6 ± 1.9	30.5 ± 6.1	0.280 ± 0.056	1.4 ± 0.3	6.34 ± 1.67	yes
G140.49+06.07_1	19.7	0.07	–	1.19	12.3 ± 0.5	46.5 ± 4.5	0.911 ± 0.089	20.4 ± 2.0	–	yes
G146.11+07.80_1	19.2	0.03	0.43 ± 0.05	0.61	1.8 ± 0.4	73.8 ± 9.7	0.619 ± 0.081	2.5 ± 0.3	1.49 ± 0.27	no
G146.11+07.80_2	14.1	0.02	–	0.17	0.1 ± 0.0	5.6 ± 0.7	0.034 ± 0.004	0.1 ± 0.0	–	yes
G147.01+03.39_1	38.7	0.06	0.25 ± 0.05	1.85	1.1 ± 0.3	23.1 ± 3.6	0.372 ± 0.058	5.6 ± 0.9	0.75 ± 0.18	no
G148.00+00.09_1	14.6	0.09	–	0.24	13.8 ± 0.6	16.0 ± 1.9	0.419 ± 0.050	16.6 ± 2.0	–	yes
G148.00+00.09_2	15.1	0.09	–	0.21	11.2 ± 0.6	14.0 ± 2.0	0.379 ± 0.056	16.3 ± 2.4	–	yes
G148.00+00.09_3	22.5	0.14	0.34 ± 0.09	0.47	2.4 ± 0.5	6.3 ± 1.5	0.257 ± 0.060	24.5 ± 5.7	0.59 ± 0.20	yes
G148.00+00.09_4	14.1	0.09	–	0.17	10.5 ± 0.8	18.7 ± 4.2	0.471 ± 0.105	17.5 ± 3.9	–	yes
G148.00+00.09_5	20.3	0.13	0.63 ± 0.10	0.40	2.1 ± 0.4	8.5 ± 2.1	0.311 ± 0.077	24.2 ± 6.0	0.98 ± 0.29	yes
G149.52-01.23_1	17.7	0.03	0.48 ± 0.08	0.35	2.5 ± 0.4	20.5 ± 10.1	0.154 ± 0.076	0.5 ± 0.3	7.30 ± 3.82	no
G149.52-01.23_2	23.3	0.03	0.47 ± 0.06	0.41	4.4 ± 0.6	14.2 ± 1.3	0.141 ± 0.012	0.8 ± 0.1	5.94 ± 0.89	no
G156.04+06.03_1	15.8	0.02	–	0.82	3.7 ± 0.4	408.2 ± 137.0	2.251 ± 0.755	4.0 ± 1.3	–	yes
G156.20+05.26_1	14.1	0.02	–	0.87	6.5 ± 0.3	205.0 ± 18.0	1.050 ± 0.092	1.6 ± 0.1	–	yes
G156.20+05.26_2	14.1	0.02	–	0.17	0.1 ± 0.0	6.8 ± 0.8	0.035 ± 0.004	0.1 ± 0.0	–	yes

TABLE 5—*Continued*

Name	FWHM[a]	$R_{\rm eff}$[b]	$\sigma_{\rm C^{18}O}$	S_{850}	$N_{\rm H_2}^{850\mu\rm m}$	$n_{\rm H_2}^{850\mu\rm m}$	$\Sigma^{850\mu\rm m}$	$M_{\rm H_2}^{850\mu\rm m}$	$\alpha_{\rm vir}$	Infrared[c]
	$''$	pc	km s^{-1}	Jy	10^{22}cm^{-2}	10^{4}cm^{-3}	g cm^{-2}	$M_\odot$		WISE
G159.52+03.26_1	29.0	0.17	1.54 ± 0.23	0.90	3.5 ± 0.7	14.3 ± 4.0	0.681 ± 0.192	90.0 ± 25.4	0.84 ± 0.27	yes
G159.52+03.26_2	23.8	0.14	1.15 ± 0.27	0.40	2.7 ± 0.5	11.4 ± 4.2	0.446 ± 0.165	39.7 ± 14.7	1.17 ± 0.51	yes
G169.14-01.13_1	17.4	0.09	0.44 ± 0.10	0.24	1.5 ± 0.3	18.1 ± 5.3	0.493 ± 0.145	21.2 ± 6.2	0.58 ± 0.22	yes
G171.34+02.59_1	15.4	0.08	0.54 ± 0.10	0.23	1.7 ± 0.3	12.9 ± 5.5	0.296 ± 0.126	9.0 ± 3.8	1.41 ± 0.65	yes
G171.34+02.59_2	17.7	0.09	0.40 ± 0.09	0.29	1.8 ± 0.6	18.0 ± 3.7	0.475 ± 0.097	19.2 ± 3.9	0.57 ± 0.17	no
G172.85+02.27_1	37.5	0.19	0.99 ± 0.13	7.20	7.8 ± 1.7	14.3 ± 2.5	0.770 ± 0.133	129.3 ± 22.4	0.43 ± 0.09	yes
G172.85+02.27_2	26.8	0.13	0.92 ± 0.10	2.82	8.5 ± 1.8	16.8 ± 2.1	0.645 ± 0.082	55.4 ± 7.0	0.66 ± 0.11	yes
G172.85+02.27_3	27.8	0.14	0.83 ± 0.10	1.32	7.1 ± 1.6	6.6 ± 1.3	0.262 ± 0.053	24.1 ± 4.9	1.41 ± 0.33	yes
G172.85+02.27_4	16.9	0.08	0.81 ± 0.06	0.41	9.7 ± 1.6	10.5 ± 0.9	0.253 ± 0.022	8.6 ± 0.7	2.36 ± 0.27	yes
G172.85+02.27_5	25.9	0.13	1.10 ± 0.16	0.79	4.6 ± 1.2	4.5 ± 2.7	0.166 ± 0.099	13.3 ± 7.9	3.18 ± 1.95	yes
G172.85+02.27_6	26.5	0.13	–	0.71	31.3 ± 1.2	6.6 ± 0.7	0.251 ± 0.026	20.9 ± 2.2	–	no
G172.85+02.27_7	24.0	0.12	0.63 ± 0.07	0.57	9.2 ± 1.8	5.8 ± 0.6	0.198 ± 0.019	13.6 ± 1.3	1.66 ± 0.24	yes
G175.20+01.28_1	23.7	0.12	–	0.80	11.8 ± 0.6	18.2 ± 2.7	0.607 ± 0.089	39.3 ± 5.7	–	yes
G176.17-02.10_1	25.3	0.37	0.21 ± 0.03	0.40	4.1 ± 0.7	2.2 ± 0.2	0.228 ± 0.025	145.4 ± 15.8	0.16 ± 0.03	no
G176.94+04.63_1	27.6	0.14	0.60 ± 0.17	0.98	2.0 ± 0.4	6.9 ± 3.5	0.282 ± 0.144	27.5 ± 14.1	0.92 ± 0.54	yes
G176.94+04.63_2	23.2	0.12	0.62 ± 0.10	0.52	2.3 ± 0.7	5.9 ± 2.2	0.204 ± 0.077	14.2 ± 5.3	1.56 ± 0.63	yes
G177.14-01.21_1	25.1	0.37	0.55 ± 0.05	1.28	7.9 ± 1.2	4.6 ± 0.3	0.486 ± 0.036	310.7 ± 22.8	0.19 ± 0.02	yes
G177.14-01.21_2	25.9	0.38	0.52 ± 0.07	0.82	6.0 ± 1.1	3.0 ± 0.3	0.320 ± 0.030	218.2 ± 20.4	0.27 ± 0.05	yes
G177.14-01.21_3	32.6	0.48	0.73 ± 0.13	1.20	5.0 ± 1.1	1.8 ± 0.2	0.240 ± 0.031	259.1 ± 33.5	0.40 ± 0.09	yes
G178.28-00.61_1	25.7	0.07	0.65 ± 0.09	1.34	3.7 ± 0.9	22.3 ± 3.5	0.462 ± 0.072	11.5 ± 1.8	1.21 ± 0.25	yes
G178.28-00.61_2	23.8	0.07	0.35 ± 0.08	0.88	3.8 ± 1.0	21.3 ± 2.8	0.408 ± 0.054	8.7 ± 1.1	0.79 ± 0.21	yes
G178.28-00.61_3	24.7	0.07	0.43 ± 0.05	0.86	5.5 ± 0.9	22.3 ± 1.9	0.444 ± 0.039	10.2 ± 0.9	0.87 ± 0.12	yes
G178.28-00.61_4	18.9	0.05	0.39 ± 0.10	0.60	3.2 ± 1.0	32.1 ± 5.2	0.489 ± 0.079	6.6 ± 1.1	0.92 ± 0.29	no
G178.28-00.61_5	17.0	0.05	–	0.36	17.3 ± 0.8	28.5 ± 3.4	0.390 ± 0.047	4.2 ± 0.5	–	no
G178.28-00.61_6	18.9	0.05	0.46 ± 0.13	0.42	1.7 ± 0.3	12.8 ± 6.7	0.195 ± 0.102	2.6 ± 1.4	2.77 ± 1.64	yes
G178.28-00.61_7	28.8	0.08	0.55 ± 0.09	0.82	5.9 ± 1.3	20.3 ± 2.7	0.471 ± 0.062	14.7 ± 1.9	0.89 ± 0.19	yes
G178.28-00.61_8	21.1	0.06	0.43 ± 0.05	0.39	3.9 ± 0.9	10.8 ± 1.2	0.182 ± 0.020	3.0 ± 0.3	2.49 ± 0.41	no
G178.28-00.61_9	17.6	0.05	0.55 ± 0.08	0.30	3.0 ± 0.7	15.2 ± 2.5	0.215 ± 0.036	2.5 ± 0.4	3.18 ± 0.72	yes
G178.28-00.61_10	26.2	0.07	0.55 ± 0.15	0.58	2.2 ± 0.3	6.9 ± 4.6	0.145 ± 0.096	3.7 ± 2.5	3.19 ± 2.30	yes

[a]The extracted clump sizes with *Gaussclumps* procedure (see Section 3.2).

[b]The clump effective radius $R_{\rm eff}$ = FWHM/$(2\sqrt{\ln 2})$. The uncertainties of $R_{\rm eff}$ are ∼10%, which will cause additional uncertainty of around 21% in the derived masses.

[c]The point source cross identification using the AllWISE Data in VizieR Online Data Catalog (see Section 2.3).